The Role of the Homeobox Transcription Factor Meis2b in Zebrafish Heart Development and Asymmetry

Dissertation

zur Erlangung des Doktorgrades

der Naturwissenschaften

Vorgelegt beim Fachbereich 15

der Johann Wolfgang Goethe-Universität

in Frankfurt am Main

Von

Almary Victoria Guerra Rodríguez

aus Barquisimeto, Venezuela

Frankfurt 2017

(D30)

vom Fachbereich Biowissenschaften (FB15) der Johann Wolfgang Goethe - Universität als Dissertation angenommen.

Dekanin: Prof. Dr. Meike Piepenbring

Gutachter: Prof. Didier Y. R. Stainier, Ph.D.

Prof. Virginie Lecaudey, Ph.D.

Datum der Disputation:

SUPERVISORS

Dr. Sven Reischauer
Department of Developmental Genetics
Max Planck Institute for Heart and Lung Research
Bad Nauheim, Germany

and

Prof. Didier Y. R. Stainier, Ph.D.
Department of Developmental Genetics
Max Planck Institute for Heart and Lung Research
Bad Nauheim, Germany

REVIEWERS

Prof. Didier Y. R. Stainier, Ph.D.
Department of Developmental Genetics
Max Planck Institute for Heart and Lung Research
Bad Nauheim, Germany

and

Prof. Virginie Lecaudey, Ph.D.
Department of Developmental Biology of Vertebrates
Institute of Cell Biology and Neuroscience
Johann Wolfgang Goethe University
Frankfurt am Main, Germany

DECLARATION

I herewith declare that I have not previously participated in any doctoral examination procedure in a mathematics or natural science discipline.

Frankfurt am Main, …….

(Signature)

Author's Declaration

I herewith declare that I have produced my doctoral dissertation on the topic of "**The Role of the Homeobox Transcription Factor Meis2b in Zebrafish Heart Development and Asymmetry"**
independently and using only the tools indicated therein. In particular, all references borrowed from external sources are clearly acknowledged and identified.

I confirm that I have respected the principles of good scientific practice and have not made use of the services of any commercial agency in respect of my doctorate.

Frankfurt am Main, ……

(Signature)

Table of Contents

Abbreviations

ALMP	Anterior Lateral Plate Mesoderm
AVC	Atrio-ventricular Canal
BAC	Bacterial Artificial Chromosome
bp	Base pairs
BSA	Bovine Serum Albumin
cds	Coding sequence
DBE	Dibenzyl ether
DEAB	4-diethylaminobenzaldehyde
DMSO	Dimethyl sulfoxide
dpf	Days post fertilization
ECM	Extracellular Matrix
EdU	5-ethynyl-2'-deoxyuridine
EGTA	Ethylene glycol-bis(β-aminoethyl ether)-N,N,N',N'-tetraacetic acid
EMT	Endothelial to Mesenchymal Transition
FHF	First Heart Field
G	Gravitational constant
h	Hour
HA	Hyaluronic Acid or Hyaluronan
HABP	Hyaluronic acid binding protein
HINGS	Heat inactivated goat serum
hpf	Hours post fertilization
HRM	High-Resolution Melt
HRMA	High-Resolution Melt Analysis
IFT	Inflow Tract
ISH	*In situ* hybridization
meis2a	Myeloid Ecotropic Viral Integration Site 2.1
meis2b	Myeloid Ecotropic Viral Integration Site 2.1
mL	milliliter
mM	Millimolar
MO	Morpholino
mpf	Months post fertilization

OFT	Outflow Tract
PBS	Phosphate Saline Buffer
PCR	Polymerase Chain Reaction
PFA	Paraformaldehyde
pH	Potential of Hydrogen
PIPES	1,4-Piperazinediethanesulfonic acid
RA	Retinoic acid
RT-qPCR	Real-Time Quantitative Polymerase Chain Reaction
s	Seconds
SHF	Second Heart Field
spaw	*southpaw*
TALEN	Transcription activator-like effector nuclease
Tg	Transgenic Line
Tg(meis2b-reporter)	*TgBAC(meis2b:GAL4FF)*^{bns15}*;Tg(5xUAS:*eGFP*)*^{nkuasgfp1a}
THF	Tetrahydrofuran
µL	microliter
HD	Homeodomain

I. Introduction

The zebrafish as an experimental model offers a number advantages over mammalian models, such as: external fertilization, small size and transparency during embryonic development, and the possibility to study organ formation *in vivo*. Furthermore, congenital heart defects do not affect the survival during the first five days post fertilization (dpf), since the zebrafish larvae are able to exchange oxygen and CO_2 by diffusion, thus permitting the study of embryos with severe cardiovascular defects. All these characteristics make the zebrafish a great candidate for the study of cardiovascular diseases that otherwise would be difficult to study using mammalian experimental models.

In this project, the zebrafish was used as an experimental model for cardiac development. However, results obtained with experiments in the zebrafish can help in understanding certain events during heart development in higher vertebrates. Therefore, this chapter is dedicated to the discussion of the zebrafish and mammalian heart formation, followed by a description of different genetic and signaling pathways that are relevant in this project.

1.1. Zebrafish Heart Development

The zebrafish has a linear heart configuration, composed by one atrium which receives the deoxygenated blood from the body and one ventricle which pumps the blood out of the heart and into the gills (Stainier 2001).

In the zebrafish, the heart is the first organ to form and function during embryonic development. As early as 5 hours post fertilization (hpf) (in the blastula stage), atrial and ventricular cardiomyocyte precursors can be found on both sides of the embryo in the lateral margin zone. At this stage, the atrial precursors are located more ventral than the ventricular precursors, and the endocardial precursors are located in the same area but without a specific organization (Fig. 1.1 A) (Stainier, Lee et al. 1993, Keegan, Meyer et al. 2004). As development progresses, the cardiomyocyte precursors involute and reach the embryonic axis in the anterior lateral plate mesoderm (ALMP) by 5 somites stage, forming two bilateral streams of cells known as the cardiac fields (Fig. 1.1 B) (Stainier, Lee et al. 1993), where they express the transcription factors *gata4*, *nkx2.5* and *hand2* (Schoenebeck, Keegan et al. 2007).

Previous studies suggest that the G-coupled Apelin receptor (*agtrl1b*) and its ligand Apelin, are important in the migration and the correct positioning of the cardiomyocyte precursors in the ALPM, where they can receive myocardial differentiation signals (Scott, Masri et al. 2007, Zeng, Wilm et al. 2007).

By 14 somites, the ventricular precursors are positioned medial to the atrial precursors and the endocardial precursors are located anterior to the cardiac fields (Fig. 1.1 B) (Bussmann, Bakkers et al. 2007, Schoenebeck, Keegan et al. 2007). The forelimb progenitors can be found posterior to the cardiac fields, and the boundaries between the pool of vascular, cardiac and forelimb progenitors are tightly regulated by retinoic acid signaling (Waxman, Keegan et al. 2008, Rydeen and Waxman 2014).

Afterwards, the endocardial precursors migrate and fuse at the midline (Fig. 1.1 C), dorsal to the cardiomyocyte precursors (Bussmann, Bakkers et al. 2007, Holtzman, Schoenebeck et al. 2007). Afterwards, the myocardial precursors meet at the midline, first by fusion of the posterior cells (Fig. 1.1 D), and then by fusion of the most anterior cells of the cardiac fields; this process of fusion forms the heart disc, where the atrial cardiomyocytes are located around the ventricular cardiomyocytes (Fig. 1.1 E) (Bakkers 2011). The heart disc is covered ventrally by the endocardial progenitors, which pass through the central ring of the heart disc and connect dorsally to the lateral dorsal aortae through the aortic arches (Bussmann, Bakkers et al. 2007).

fibronectin, a gene that encodes an extracellular matrix (ECM) protein, is important in the migration of the bilateral heart fields to the midline. In *fibronectin* mutants (*natter* mutants), the cardiomyocyte progenitors in the heart fields fail to fuse at the midline, leading to a cardia bifida phenotype (Trinh and Stainier 2004). Mutations in other genes that are involved in regulating *fibronectin* levels, such as *s1p* (*two-of-hearts*/*toh* mutant) or its receptor *s1p2* (*miles-apart*), also cause cardia bifida (Bakkers 2011, Staudt and Stainier 2012). Therefore, regulation of the heart disc formation is important for proper heart development.

After the heart disc is formed, the cells start to migrate and rotate asymmetrically to form the heart tube (de Campos-Baptista, Holtzman et al. 2008, Rohr, Otten et al. 2008, Smith, Chocron et al. 2008). By 26 somites (24 hpf), as a result of this asymmetrical migration of the cardiomyocytes, the heart tube is tilted to the left side of the embryo (a process known as cardiac jogging), with the future atrium located anterior to the future ventricle (Bakkers 2011, Staudt and Stainier 2012). Furthermore, the endocardial cells, which were previously

located ventral to the heart disc, now line the interior of the heart tube and connect posteriorly to the dorsal aortae (Bussmann, Bakkers et al. 2007, Holtzman, Schoenebeck et al. 2007).

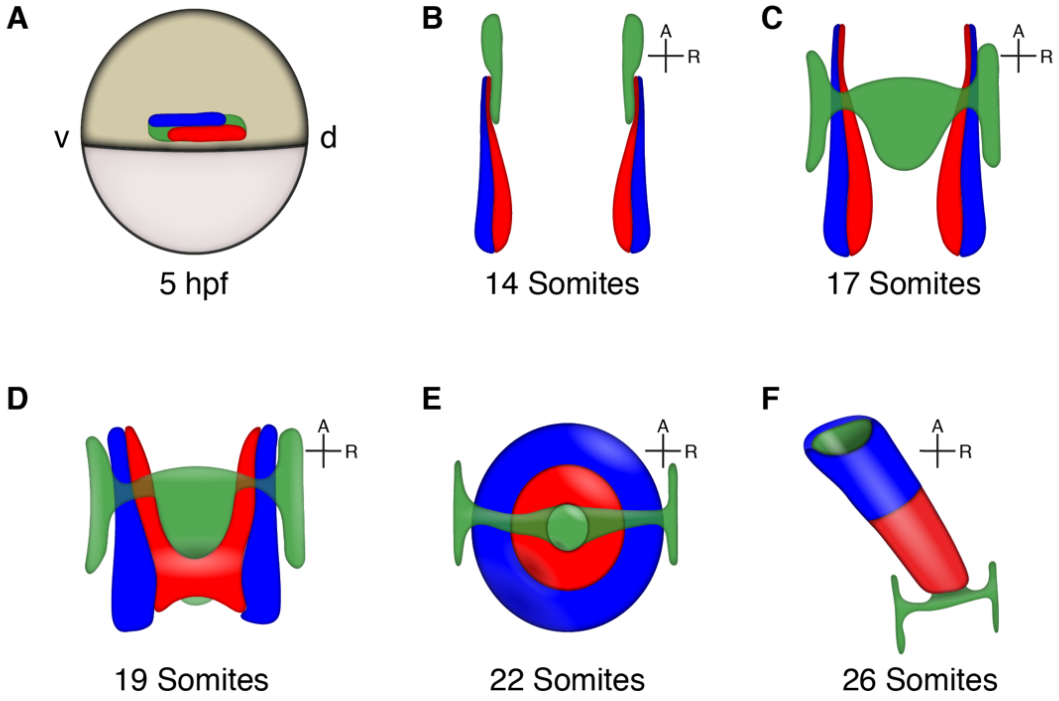

Figure 1.1. Schematic representation of the formation of the heart tube in the zebrafish. **(A)** Endocardial (green), atrial (blue) and ventricular (red) myocardial precursors can be tagged in the blastula stage. **(B)** By 14 somites, myocardial precursors are arranged bilaterally and form the heart fields, with the ventricular precursors medial to the atrial precursors, and the endocardial precursors anterior to the heart fields. **(C)** Endocardial precursors fuse at the midline by 17 somites stage. **(D)** The most posterior myocardial precursors meet at the midline, dorsal to the endocardial precursors. **(E)** The heart disc is formed, with the ventricular precursors located in the center of the disc. The endocardial cells cover the ventral side of the heart disc and pass through the ring in the disc, and connect to the aortic arches at 22 somites stage. **(F)** The heart tube is formed, with the endocardial cells lining the interior of the heart and the atrial cardiomyocytes located anterior to the ventricular cells.

The migration of the cells in the heart disc is regulated by left-right (L-R) signaling pathways (these pathways will be discussed in detail later in this chapter). Nodal and BMP signaling genes are asymmetrically expressed in the ALPM, and control left-right heart morphogenesis by regulation of the direction and the speed of the cardiomyocyte migration during heart tube formation (de Campos-Baptista, Holtzman et al. 2008, Smith, Chocron et al. 2008).

Other genes also participate in the formation of the heart tube; for example, the heart disc in *has2* (*hyaluronan synthase 2*) mutants fail to rotate and, as a consequence, the heart disc is

formed in the midline of the embryo instead of the normal leftward displacement that occurs in wildtype (WT) fish (Smith, Chocron et al. 2008).

During heart tube extension, *nkx2.5* and *nkx2.7* are important in determining the number of atrial and ventricular cardiomyocytes. *nkx*-deficient fish have normal heart disc formation, but start showing abnormalities during heart tube development, with a short ventricle and a surplus of atrial cardiomyocytes (Targoff, Schell et al. 2008).

After the heart tube is assembled, it inclines towards the right side of the embryo, and the arterial and venous poles rotate in different directions and speeds, leading to a torsion of the heart tube, a process known as heart looping (Smith, Chocron et al. 2008, Bakkers 2011). This process results in a ventricle positioned on the right side and a more posterior atrium located on the left side of the midline of the embryo. At this point, the atrium and ventricle are separated by a narrow segment called the atrioventricular canal (AVC), where the valves will be formed.

The direction of cardiac jogging is regulated by left-right signals and, usually, a leftward migration of the heart tube is followed by a rightward looping of the heart. However, this is not always the case, and it is still not clear which mechanisms are responsible for heart looping (reviewed by (Bakkers, Verhoeven et al. 2009)).

A series of morphogenetic events follow after heart looping; however, they will not be discussed in depth in this chapter. Some of these events include the formation of the atrioventricular valves in the AVC, which starts at 48 hpf. The valves are key for proper heart function, since they ensure the unidirectional blood flow from atrium to ventricle, and prevent the retrograde blood flow inside the heart (reviewed in (Staudt and Stainier 2012). A second key event is heart trabeculation, which starts at around 60 hpf, and consists in the growth of finger-like projections into the ventricular lumen, which are important for the contraction of the ventricle and in the electrical conduction in the heart (reviewed in (Staudt and Stainier 2012)). As a summary, some of the most important steps during cardiac development in the zebrafish have been mentioned above: formation of the bilateral cardiac fields, formation of the heart disc, heart tube and AV valves, and trabeculation.

There is another important event during heart development: the contribution of cells from the first and second heart fields (FHF and SHF, respectively) to different regions of the heart. During cardiac development, two events of cardiomyocyte differentiation can be observed: the earliest differentiation event corresponding to the FHF, and a second corresponding to

the SHF. These two waves of cardiomyocyte differentiation are very important for proper cardiac development (Liu and Stainier 2012) and some of the most relevant details about SHF are discussed below.

1.2. Second heart field

Mammalians have four-chambered hearts, with two ventricles and two atria which allow the separation of the systemic and pulmonary circulations, constituting an evolutionary advantage in comparison to the fish, who have two-chambered hearts and only one circulatory system (Fig. 1.2). The separation of pulmonary and systemic circulations happened during the transition from aquatic to terrestrial life, and it has been proposed that the cardiac chambers dedicated to the newly formed pulmonary circulation, such as the right ventricle, arise from the second heart field (SHF) (Hillenius and Ruben 2004, Olson 2006, Koshiba-Takeuchi, Mori et al. 2009).

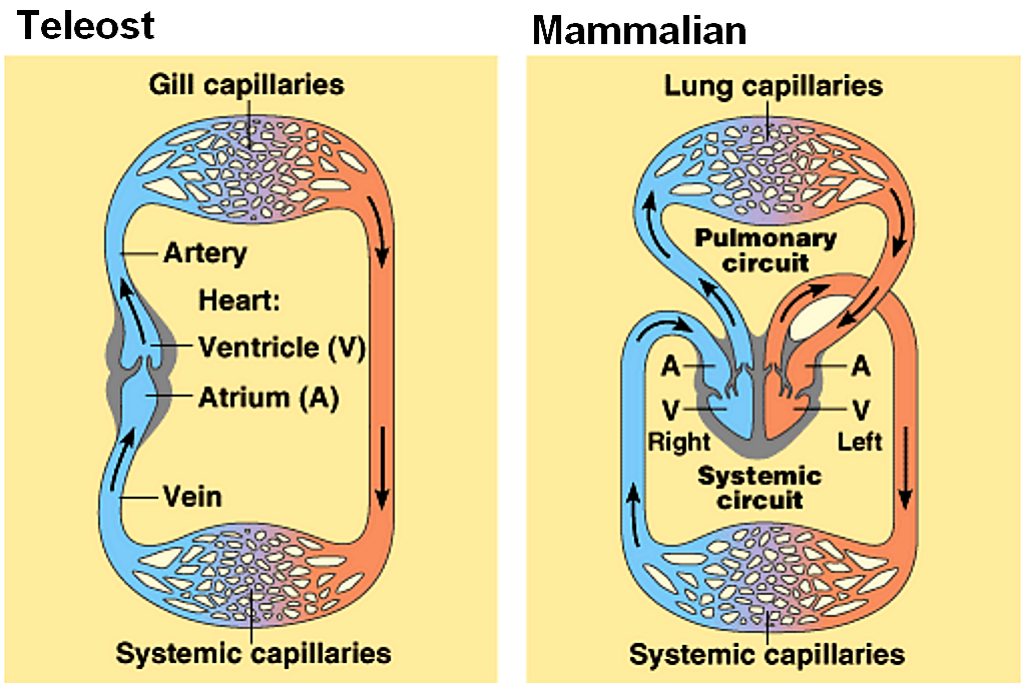

Figure 1.2. Cardiovascular systems of teleost and mammalians. The teleost fish have two-chambered hearts consisting of one atrium and one ventricle. Mammalians possess fully septated four-chambered hearts composed of two atria and two ventricles, allowing the separation of the pulmonary and systemic circuits. Modified from (Moyes and Schulte 2005)

Surprisingly, the zebrafish also exhibits a SHF contribution to the arterial and venous pole, despite having only one atrium and ventricle. In the ALMP, the SHF cells are initially located medio-cranially in the bilateral heart fields (Hami, Grimes et al. 2011). After the heart tube is formed, a late addition of a population of cells derived from the SHF contributes to the venous and the arterial poles of the tube. It has been reported that *isl1*+ cells contribute to addition of cardiomyocytes to both poles of the heart. Furthermore, expression of *isl1* is important in the formation of the pacemaker cells in the atrium (Fig. 1.3) (de Pater, Clijsters et al. 2009, Hami, Grimes et al. 2011, Witzel, Jungblut et al. 2012).

The SHF cells added to the arterial pole of the heart express the *latent TGF-ß binding protein 3* (*ltbp3*), and contribute cardiomyocytes to the outer curvature of the ventricle and smooth muscle cells in the outflow tract (Fig 1.3). Moreover, an interaction between Nkx2.5 and Ltbp3 was revealed, suggesting a role for Nkx2.5 in the contribution of SHF cells to the heart (Zhou, Cashman et al. 2011, Guner-Ataman, Paffett-Lugassy et al. 2013). Last, the process of expansion of the SHF derived cells in the heart, requires Fgf, Bmp and Hh signaling (Marques, Lee et al. 2008, de Pater, Clijsters et al. 2009, Hami, Grimes et al. 2011).

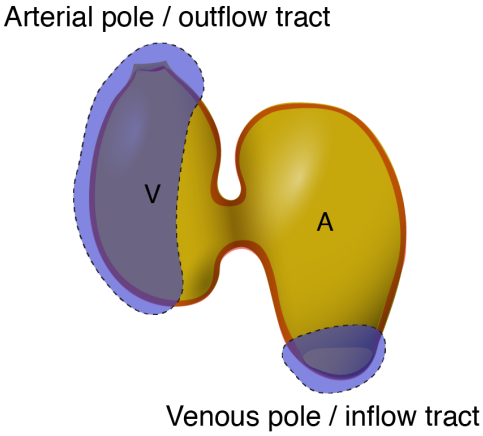

Figure 1.3. Second heart field in the zebrafish heart. At 72 hpf, the contributions of the SHF derived cells can be observed in the outer curvature of the ventricle, outflow tract and in the inflow tract (purple areas). A, atrium. V, ventricle.

1.3. Heart development in mammals

As previously mentioned, mammals have four-chambered hearts consisting of two atria and two ventricles. Despite the notable anatomical differences, the cellular and genetic mechanisms controlling cardiac development in mammals are very similar to those found in

the teleost, which is an advantage when using the zebrafish as an experimental model for heart diseases.

In mouse, at E7.5, the cardiac progenitors are arranged in the first and second heart fields forming the cardiac crescent. The peak of the crescent is located cranially, while its two tails extend caudally (Fig. 1.4 Cardiac Crescent) (Reviewed in (Harvey 2002)). The SHF progenitors are located anterior and medial to the FHF progenitors (Waldo, Kumiski et al. 2001). Then, the cardiac crescent fuses at the midline, forming the linear heart tube. Additionally, the cells of the FHF differentiate and proliferate during the formation of the heart tube, while the SHF progenitors remain undifferentiated and are located dorsally to the heart tube (reviewed by (Buckingham, Meilhac et al. 2005)).

In mammals, the anterior SHF progenitors give rise to the right ventricle and the outflow tract, while the posterior SHF progenitors form the inflow tract and contribute to the atria. In contrast, FHF progenitors form the left ventricle and contribute to both atria. As a consequence, both atria show contribution from both FHF and SHF progenitors (Zaffran, Kelly et al. 2004, Buckingham, Meilhac et al. 2005, Rochais, Mesbah et al. 2009).

The FHF progenitors express *Tbx5* and an early wave of *Nkx2.5* (Bruneau, Nemer et al. 2001, Stanley, Biben et al. 2002, Takeuchi, Ohgi et al. 2003). In contrast, the SHF can be identified by the expression of *Isl1, Fgf8* and *Fgf10* (Kelly, Brown et al. 2001, Cai, Liang et al. 2003, Ilagan, Abu-Issa et al. 2006, Moretti, Caron et al. 2006) but become downregulated as the linear heart tube is formed and other transcription factors such as *Nkx2.5*, *Gata4* and *Mef2c* become highly expressed in the cardiac cells (Waldo, Kumiski et al. 2001).

After the heart tube is formed, the cardiac chambers start to balloon as the atrial and ventricular cells differentiate and proliferate. Cardiac septation occurs from stage E10 and is only completed after birth (Fig. 1.4). Correct chamber septation is fundamental for the proper function of the heart.

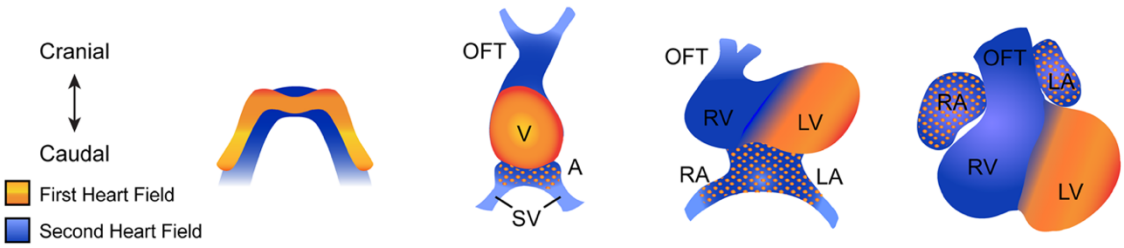

Stage	Cardiac Crescent	Linear Heart Tube	Looping Heart	Chamber Specialization/ Septation
Mouse Embryo Stage	E7.5	E8.0	E9-12	E10+
Human Embryo Stage	Day 15	Day 20	Day 28-30	Day 32+
Key Regulators	GATA4 NKX2.5 MESP1/2 ISL1 BAF60C MEF2C	GATA4 NKX2.5 TBX5 TBX20 MEF2C	GATA4 NKX2.5 TBX5 MEF2C HAND1/2	GATA4 NKX2.5 TBX5 PITX2 TBX1

Figure 1.4. Overview of mammalian embryonic heart development. The table shows the different stages of heart development in mouse and the equivalent time in humans, as well as the most important transcription factors controlling cardiac embryonic formation. Taken from (Paige, Plonowska et al. 2015).

The process of atrial septation starts with the formation of the *septum primum*, which originates from the dorsal part of the common atrium and extends until the AV cushions, leaving a small opening called the *ostium primum* that allows the movement of blood between the atria. As the *ostium primum* closes, cell death produces another fenestration in the upper side of the *septum primum* (Webb, Brown et al. 1998, Kim, Viragh et al. 2001). This second opening is called *ostium secundum*. Another fold appears in the right atrium, close to the *septum primum*, this fold will develop as the *septum secundum*, which overlaps with the *ostium primum*. However, the *septum secundum* is also not completely closed; the fenestration in the *septum secundum* is called the oval foramen, and it allows blood flow from the right to the left atrium. After birth, when the blood pressure in the left atrium increases, the *septum primum* and *secundum* are pushed together, which closes the fenestrations in the septa, leading to the definitive formation of the inter-atrial septum (Wessels, Anderson et al. 2000, Lamers and Moorman 2002).

Ventricular septation happens simultaneously to the atrial septation, and it starts with folding and fusion of the anterior ventricular wall that extends to the interior of the common ventricle towards the AV area. A fenestration called the interventricular foramen is left open until the

aorticopulmonary septum is formed (a septum that separates the truncus arteriosus into the aortic and pulmonary artery). Afterwards, the interventricular foramen is then closed due to the contribution of endocardial tissue from the ventricular septum, the AV endocardial cushions and the aorticopulmonary septum (Lamers and Moorman 2002, Anderson, Webb et al. 2003).

Once the heart is completely formed, each chamber performs its own function within the organ: the right atrium receives deoxygenated blood from the body and pumps it into the right ventricle, which pushes the blood into the pulmonary artery and into the lungs for oxygenation. Meanwhile, the left atrium receives the oxygenated blood from the lungs and pushes it into the left ventricle and then to the body. The proper function of each chamber is crucial for the overall cardiac performance, and diseases affecting chamber morphogenesis can greatly compromise the proper blood circulation through the body. Therefore, the following parts of this chapter are dedicated to the description of the importance of cardiac chamber identity and function in heart diseases.

1.4. Congenital heart defects

Congenital heart diseases (CHDs) are the most common type of birth defects in humans, affecting nearly 1% of live births (Hoffman 1995). CHDs arise when the heart is not correctly formed during development, impeding the proper function of the heart. CHD can be caused by external factors (such as certain medicines taken by the mother during pregnancy) or by internal factors such as mutations (Schott, Benson et al. 1998, Garg, Kathiriya et al. 2003, Li, Klena et al. 2015, Ang, Rivas et al. 2016).

CHDs can be classified into three main groups: cyanotic heart disease, left-sided obstruction defects and septation defects (Bruneau 2008). Children with cyanotic heart disease appear blue due to the mixing of oxygenated and deoxygenated blood; and the following defects form part of this category: transposition of the great arteries, tetralogy of Fallot, double outlet right ventricle and persistent truncus arteriosus. The left-sided obstruction defects include: hypoplastic left heart syndrome, mitral and aortic stenosis, aortic coarctation and interrupted aortic arch (Bruneau 2008). The most common septation defects are: atrioventricular septal defects, atrial septal defects (ASDs) and ventricular septal defects (VSDs). The ASDs and VSDs are the most relevant for this study and therefore, are described below:

1.4.1. Atrial Septal Defects:

These defects happen when the inter-atrial septum is not completely closed or is absent, causing a mix of oxygenated and deoxygenated blood between the atria (Fig. 1.5 B) (Lo, Yu et al. 2010). ASDs are often associated with cardiac conduction defects since mechanisms responsible for atrial septation can be involved in sinoatrial node formation, which is located in the right atrium (Zaidi and Brueckner 2017).

1.4.2. Ventricular Septal Defects:

Similar to the ASDs, the VSDs occur when the interventricular septum is not closed or did not form at all, allowing the passing of blood between the ventricles. Additionally, when the fenestration between the pulmonary artery and the left ventricle is not closed, the oxygenated blood from the ventricle can pass into the pulmonary artery, which carries the deoxygenated blood to the lungs. This defect can significantly decrease the amount of oxygenated blood that goes into the body (Fig. 1.5 C) (Lo, Yu et al. 2010)

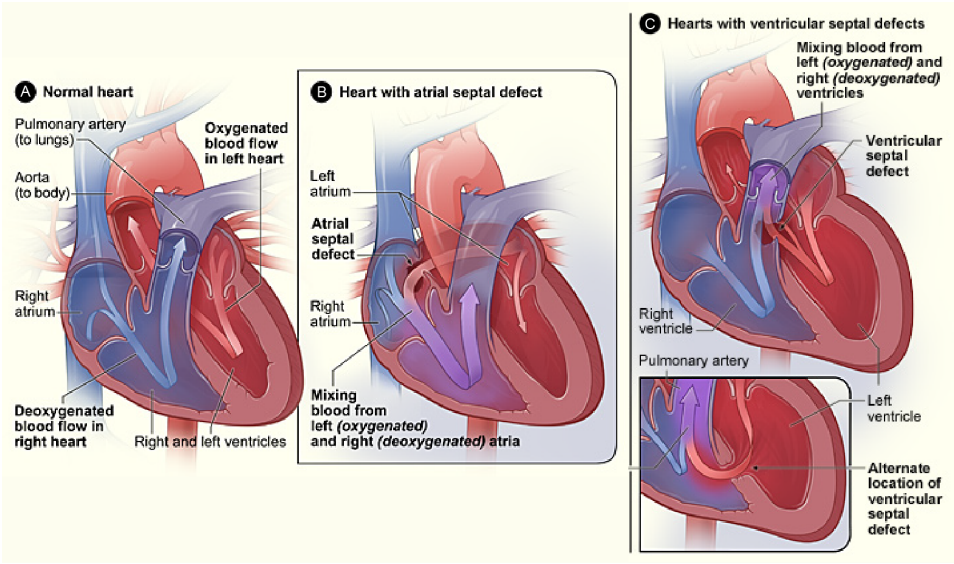

Figure 1.5. Atrial and ventricular septal defects. **(A)** Schematic illustration of a healthy human heart. **(B)** Heart showing an incomplete atrial septum formation. **(C)** Heart with a ventricular septal defect, allowing blood from the left ventricle into the pulmonary artery (top panel) and an interventricular septum malformation (bottom panel). Modified from nhlbi.nih.gov.

1.5. Determination of cardiac left-right asymmetry

The establishment of the three body axes (anterior-posterior, dorsal-ventral and left-right) is key to the organization of the vertebrate body plan. The heart has a clear left-right asymmetric pattern, which can be evidenced not only by the differential gene expression in each chamber but also in the anatomy of the heart (Hamada 2010). Cardiac asymmetry is linked to chamber identity, which, at the same time, is also linked to the particular functions of each heart chamber. Several signaling pathways are involved in the establishment of the left-right asymmetry, the most important are discussed below:

1.5.1 Nodal Signaling

The Nodal signaling pathway plays an important role in the asymmetric patterning of different organs during embryonic formation, and its function is highly conserved among species. In mammals, there is one single *Nodal* gene, while in the zebrafish there are three orthologues: *cyclops*, *squint* and *southpaw* (*spaw*), where only the latter is important for cardiac asymmetric development, as reviewed in (Shen 2007).

Nodal/spaw are expressed on the left side of the lateral plate mesoderm (LPM), and cells that receive Nodal signals on this side will specifically contribute to the left side of visceral organs. Cells located on the right half of the LPM that do not receive Nodal signals will contribute to the right side of the visceral organs. Nodal is capable of inducing its own expression via a positive-feedback loop, and alterations in *Nodal* asymmetric expression lead to abnormal organization and development of the gut and heart (Yokoyama, Copeland et al. 1993, Horne-Badovinac, Rebagliati et al. 2003, Long, Ahmad et al. 2003, Baker, Holtzman et al. 2008).

Nodal is a TGFß family ligand and can interact with type I and II TGFß receptors. However, Nodal requires CRYPTIC or CRIPTO (One-eyed pinhead in zebrafish) as co-receptors (Schier and Shen 2000). Additionally, Smad2 and Smad4 are also key intracellular components of the Nodal pathway and help activate the transcription of downstream genes (Shen 2007).

There are several downstream targets and proteins involved in the Nodal signaling pathway and in this chapter, I focus on *Lefty1-2* and *Pitx2*.

1.5.2. Lefty1 and Lefty2

The *Lefty* genes are also asymmetrically expressed in the LPM. In mouse, during left-right axis formation, *Lefty1* is expressed in the presumptive floor plate and lowly expressed on the left LPM, while *Lefty2* is lowly expressed in the presumptive floor plate and highly expressed on the left side of the LPM (Meno, Ito et al. 1997). In contrast, in the zebrafish *lefty1* is initially expressed in the notochord but after the left-right patterning is established *lefty1* and *2* are expressed on the left side of the LPM.

Lefty1 and *2* expressions are induced by Nodal signaling and, at the same time, LEFTY1 and 2 act as NODAL antagonists by competitively interacting with CRYPTIC or CRIPTO (Cheng, Olale et al. 2004). Therefore, LEFTY regulates Nodal activity and expression via a negative-feedback loop. Furthermore, it has been proposed that expression of *Lefty1* in the embryo midline, inhibits the expression of *Nodal* on the right side of the LPM (Fig. 1.6) (Meno, Shimono et al. 1998, Bisgrove, Essner et al. 1999).

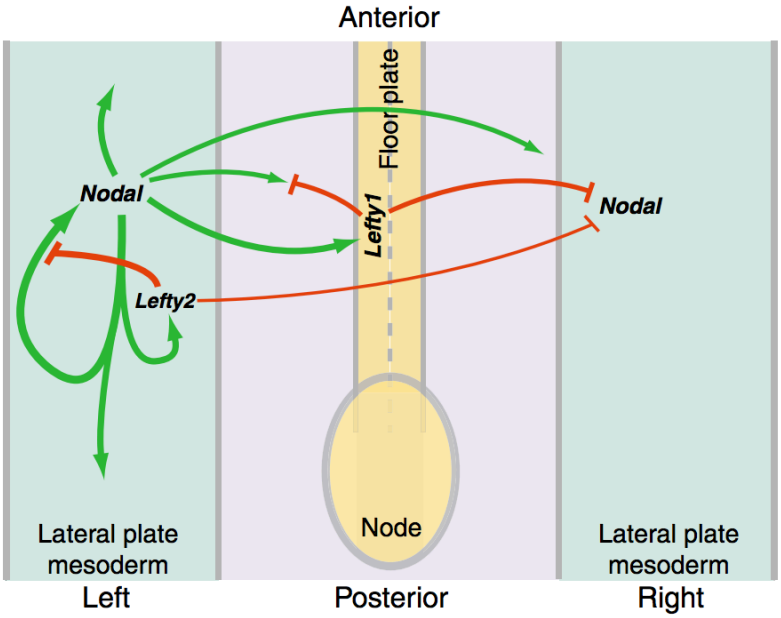

Figure 1.6. Nodal signaling pathway during left-right patterning specification in the mouse embryo (3-8 somites). Nodal regulates its own expression in the LPM via a positive-feedback loop, and at the same time NODAL induces the expression of *Lefty1* and *Lefty2*. LEFTY2 downregulates *Nodal* expression in the left LPM, while LEFTY1 suppresses Nodal expression in the midline and prevents the spreading of Nodal signals to the right LPM.

In mouse, absence of *Lefty1* causes the loss of asymmetric expression of *Nodal*, *Lefty2* and *Pitx2* as these genes become expressed on the left and right side of the LPM. Additionally,

Lefty1$^{-/-}$ embryos show visceral left isomerism, meaning that the liver, lungs and heart displayed a left-sided identity of both the right and left sides (Meno, Shimono et al. 1998). In the zebrafish, *lefty2* is expressed in the left half of the heart disc, and lineage tracing experiments have shown that, during the formation of the heart tube, the *lefty2*-expressing cells move to the dorsal half of the heart tube (Smith, Chocron et al. 2008). *Lefty2* null mutant mice die at early embryonic stages and fail to form structures such as the node, notochord and somites. These results suggest that LEFTY2 plays an important role during gastrulation (Meno, Gritsman et al. 1999).

1.5.3 Pitx2

PITX2 is a homeobox transcription factor involved in left-right signaling during embryonic development of the heart and other organs. Mutations in *Pitx2* cause Axenfeld-Rieger syndrome in humans, which is characterized by ocular malformations, dental anomalies and facial dysmorphisms (Semina, Reiter et al. 1996). Furthermore, mutations in *Pitx2* have been linked to congenital cardiac defects in humans such as atrial and ventricular septal defects, as well as endocardial cushion defects and atrial fibrillation (Mammi, De Giorgio et al. 1998, Gudbjartsson, Arnar et al. 2007, Franco, Chinchilla et al. 2012, Zhao, Peng et al. 2015).

Pitx2 has three splice isoforms: *Pitx2a*, *Pitx2b* and *Pitx2c* (in humans, a fourth *Pitx2* variant has been identified, *Pitx2d*). However, only *Pitx2c* is expressed in the heart and is involved in left-right asymmetric cardiac development (from now on, Pitx2 refers to Pitx2c, since this is the only isoform that will be discussed in this manuscript) (Martin, Amendt et al. 2010). During heart development in mammals, *Pitx2* is expressed on the left LPM, on the left cardiac crescent, and subsequently on the left side of the heart tube (Fig. 1.7) (Campione, Ros et al. 2001). During heart looping, *Pitx2* expression becomes restricted to the ventral side of the forming ventricles and on the left atrium. After the heart is formed, *Pitx2* expression is downregulated in the ventricles while a high expression in the left atrium remains until adulthood, as reviewed in (Franco and Campione 2003, Franco, Chinchilla et al. 2012).

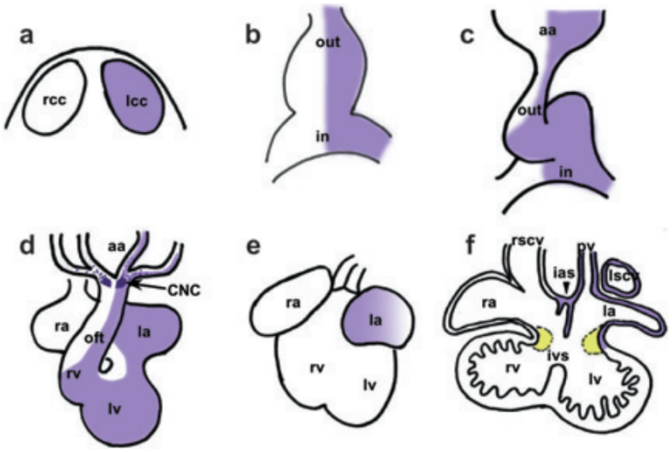

Figure 1.7. *Pitx2c* expression during heart development in mouse. Purple areas indicate *Pitx2* expression. rcc, right cardiac crescent; lcc, left cardiac crescent; out, outflow; in, inflow region; ias, interatrial septum; ivs, interventricular septum; la, left atrium; lv, left ventricle; oft, outflow tract; pv, pulmonary veins; ra, right atrium; rv, right ventricle. Taken from (Franco and Campione 2003).

Global knockout of *Pitx2* leads to embryonic lethality and cardiovascular defects such as double-outlet right ventricle, right atrial isomerism, ASDs and VSDs (Lin, Kioussi et al. 1999, Liu, Liu et al. 2002, Tessari, Pietrobon et al. 2008), while specific *Pitx2* myocardial knockout leads to right cardiac chamber enlargements, hypertrophy of the interventricular septum and overall cardiac dysfunction (Tessari, Pietrobon et al. 2008).

Interestingly, mutations in *Pitx2* in mouse also lead to atrial fibrillation. In WT conditions, PITX2 directly represses *Shox2* expression in the left atrium; therefore, *Shox2* is exclusively expressed in the right atrium, where it works together with NKX2.5, TBX3 and HCN4 in the development of the sinoatrial node, which is responsible for originating the heart beat (Mommersteeg, Hoogaars et al. 2007, Espinoza-Lewis, Yu et al. 2009, Wang, Klysik et al. 2010).

Pitx2 expression in the left LPM can be initiated by FOXH1 binding to the *Pitx2* enhancer region, and further regulated by NKX2-5 (Shiratori, Sakuma et al. 2001, Shiratori, Yashiro et al. 2006). FOXH1 is a transcription factor which is a Nodal signaling effector, therefore it is accepted that *Pitx2* is a downstream target of Nodal signaling. In general, there is strong evidence that *Pitx2* is a key factor in maintenance of the left atrial identity (Tessari, Pietrobon et al. 2008, Franco, Christoffels et al. 2014).

1.5.4. Bmp Signaling

Bmp signaling is also important in determining cardiac left-right asymmetry during development by regulating Nodal signaling. In the zebrafish, the absence of Bmp signaling at the end of gastrulation leads to expression of *spaw* in the right and left LPM, while ectopic Bmp expression results in abolishment of *spaw* expression in the LPM (Chocron, Verhoeven et al. 2007). Knock-down of *bmp4* inhibits *lefty1* expression in the midline; therefore, as mentioned before, the absence of *lefty1* leads to expansion of Nodal signaling to the right LPM (Monteiro, van Dinther et al. 2008).

1.5.5. Tbx Transcription Factors

The T-box family of transcription factors are involved in cardiac lineage determination, chamber specification, valve development and conduction system development. *Tbx1*, *Tbx2*, *Tbx3*, *Tbx5*, *Tbx18* and *Tbx20* are all involved in cardiac development (Plageman and Yutzey 2005). Especially in humans, mutations in *TBX5* cause the Holt-Oram Syndrome, which is characterized by abnormal left-right asymmetric development of the upper limbs, as well atrial and ventricular septal defects and cardiac conduction defects (Newbury-Ecob, Leanage et al. 1996, Plageman and Yutzey 2005). Furthermore, in mouse, *Tbx5* is required in the SHF for the development of the atrial septum (Xie, Hoffmann et al. 2012).

Studies in the zebrafish revealed that *tbx16* is expressed in the perinodal area, around the Kupffer's vesicle (a ciliated organ that creates a directional flow, triggering the asymmetric expression of genes such as *spaw* (Essner, Amack et al. 2005), where it promotes the expression of *spaw* at around 4-6 somites stage therefore, influencing the initial break of the embryonic left-right asymmetry (Fig. 1.8), as reviewed by Bakkers et al. (Bakkers, Verhoeven et al. 2009).

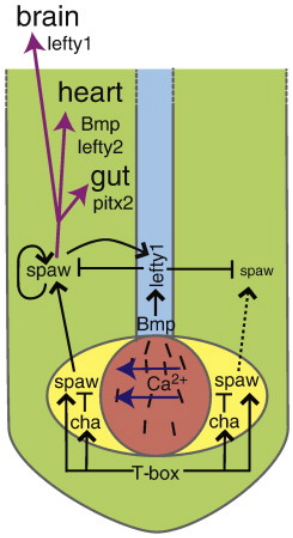

Figure 1.8. Role of Tbx16 in the initial expression of *spaw*. Tbx16 and Charon are the first to promote the expression of the Nodal-related gene *spaw* in the perinodal area (yellow). The directional flow caused by the Kupffer's vesicle (red) is then responsible for the accumulation of Southpaw on the left side of the LPM. Midline (blue); LMP (green). Taken from (Bakkers, Verhoeven et al. 2009).

1.6. Retinoic acid signaling in heart development

Retinoic acid (RA) is the active form of Vitamin A. RA acts as a signaling molecule that controls many events during embryonic anterior-posterior patterning, morphogenesis and organogenesis (Niederreither and Dollé 2010). Once it is in the nucleus, RA binds to one of the three Retinoic Acid Receptors (RARs) or to one of the three Retinoid X Receptors (RXRs), which then bind to the RARE (Retinoic Acid Response Elements) DNA sequence and activate the transcription of target genes (Rhinn and Dolle 2012). The cytochrome P450 26 subfamily (CYP26A1, CYP26B1 and CYP26C1) are responsible for the degradation of RA; this process is very important to prevent inappropriate RA signaling in certain cell types. The enzymes that carry out the last step in the synthesis of RA are RALDH1, RALDH2 and RALDH3 (also known as ALDH1-3); however, RALDH2 (Aldh1a2 in zebrafish) is the most important of these proteins and responsible for the earliest RA synthesized during development (Rhinn and Dolle 2012).

Mutations in *Raldh2* in mouse are lethal and cause severe cardiac defects such as hypoplastic atria and sinus venosus, absence of endocardial cushion formation, underdevelopment of the ventricular chamber, and persistent truncus arteriosus among other defects (Niederreither, Subbarayan et al. 1999, Niederreither, Vermot et al. 2001). In zebrafish, the *aldh1a2* (*neckless*, *nls*) mutants exhibit an excess of cardiomyocytes, and anterior and lateral

expansion of cardiac markers such as *nkx2.5* and *myl7*, as a consequence of an excess of cardiac progenitor cells (Begemann, Schilling et al. 2001, Keegan, Feldman et al. 2005). The same outcome is observed when Aldh1a2 is inhibited by the use of BMS or DEAB (Aldh inhibitors) (Waxman, Keegan et al. 2008).

Zebrafish embryos treated with BMS at 40% epiboly showed a dramatic excess of cardiomyocyte progenitors in the heart field at 6 and 18 somites. This effect gradually decreased in embryos that were treated with BMS at later stages (75% epiboly and tailbud), suggesting that RA signaling is needed to control the number of cardiomyocyte progenitors before gastrulation rather than at later developmental stages. Fate-map experiments determined that RA signaling is required during gastrulation in the lateral margin zone to restrict the size of the myocardial progenitor pool, thus defining a limit of the cardiac fields (Keegan, Feldman et al. 2005). Furthermore, embryos treated with exogenous RA show an anterior extension of the characteristics from posterior (posteriorization); in other words, anterior structures are underdeveloped (small heads, eyes and fins) but posterior structures are enlarged (Stainier and Fishman 1992, Waxman and Yelon 2009)

In the ALPM, the vascular progenitors are positioned anteriorly to the cardiac progenitors, and the forelimb progenitors are located posteriorly to the cardiac progenitors; RA signaling regulates the boundaries between these pool progenitors in the ALMP (Fig. 1.9 A) (Waxman, Keegan et al. 2008, Rydeen and Waxman 2014). Zebrafish embryos with excess of RA show reduced number of cardiomyocytes and an anterior shift in the pool of cardiac progenitors with respect to the notochord (Fig. 1.9 B) (Keegan, Feldman et al. 2005, Waxman and Yelon 2009, Rydeen and Waxman 2014), while deficiency of RA signaling results in a posterior shift of the cardiac progenitors and a surplus in the cardiomyocyte number (Fig. 1.9 C) (Keegan, Feldman et al. 2005, Waxman, Keegan et al. 2008). This posterior shift is due to RA signaling directly regulating *hoxb5b* (a RA-responsive gene) expression within the forelimb field. Hoxb5 is required to restrict the number of atrial cells arising from the adjacent heart field; therefore, in the absence of Hoxb5b (caused by a decrease in RA levels), cardiomyocytes proliferate at a higher rate and fill the space of the forelimb progenitors (Waxman, Keegan et al. 2008).

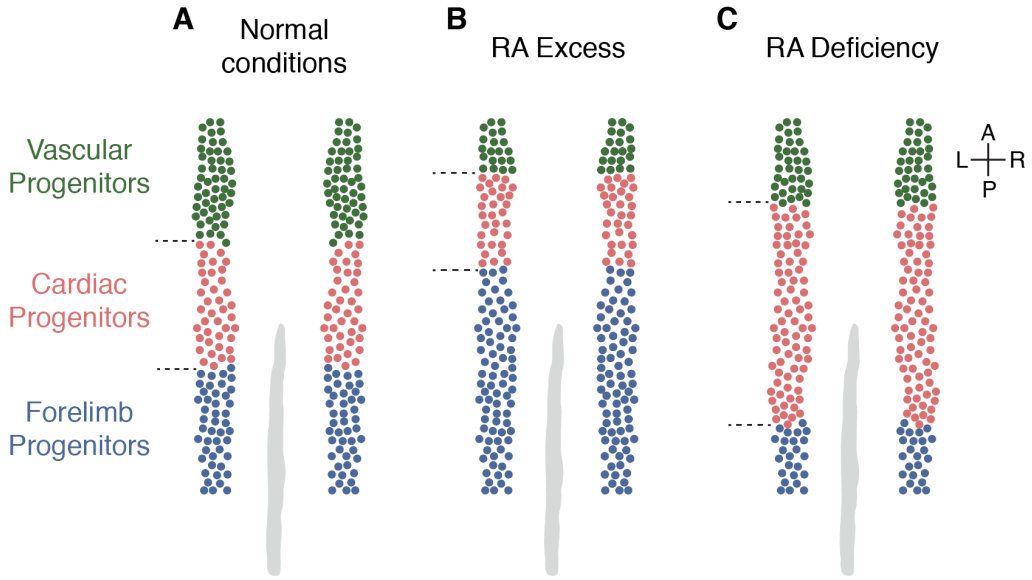

Figure 1.9. RA signaling regulates the boundaries between the pools of vascular, cardiac and forelimb progenitors **(A)**. **(B)** In RA excess conditions, there is an anterior shift in the pool of cardiac progenitors, and a decrease in the number of cardiomyocytes. **(C)** When there is deficiency of RA, the number of cardiomyocytes increases and there is a significant posterior shift and a less marked anterior shift in the pool of cardiac progenitors. Vascular, green; cardiac, pink; forelimb, blue; notochord, gray.

Interestingly, *Raldh2* mutant mice display a posterior expansion of the anterior cells of the SHF territory. The SHF cells of *Raldh2* mutants fail to differentiate and form beating cardiomyocytes, compromising the formation of the SHF derived structures such as the outflow tract, right ventricle and part of the atria (Ryckebusch, Wang et al. 2008, Sirbu, Zhao et al. 2008).

In the zebrafish, *cyp26*-deficient embryos (therefore, embryos with excess of RA) show a decrease in the number of smooth muscle cells from the SHF added to the outflow tract and an extrusion of the ventricular cardiomyocytes from the heart tube, leading to smaller ventricles in comparison to WT siblings (Rydeen and Waxman 2016).

In general, RA is very important in determination of the anterior-posterior (outflow-inflow) patterning of the heart. At tailbud stages, treatments with DEAB, or with exogenous RA, results in hearts with outflow, or inflow dominance, respectively (reviewed by (Xavier-Neto, Davidson et al. 2010)). To summarizing, heart development is a complex process which involves the orchestration of several mechanisms, out of which left-right asymmetry, anterior-posterior patterning, and first and second heart field are the most important for this study.

1.7. Meis2 transcription factors

1.7.1. The *MEIS* proteins

The Meis proteins are transcription factors that belong to the TALE class of proteins. The TALE (Three-aminoacid-loop-extension) transcription factors have a conserved 60 residue long helix-loop-helix homeodomain (HD), with three aminoacid extension between the first and second helix (Burglin 1997). This class of proteins is composed of two families: PBC (which is formed by Pbx1-4) and MEINOX, the latter further divides in PREP and MEIS subfamilies (Longobardi, Penkov et al. 2014). In mammals, the MEIS subfamily consists of three genes: *Meis1*, *Meis2* and *Meis3*, while the zebrafish subfamily is formed by *meis1a*, *meis1b*, *meis2a*, *meis2b* and *meis3* (data from ensembl.org). In contrast, *Drosophila* and nematodes have only one orthologue called Homothorax (Hth) (Merabet and Mann 2016).

The basic structure of the Meis proteins is shown in Fig. 1.10. The HD domain is conserved throughout the TALE class and constitutes the DNA binding domain of these transcription factors. Closer to the N-terminus, the MEIS-A and MEIS-B interaction domains can be found, these domains are conserved only within the MEINOX family and are crucial for the protein-protein interaction of Meis and Prep with other binding partners such as Pbx and Hox (Penkov, Mateos San Martin et al. 2013, Longobardi, Penkov et al. 2014).

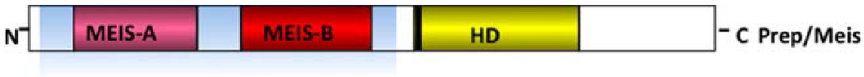

Figure 1.10. Basic structure of the Meis proteins. All Meis proteins have MEIS-A and B interaction domains (pink and red, respectively) and the DNA binding Homeodomain (HD, yellow). Taken from (Longobardi, Penkov et al. 2014).

1.7.2. Meis interaction partners

The Meis proteins form complexes with Pbx, Prep and Hox transcription factors (Longobardi, Penkov et al. 2014). Hox genes are important for anterior-posterior axis development, and depending on the cofactor interacting with the Hox protein, the binding specificity of Hox can be modified. The main families of Hox cofactors are the Meis, Prep and PBC families (Merabet and Mann 2016). Furthermore, Pbx proteins interact with Meis or Prep (Chang, Jacobs et al. 1997, Knoepfler, Calvo et al. 1997), and at the same time, Pbx proteins can interact with Hox proteins through their HD, thus allowing the formation of trimers Pbx-Hox-Meis, which alters the binding specificity of Hox. Furthermore, all Meis

proteins (but not Prep) can interact with posterior Hox proteins (Williams, Williams et al. 2005).

Additionally, it has been reported that during the development of cranial structures in mouse, MEIS1/2 interactions with anterior Hox proteins (HOXA2) enhance Meis binding to specific sites, which provide the second branchial arch with its anatomical identity, thus revealing the importance of Hox-Meis complexes in anterior embryonic development (Amin, Donaldson et al. 2015). Interestingly, when Pbx binds Meis, the DNA binding and selectivity increases, and both HDs are required to bind to the DNA target sequence. A mutation in the HD of Meis or Pbx is sufficient to prevent binding of the Pbx-Meis complex to the DNA (Longobardi, Penkov et al. 2014). Furthermore, it has been proposed that Pbx-Meis interactions influence a shift of the Pbx proteins from promoters containing Pbx-Hox binding motifs to others containing Pbx-Meis motifs (Knoepfler, Calvo et al. 1997). Additionally, during chick and mouse limb development, *Meis1/2* and *Pbx1* expressions are restricted to the proximal domains of the forming limbs, where MEIS1 regulates PBX1 activity by promoting the nuclear import of PBX1. Together, MEIS1/2-PBX1 are essential to specify cell fates and differentiation patterns along the proximo-distal axis of the limb (Mercader, Leonardo et al. 1999).

1.7.3. Meis1-3 mutants and knockdowns, and *Meis* upstream regulators

In recent years, it has been reported that mutations in *Meis2* in humans cause ASDs and VSDs and left-sided obstruction defects (Louw, Corveleyn et al. 2015). In addition to the CHDs, mutations in *Meis2* also cause cleft palate, mental retardation, delayed motor development, facial dysmorphism, epilepsy (Erdogan, Ullmann et al. 2007, Chen, Lin et al. 2008, Crowley, Conlin et al. 2010, Louw, Corveleyn et al. 2015), and more recently, autism spectrum disorder (Shimojima, Ondo et al. 2017), although the molecular pathway in which MEIS2 works has yet to be investigated.

In mouse, mutations in *Meis2* affect neural crest-derived tissues, causing defects in cranial nerve development, malformations in craniofacial bones and cartilages, delayed ocular development, and small body and liver size. *Meis2* mutant mice die between E13.5 and E14.5 due to strong hemorrhaging and display congenital heart defects such as persistent truncus arteriosus, and absence of the aortic and pulmonary valves (Machon, Masek et al. 2015).

As previously mentioned, there are two paralogues of *Meis2* in the zebrafish: *meis2a* and *meis2b*. Paige et al. showed that *meis2b* had a temporal chromatin signature similar to those genes encoding important cardiac regulators such as *nkx2.5* or *myh6* (Paige, Thomas et al. 2012). Additionally, they showed that knockdown of *meis2b* led to delayed cardiac looping and slower heart rate (Fig. 1.11) (Paige, Thomas et al. 2012). In contrast, *meis2a* knockdown causes craniofacial defects including the fusion of viscerocranial cartilages and ectopic cartilage formation (Melvin, Feng et al. 2013).

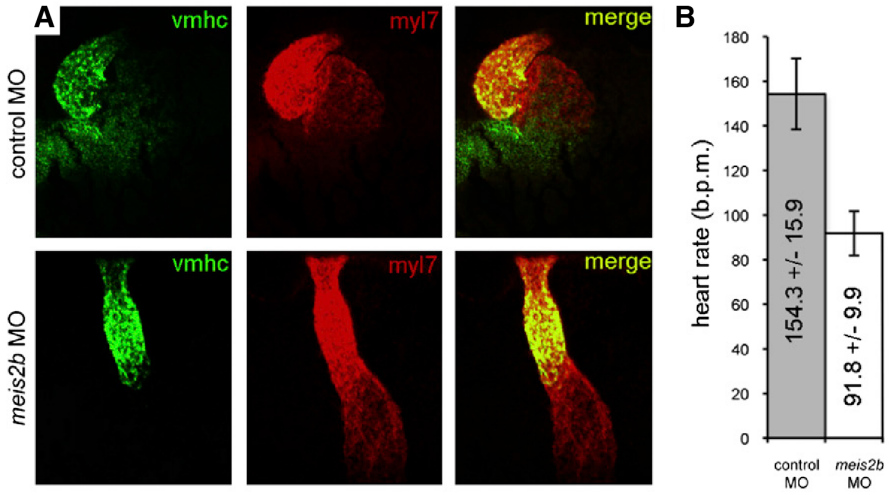

Figure 1.11. *meis2b* knockdown causes defects in cardiac development. **(A)** Fluorescent *in situ* hybridization against *ventricular myosin heavy chain* (*vmhc* in green) and *myl7* (red) in control morpholino (upper panel) and *meis2b* splice morpholino (bottom panel) show absence of heart looping at 48 hf. **(B)** Heart rate is significantly lower in 72 hpf *meis2b* morphants compared to control conditions. Modified from (Paige, Thomas et al. 2012)

Another Meis protein that affects embryonic heart development is Meis1. *Meis1* knockout in mouse leads to subcutaneous hemorrhage and lethality between E14.5 and E15.5, VSD and overriding aorta; interestingly this phenotype resembles the cardiac anomalies caused by mutations in *Pbx1*, suggesting an important interaction between PBX1 and MEIS1 during heart development (Stankunas, Shang et al. 2008). Furthermore, *Meis1* is also important in regulating the cell cycle of postnatal cardiomyocytes in mice, suggesting a role of *Meis1* in cardiomyocyte proliferation and cardiac regeneration (Mahmoud, Kocabas et al. 2013). In contrast, *Meis3* is involved in pancreas development and it induces posterior hindbrain patterning and neuronal differentiation, as summarized in (Uribe and Bronner 2015).

Little is known about what pathways are upstream of the *meis* genes and how is their expression regulated. However, there is strong evidence that *Meis1* and *Meis2* are (direct or

indirect) downstream targets of RA signaling (Oulad-Abdelghani, Chazaud et al. 1997, Savory, Edey et al. 2014). Previous reports show that *Meis1* and *Meis2* are important during chick limb development by determining the proximal limb compartment (Capdevila, Tsukui et al. 1999, Mercader, Leonardo et al. 1999). During limb budding, RA signaling is required to restrict *Meis1* and *2* expression to the proximal domains; ectopic RA signals in the distal domain of the limb bud leads to ectopic expression of *Meis1* and *Meis2* in the same area (Mercader, Leonardo et al. 2000). Moreover, recent studies have revealed a role for RA signaling during proximal-distal patterning and branching morphogenesis of the chick lung, where *Meis1* and *Meis2* expression is significantly induced after treatment with excess RA (Fernandes-Silva, Vaz-Cunha et al. 2017). Altogether, these data suggest that RA signaling can regulate *Meis1* and *Meis2* expression in different tissues, and is important in the patterning of lung and limb during development.

To summarize, it has become evident that the *Meis* genes have several roles during embryonic development. Specifically, *Meis2* and its zebrafish orthologue *meis2b* are important in atrial and ventricular septation, formation of the aortic pulmonary valves, separation of the pulmonary trunk and aorta, cardiac looping and heart rate (Paige, Thomas et al. 2012, Louw, Corveleyn et al. 2015, Machon, Masek et al. 2015). However, how Meis2 works at the cellular level, in which genetic pathways Meis2 is involved, what are its downstream targets, and how it regulates all of these important cardiac developmental processes is still unknown (Longobardi, Penkov et al. 2014). Furthermore, regulation of *Meis* expression by RA signaling has been proposed in different tissues (Mercader, Leonardo et al. 2000, Fernandes-Silva, Vaz-Cunha et al. 2017), but how *Meis2* expression is regulated in the heart remains to be determined. All these reasons make Meis2b a good candidate for further studies on cardiac development. Therefore, this work focuses on dissecting the role of Meis2b during zebrafish heart development.

II. Aim of the Project

Congenital heart malformations represent the most common type of birth defects and constitute a leading cause of mortality in newborns (Hoffman 1995, Hoffman 1995). Numerous genetic pathways control embryonic heart formation, and mutations in several genes have been associated with defects in cardiac development in humans (Mammi, De Giorgio et al. 1998, Bruneau 2008, Prendiville, Jay et al. 2014, Ang, Rivas et al. 2016). In humans, mutations in *MEIS2* lead to congenital heart defects such as atrial and ventricular septal defects and persistent truncus arteriosus (Erdogan, Ullmann et al. 2007, Chen, Lin et al. 2008, Crowley, Conlin et al. 2010, Louw, Corveleyn et al. 2015, Machon, Masek et al. 2015). In zebrafish, knockdown of *meis2b* leads to delayed cardiac development, cardiac looping defects and slower heart rate (Paige, Thomas et al. 2012). However, the exact role of *MEIS2* and its orthologue *meis2b*, during heart formation is not clear. Therefore, the main goal of this project was to determine the function of *meis2b* in cardiac development in the zebrafish.

Seeking to take advantage of the zebrafish model because of their small size, transparency, and survival during embryonic development despite severe cardiac defects, the zebrafish was chosen as an experimental model to answer the main aim of this study and its specific aims, as shown below:

1st Aim: To determine the expression pattern of *meis2b* heart development until adulthood.

2nd Aim: To study the effect of *meis2b* loss-of-function in heart development and function.

3rd Aim: To determine possible upstream regulators of Meis2b in the heart.

4th Aim: To determine possible downstream targets of Meis2b in the heart.

III. Materials

3.1. Disposable Laboratory Equipment

Table 3.1. Disposable equipment.

Material	Model	Supplier
Bacterial culture tubes	13mL PP Tube Sterile	Greiner Bio-one
Cell culture plates	10cm	Greiner Bio-one
Cell culture plates	6-well cell culture plate, cellstar	Greiner Bio-one
Cell culture plates	12-well cell culture plate, cellstar	Greiner Bio-one
Cover slips	24 X 60mm #1	Thermo Scientific
Falcon tubes	15mL, 50mL	Greiner Bio-one
Glass Capillaries	1.00OD X 0.58ID X 100mm	Hardvard Apparatus
Microscope slides	Menzel Gläser Superfrost UltraPlus	Thermo Scientific
Nitril gloves		Gen-X
Pasteur pipettes	2,5mL	Sarstedt
PCR tubes	8er SoftStrips 0,2mL	Bio Zym
Pipette filter tips	FT10, FT20, FT100, FT200, FT1000	Greiner Bio-one
Plastic pipettes	5mL, 10mL, 25mL Cellstar	Greiner Bio-one
Reaction tubes	1,5mL, 2mL safe-lock tubes	Eppendorf
Thin pipette tips for capillary filling	20µL Physio Care Concept	Eppendorf
Tissue cassettes	C-0250-YL	Thermo Scientific

3.2. Laboratory Equipment

Table 3.2. Miscellaneous equipment

Material	Model	Supplier
Analytical balance	Explorer	OHAUS
Aquatic system		Techniplast
Bacterial incubator	Innova 4200	New Brunswick Scientific
Balance	M-Power	Sartorius Laboratory
Cooling centrifuge	5424R	Eppendorf
Electrophoresis chamber	B2 Separation System	OWI
Forceps	Inox 55	Dumont
Glass beakers	Duran	Schott
Glass bottles	Duran	Schott
Glass Erlenmeyer flasks	Duran	Schott
Glass measuring cylinder	Duran	Schott
Heating block	Digital heatblock	VWR
ImmEdge Pen	H-4000	Vector Laboratories, Inc.
Injection pump	Pneumatic Picopump PV820	World Precision Instruments
Magnetic heating plate	VMS-C7	VWR
Micromanipulator	MM 33 Right	World Precision Instruments
Micropipette Puller	Horizontal puller P-1000	Sutter Instruments
Micropipettes	Research	Eppendorf
Microtome	Paraffin microtome 1516	Leitz
Optical dishes	Glass bottom culture 35mm dishes	Ibidi
Paraffin Pouring Station	EC 350	Formafix Global Technologies
PCR cycler	Eppendorf Vapo Protect Master Cycler Pro PCR Machine	Eppendorf

pH meter	Five easy	Mettler Toledo
Real-Time PCR cycler	Eco Realtime PCR System	Illumina
Real-Time PCR cycler	CFX Connect Real-Time System	Bio-Rad
Spectrophotometer	Nanodrop 2000c	PeqLab
Table-top centrifuge	5424 and 5810R	Eppendorf
Tissue homogenizer	Bullet Blender 24 Gold	Next Advance
Vortex	Vortex Genie 2	Scientific Industries
Water bath	14L waterbath, 1003	GFL
Water bath for paraffin sections	Paraffin stretch bath, 1052	GFL

3.3. Microscopes

Table 3.3. Employed microscopes.

Microscopes	**Model**	**Supplier**
Confocal microscope	LSM700, LSM 780, LSM800, LSM880	Zeiss
Dissecting microscope	SteREO Discovery.V8	Zeiss
Dissecting microscope	Stemi 2000	Zeiss
Stereo microscope	SMZ25	Nikon
Widefield Microscope	Axio Imager 2	Zeiss

3.4. Chemicals

Table 3.4. List of all employed chemicals.

Name	**Supplier**
20X SSC	Ambion
4-diethylaminobenzaldehyde	Sigma
Agarose	peqLab
Alcian blue 8GX	Sigma
Alizarin red S	Sigma

Ampicillin	Calbiochem
Blocking reagent	Roche
Bouin's solution	Sigma
Bovine serum albumin	Sigma
BSA	Sigma
Chloroform	Merck
DAPI	Sigma
Dichloromethane	Sigma
Dimethyl sulfoxide	Sigma
EdU	Life Technologies
EGTA	Sigma
Ethanol	Carl Roth
Formaldehyde	Santa Cruz Biotechnology
Formamide	Sigma
Glacial acetic acid	Carl Roth
Glutaraldehyde	Sigma
Glycerol	Sigma
Goat serum	Sigma
H_2O_2	Sigma
HCl	Sigma
Heparin	Sigma
KCl	Sigma
KH_2PO_4	Sigma
KOH	Sigma
Low melt agarose	Carl Roth
Low melting agarose	Carl Roth
Methanol	Carl Roth
$MgCl_2$	Sigma
$MgSO_4$	Sigma
Na_2HPO_4	Sigma
NaCl	Sigma
NaH_2PO_4	Sigma
NBT/BCIP	Roche

OCT mounting medium for cryosections	Tissue-tek
Paraformaldehyde	Sigma
PBS tablets	Sigma
Phenol red	Sigma
PIPES	Sigma
ProLong Diamond Antifade Mountant	Molecular Probes by Life Technologies
Retinoic acid	Sigma
SDS	Sigma
Sheep serum	Sigma
Tetrahydrofuran	Sigma
Tricaine	Pharmaq
Trichrome stain (Masson) kit	Sigma
Tris	Carl Roth
Triton X-100	Sigma
TRIzol Reagent	Invitrogen
tRNA	Sigma
Tween 20	Sigma
Weigert's iron hematoxylin	Sigma
Xylene	Carl Roth

3.5. Buffers

Table 3.5. List of all employed buffers.

Name	**Content**
4% PFA	PBS 4% PFA pH 7,35
Acid-Formalin-Ethanol fixative	PBS 3,7% Formaldehyde 70% Ethanol

	5% Glacial acetic acid
Acid-free staining solution	Part A: 0,02% alcian blue 200mM $MgCl_2$ 70% ethanol Part B: H_2O 0,5% alizarin red S Working solution: 1mL part A + 10µL part B
Alkaline Tris Buffer	100mM Tris-HCl pH 9,5 50mM $MgCl_2$ 100mM NaCl 0,1% Tween 20
Bleaching solution	1,5% H_2O_2 1% KOH
Blocking buffer for HA staining	PBST 1% BSA 2% HINGS
E3 Embryo Medium	
Fish Fix	22,6mM NaH_2PO_4 76,9mM Na_2HPO_4 0,12mM $CaCl_2$ 4% w/v Sucrose 4% Paraformaldehyde pH 7,35
HM$^-$	50% deionized formamide 5X SSC 0,1% Tween 20 50µg/mL heparin pH 6.0 (adjusted with 1M citric acid)
HM$^+$	50% deionized formamide 5X SSC

	0,1% Tween 20 50µg/mL heparin RNase-free tRNA pH 6.0 (adjusted with 1M citric acid)
ISH Staining Solution	10mL Alkaline Tris buffer 175µL NBT/BCIP
MBST	100mM Maleic Acid 150mM NaCl pH to 7,5 0,1% tween 20
PBDT	PBS 1% BSA 1% DMSO 0,25% Triton X-100
PBS	137mM NaCl 2,7mM KCl 10mM Na_2HPO_4 1,8mM KH_2PO_4
PBST	PBS 0,1% Triton X-100
PBT	PBS 0,1% Tween 20
Pre-hybridization solution for ISH on paraffin sections	(RNAse free) 50% formamide 5x SSC pH 4,5 50µg/mL yeast tRNA 1% SDS 50µg/mL Heparin 5X Gendhardt's solution

3.6. Enzymes, Antibodies, Kits

Table. 3.6. List of all employed enzymes, antibodies, kits, cells.

Name of Reagent	Reference number	Supplier
2X Kapa2G Fast Ready Mix + Dye	KM5101	Kapa Biosystems
Alexa Fluor 488 Donkey-anti-rabbit	A21206	Life Technologies
Alexa Fluor 488 Goat-anti-chicken	A11039	Life Technologies
Alexa Fluor 568 Donkey-anti-mouse	A10037	Life Technologies
Anti-digoxigenin-AP Fab Fragments	1093274	Roche
anti-dsRed Rabbit Polyclonal Antibody	632496	Clontech
AvrII Restriction Enzyme	R0174S	NEB
BamHI-HF Restriction Enzyme	R3136L	NEB
Chicken Anti-GFP antibody	GFP-1020	Aves Labs. Inc.
ClaI Restriction Enzyme	R0197L	NEB
Click-iT EdU Alexa Fluor 647 Imaging Kit	C10340	Life Technologies
Competent cells	dh5α	
DIG RNA Labeing Mix 10X	11277073910	Roche
DNaseI	M610A	Promega
Eag-HF Restriction Enzyme	R3505S	NEB
EcoRV-HF Restriction Enzyme	R3195S	NEB
GeneJET Gel Extraction Kit	K0692	Thermo Scientific
GeneJET PCR Purification Kit	K0701	Thermo Scientific

GeneJET Plasmid Miniprep Kit	K0503	Thermo Scientific
Hyaluronic Acid Binding Protein, Bovine Nasal Cartilage, Biotynilated	385911	Calbiochem
Maxima First Strand cDNA Synthesis Kit for RT-qPCR	K1641	Thermo Scientific
Maxima SYBR Green qPCR Master Mix	K0241	Thermo Scientific
mMESSAGE mMACHINE SP6 Transcription Kit	AM1340	Invitrogen
Mouse anti-Isl1	39.4D5	Developmental Studies Hybridoma Bank
PCR Master Mix	AB-0575/DC	Thermo Scientific
pGEM-T easy cloning kit	A1360	Thermo Scientific
Proteinase K	03115879001	Roche
Recombinant RNasin Ribonuclease inhibitor	N251A	Promega
RNAscope® Multiplex Fluorescent Reagent Kit	320850	Advanced Cell Diagnostics Srl
SP6 RNA Polymerase	P108B	Promega
Streptavidin Alexa Fluor 555	S32355	ThermoFischer Scientific
T4 DNA Ligase	M02025	NEB
T7 RNA Polymerase	P207B	Promega
XhoI Restriction Enzyme	R0146S	NEB
Zymo RNA cleaner	R1016	Zymo Research

IV. Methods

4.1. Zebrafish husbandry and transgenic and mutant lines

Embryos and adult zebrafish were maintained and handled under standard conditions as previously described (Westerfield 2000). Briefly, zebrafish embryos were collected and raised until five dpf in E3 embryo medium in an incubator at 28,5ºC. Afterwards, the larvae were transferred to an aquarium system from Techniplast and were raised until adulthood with a 14 h/10 h light/darkness cycle. Animal housing and experiments were approved by the MPG animal committee in concordance with the European regulations.

The transgenic and mutant lines used in this study include:

- *Tg(myl7:LIFEACT-GFP)^{s974}* (Reischauer, Arnaout et al. 2014)
- *Tg(-5.1myl7:nDsRed2)^{f2}* (Mably, Burns et al. 2003)
- *Tg(5xUAS:EGFP)^{nkuasgfp1a}* (Asakawa, Suster et al. 2008)
- *Tg(myl7:mCherry)^{chb1}* (Langenbacher, Huang et al. 2012)
- *TgBAC(meis2b:GAL4FF)^{bns15}* (Guerra et al., manuscript in preparation).
- *meis2b^{s988}* (Guerra et al., manuscript in preparation).
- *Tg(kdrl:Hsa.HRAS-mCherry)^{s896}* (Chi, Shaw et al. 2008)
- *Tg(vmhc:mCherry-Eco.NfsB)^{s957}* (Zhang, Han et al. 2013)
- *Tg(kdrl:NLS-mCherry)^{is4}* (Wang, Kaiser et al. 2010)
- *Tg(myl7:BFP-CAAX)^{bns193}* (Guerra et al., manuscript in preparation).

4.2. DNA extraction

Tissue samples were incubated with 40µL Tris Buffer and incubated at 95ºC for ten minutes. Afterwards, 5µL of Proteinase K were added (stock concentration 10.000µg/mL), followed by incubation at 55ºC for 3h to overnight and then vortexed to help disintegrate the tissue. To deactivate the Proteinase K, the samples were incubated at 95ºC for ten minutes. The DNA samples were stored at 4ºC until used, or at -20ºC for long term storage.

4.3. RNA extraction and cDNA synthesis

Using the Bullet Blender, the tissue of interest was homogenized with 250µL TRIzol Reagent. After homogenization, the samples were kept at room temperature for ten minutes. Next, 65µL chloroform was added and the tubes were constantly shaken for two minutes and then incubated at room temperature for three minutes. Next, the samples were centrifuged for 15 minutes at 10.000g at 4ºC and the supernatant was transferred to a clean, autoclaved 1,5mL tube. To precipitate the RNA, one volume of isopropanol was added then, the tubes were briefly vortexed, and afterwards were incubated for 1h on ice. Last, the samples were centrifuged for 20 minutes at 4ºC with maximum speed.

After removal of the supernatant, the pellet was washed with 1mL of 75% ethanol / H_2O and again centrifuged at 4ºC with maximum speed for 15 minutes. The supernatant was carefully removed and the RNA air dried. Then, the RNA was resuspended in 85µL autoclaved water. To eliminate the possible DNA contamination from the samples, 10µL of DNaseI buffer and 5µL of DNaseI were added and the tubes were incubated for 30 minutes at 37ºC. Afterwards, the RNA was cleaned with Zymo RNA cleaner, following manufacturer's instructions.

1µg of RNA was used to synthesize cDNA with the Maxima First Strand cDNA synthesis kit for RT-qPCR, following manufacturer's instruction.

4.4. Ligation

For TA cloning, the PCR product was ligated into a pGEM-T easy vector by mixing:

- 3,5µL of PCR product
- 5µL of 2X ligation buffer
- 0,75µL pGEM-T easy linearized vector
- 0,75µL T4 DNA ligase
- The mix was incubated at room temperature for 3h to overnight.

For ligations following digestion with restriction enzymes, the reactions were set in the following way:

- 100ng insert
- 50ng vector
- 1µL T4 10X ligation buffer

- 0,75µL T4 ligase
- H_2O until 10µL
- The mix was incubated at room temperature for 3h to overnight.

4.5. Transformation

After thawing the competent cells, 6µL of the plasmid were added and the cells were incubated for 20 minutes on ice. Afterwards, the cells were heat shocked at 42ºC for one minute and were put back on ice for five more minutes. 300µL of LB medium were added and the cells were recovered for 30-40 minutes at 37ºC with slow agitation. Finally, 150µL of the cell culture were spread on agar plates containing ampicillin (if the pGEM-T easy plasmid was used, 75µL of X-Gal was added to the agar plate, before the spreading of the bacteria culture). The plates were incubated overnight at 37ºC. The following day, the colonies were selected (white colonies were selected when using the pGEM-T easy plasmid) and were grown for at least 6h in a liquid LB medium containing ampicillin. Finally, the plasmid was recovered using the Plasmid Miniprep Kit, following manufacturer's instructions.

4.6. EdU injections

Eight *meis2b*$^{-/-}$ fish and eight WT siblings of three mpf were anesthetized in 0,02% tricaine. EdU was injected intraperitoneally (200µg/g of body weight). After injection, the fish were allowed to recover for 30 minutes in a tank without tricaine and then were placed back in the fish system for four days before extraction of the heart.

4.7. EdU detection in adult hearts

EdU was detected with Click-iT EdU Alexa Fluor 647 Imaging Kit, following manufacturer's instructions, with minor modifications. After antibody staining against DsRed, the hearts were washed with PBS and then fixed (3,7% PFA / PBS) for 15 minutes at room temperature. Afterwards, the hearts were washed twice with 3% BSA / PBS and then incubated with PBS / 0,5% Triton X-100 for 20 minutes at room temperature. Next, the samples were washed twice with PBS/3% BSA. Then, the Click-iT reaction cocktail was prepared as shown in Table 4.1 and used immediately. The samples were incubated in

darkness with the Click-iT reaction cocktail for 25 minutes. After this time, the solution was replaced with a fresh reaction cocktail fresh and the samples were kept in the darkness for 25 minutes. Finally, the samples were washed with three times with PBS/3% BSA.

Table 4.1. Components of the Click-iT reaction cocktail

Reaction components	**Amount added**
1X Click-iT reaction buffer	4,3mL
$CuSO_4$	200µL
Alexa Fluor 647 azide	12,5µL
Reaction buffer additive	500µL
Total volume	5mL

Modified from manufacturer's manual.

4.8. Whole-mount antibody staining in adult hearts

The hearts from adult *Tg(-5.1myl7:nDsRed2)* zebrafish were fixed overnight at 4ºC with Fish Fix. Next, the hearts were washed with PBS and then gradually dehydrated with Methanol (25% methanol / PBS; 50% methanol / PBS; 75% methanol / PBS; and then 100% methanol) in five-minute washes and were kept at -20ºC in 100% methanol for at least 24h. Hearts were gradually rehydrated to PBS with successive washes (75% methanol / PBS; 50% methanol / PBS; 25% methanol / PBS) for five minutes each wash.

Due to the thickness of the cardiac tissue, penetration of the antibody is limited. Therefore, two different permeabilization protocols were used: first, after heart rehydration, all PBS was removed from the tube and 100% methanol was immediately added and the samples were incubated at -80ºC for 1h. Afterwards, the methanol was removed, and the samples were incubated for 1h at room temperature with PBS. This procedure was repeated seven times. Finally, hearts were kept overnight at 4ºC with 100% methanol, and then hearts were rehydrated with PBS. For the second step of permeabilization, all PBS was removed, and 1mL of cold acetone was added, and the samples were incubated at -20ºC for 20 minutes.

Next, the hearts were rehydrated again with PBS and then blocked for two to five hours at room temperature with PBDT/2% goat serum. The samples were incubated for five days at 4ºC with anti-dsRed antibody diluted 1/500 in PBDT with constant rotation. The primary

antibody was removed by washing with PBDT at room temperature ten times for 30 minutes each. The samples were incubated at 4ºC for five days with the secondary antibody (Donkey-anti-rabbit Alexa Fluor 488), diluted to 1/500 in PBDT. Afterwards, the samples were washed ten times, for 30 minutes with PBDT.

4.9. iDisco tissue clearing for adult hearts

Tissue clearing was performed as described in (Renier, Wu et al. 2014). Briefly, after EdU detection, the samples were incubated overnight in 10mL of 50% v/v THF / H_2O (Sigma). Afterwards, samples were incubated in 10mL of 80% THF / H_2O for 1h and then twice for 1h with 100% THF. Then, the samples were transferred to a 2mL tube with dichloromethane until they sank at the bottom of the tube. Finally, the samples were incubated in DBE until clear and then stored in darkness at room temperature until imaged.

4.10. RNA probe preparation for *in situ* hybridization

For synthesizing the antisense RNA probe for ISH, the protocol described in (Thisse and Thisse 2008) was followed with some modifications. A PCR was performed on the previously prepared cDNA as described in Tables 4.2 and 4.3, and using the combination of primers listed in Table 4.4. The primers were chosen to the span intron-exon boundaries and so that the resulting probes were between 800 and 1000bp long. The anti-sense probe for *ntl* was kindly provided by Dr. Michelle Collins.

Table 4.2. Amplification of cDNA by PCR

Component	Amount per reaction	Final amount/concentration
Template cDNA	0,5µL	10-100ng
Forward primer (100µM)	0,5µL	0,5µM
Reverse primer (100µM)	0,5µL	0,5µM
Kappa PCR 2X master mix	50µL	1X
Water	48,5µL	-
Total volume	**100µL**	-

Modified from (Thisse and Thisse 2008).

Table 4.3. PCR conditions for ISH RNA probe synthesis

Cycle number	Denature	Anneal	Extend
1	95ºC, 4 minutes	-	-
2-36	95ºC, 30 s	55ºC, 30 s	72ºC, 1 minute
37	-	-	72ºC, 7 minutes

Taken from (Thisse and Thisse 2008).

Table 4.4. List of primers for ISH RNA probe synthesis

Probe	Forward	Reverse
meis2b	CAGATCACAATCCAGCATCC	TCTGATGGCTAGGTGAGGAG
myl7	AGACCAACAGCAAAGCAGAC	TGATGCTCTACTCATAGTCAAGG

After the PCR, the product was loaded in a 1% agarose gel, the desired product band was then excised and the product was cleaned using the Gel Extraction Kit and following manufacturer's instructions. Afterwards, the PCR product was ligated into pGEM-T easy plasmid and then transformed. Three colonies were picked from the agar plate and grown in LB medium containing ampicillin. Afterwards, the plasmids were extracted with the Miniprep Extraction Kit and were sequenced with T7 and SP6, in order ensure the correct sequence and the direction in which the PCR product was inserted into the vector plasmid.

Afterwards, a PCR with T7 (forward) and SP6 (reverse) primers was made with the conditions shown in Table 4.3 and the PCR product was cleaned with the PCR Purification Kit.

For the RNA anti-sense probe synthesis, the reaction was carried as indicated in Table 4.5. To check the quality of the RNA probe, 1µL of the product was loaded in a 1% agarose gel, a single band was observed in all cases, indicating that the RNA was not degraded.

The rest of the RNA probe was cleaned using the Zymo RNA cleaner and following manufacturer's instructions. After cleaning, the probe was diluted in HM^+ to a final concentration of 1µg/mL and stored at -20ºC until used.

Table 4.5. RNA probe synthesis reaction

Component	Amount	Temperature/Time
Template: PCR product	400µg	37ºC 2,5 to 3h
10X DIG labeling mix	4µL	
5X Transcription Buffer	8µL	
RNase inhibitor	2µL	
T7 or Sp6 enzyme	2µL	
RNase free water	Up to 40µL	
DNaseI	2µL	37ºC for 30 minutes

4.11. Whole-mount *in situ* hybridization

Whole-mount ISH was performed as described in (Thisse and Thisse 2008) with minimal modifications. Samples were fixed overnight at 4ºC with Fish Fix. Later, the samples were washed with PBS and successively dehydrated with methanol washes for five minutes each (25% methanol / PBS, 50% methanol / PBS, 75% methanol / PBS, 100% methanol). Samples were kept in 100% methanol at -20ºC for at least 2h or up to one month. The ISH protocol was performed in three days, as explained below:

4.11.1. Day 1 ISH – Permeabilization and Hybridization

Dehydrated samples were kept on the bench until room temperature was reached (approximately 15 minutes). Afterwards, the samples were successively rehydrated with five-minute washes with methanol (75% methanol / PBS, 50% methanol / PBS, 25% methanol / PBS) and washed four times for five minutes with PBT.

Permeabilization was performed with proteinase K in PBT (10µg/mL), the time of digestion varied according to the age of the fish as described in Table 4.6.

Table 4.6. Duration of tissue permeabilization for ISH

Developmental stage	Duration of treatment
1 cell – tailbud stage	30 s

Tailbud – 8 somites stage	1 minute
9 – 18 somites stage	3 minutes
18 somites stage – 36 hpf	10 minutes
36 hpf – 5 dpf	30 minutes

Modified from (Thisse and Thisse 2008).

After permeabilization, samples were fixed with Fish Fix for 20 minutes and then washed four times with PBT for five minutes. Posteriorly, the samples were prehybridized with HM^+ for 2-5h at 70ºC. Then, HM^+ was substituted with the RNA probe, diluted in HM^+ to a concentration of 1μg/mL and the samples were incubated to 70ºC overnight.

4.11.2. Day 2 ISH – Blocking and antibody detection

The solutions were gradually changed from HM^+ to 2X SSC, through a series of ten-minute washes at 70ºC with 75% HM^- / 2X SSC; 50% HM^- / 2X SSC; 25% HM^- / 2X SSC and twice with 2X SSC. Posteriorly, two washes with 0,2X SSC for 30 minutes at 70ºC.

Afterwards, the 0,2X SSC solution was progressively replaced with PBT at room temperature, doing ten-minute washes with: 75% 0,2X SSC / PBT; 50% 0,2X SSC / PBT; 25% 0,2X SSC / PBT and finalizing with two washes of 100% PBT.

Then, the samples were blocked with blocking buffer for 3-4h at room temperature with PBT / 2% sheep serum / 2mg/mL BSA. Later, the solution was replaced with anti-DIG antibody, diluted in blocking buffer to 1/10.000 and the samples were incubated overnight at 4ºC.

4.11.3. Day 3 ISH – Staining

To eliminate the excess of anti-DIG antibody, the samples were washed six times for 15 minutes with PBT at room temperature. Afterwards, all excess of PBT was removed from the samples, and the solution was replaced with alkaline Tris buffer and incubated three times for five minutes.

Then, the samples were transferred to 6- or 12-well culture plates and were incubated in darkness with 1mL of the staining solution until the desired staining intensity was reached (depending on the RNA probe, the time average incubation time was between 1-2h).

To stop the staining reaction, the samples were transferred to 1,5mL tubes and the staining solution was replaced with three washes for five minutes with PBT, followed by 20 minutes fixation with Fish Fix, and then repeating the washes with PBT.

To eliminate the background staining, the samples were incubated with 50% methanol/PBT for five minutes, then in 100% methanol for ten minutes. Afterwards, the methanol was replaced with fresh 100% methanol, and the samples were incubated for 30 minutes and then rehydrated with PBT. The samples were stored at 4ºC in PBT until imaged.

4.12. *In situ* hybridization on paraffin sections

4.12.1. Tissue processing

Adult hearts were extracted and fixed with 4% PFA/PBS at 4ºC overnight. Washed twice for ten minutes with PBS and then gradually dehydrated with ten-minute washes with 30% ethanol / H_2O, 50% ethanol / H_2O, twice with 70% ethanol / H_2O, 80% ethanol / H_2O, 90% ethanol / H_2O, 95% ethanol / H_2O, 3 times with 100% ethanol. To preserve the RNA in the sample, all washes were performed in sterile conditions. The hearts were transferred to a plastic cassette and washed twice in xylene for 20 minutes at room temperature and then in 50% xylene/50% paraffin at 65ºC for 1h. Afterwards, the cassettes were transferred to 100% paraffin at 65ºC for 2-3h and then overnight in fresh paraffin. The hearts were mounted in paraffin blocks and stored at 4ºC for up to one month. The sections were made with 12µm thickness.

4.12.2. Hybridization

The slides were dewaxed in xylene for 10 minutes. Then gradually rehydrated with 100% ethanol, 95% ethanol / H_2O, 90% ethanol / H_2O, 80% ethanol / H_2O, 70% ethanol / H_2O, 50% ethanol / H_2O, 30% ethanol / H_2O and 100% water for 30s, each wash. Then, three washes in PBS for 3 minutes. To permeabilize the tissue, the sections were incubated in 15µg/mL proteinase K in PBS for ten minutes and fixed with 4% PFA / PBS for five minutes and then washed with PBS. Afterwards, 200µL of the pre-hybridization solution were added and the slides were incubated at 65ºC for 1h. Finally, the probe was added to a final concentration of 1µg/mL and incubated overnight at 65ºC.

4.12.3. Antibody detection

The sections were washed for ten minutes in 5X SSC at 70ºC, twice in 0,2X SSC for 30 minutes. The slides were rinsed in MBST. After, the tissue was blocked with 2% blocking reagent / 5% sheep serum / MBST at room temperature for 1-2h. Finally, the antibody was diluted 1:4000 in 2% blocking reagent / 1% sheep serum / MBST and the sections were incubated overnight at 4ºC.

4.12.4. Staining

The excess of antibody was eliminated with 30-minute washes in MBST at room temperature. Then, the slides were incubated three times for five minutes in alkaline Tris buffer. Afterwards, 200µL BM Purple were added, and the slides were kept in the dark until the desired intensity of the staining was reached. Afterwards, the slides were washed in PBT pH 4,5 to stop the staining reaction and then fixed in 0,2 glutaraldehyde / 4% PFA / PBS at room temperature for 1-2h, then washed three times for five minutes in PBS and finally mounted with a drop of Mowiol.

4.13. RNAscope

The low expression levels of *pitx2*, make it difficult to precisely determine its expression pattern in the mature zebrafish heart. Thus, RNAscope, an alternative and more sensitive ISH technique, was employed. The probe for detecting *pitx2* transcripts was designed by Advanced Cell Diagnostics. Whole-mount RNAscope was performed as described in (Gross-Thebing, Paksa et al. 2014) on five wpf hearts that carried the *Tg(meis2b-reporter)*. For imaging, the hearts were mounted on a glass slide with ProLong Diamond mountant and imaged with a Zeiss LSM880 or LSM800 confocal microscope.

4.14. Trichrome

Hearts were embedded in paraffin, following the same procedure previously explained in "*In situ* hybridization on paraffin sections; tissue processing", paraffin sections had 8-10µm thickness. After rehydration of the sections, the slides were incubated in preheated Bouins solution at 56ºC for 15 minutes. Then, the slides were cleaned under running water until all color from the previous solution had disappeared. Afterwards, the slides were immersed in

Weigert's Iron Hematoxylin solution for five minutes, then briefly rinsed in 1% HCl / Ethanol and then washed in H_2O for five minutes.

Next, the slides were stained with phosphotungstic/phosphomolybdic acid solution for 15 minutes and then immediately transferred to an Aniline Blue solution. Then, the slides were washed in 1% acetic acid/H_2O. Last, the sections were gradually dehydrated by fast washes in 90% ethanol/H2O and 100% ethanol and finally in xylene. A drop of mowiol was used to mount the tissue. The sections were stored at room temperature until imaged.

4.15. Whole-mount Antibody Staining for Isl1

Antibody staining for Isl1 was performed as described in (Dong, Munson et al. 2007, Witzel, Jungblut et al. 2012) with some modifications. Briefly, embryos of 30 hpf and 48 hpf, carrying the *meis2b*-reporter were fixed with 2% formaldehyde in 0,1M PIPES / 1mM $MgSO_4$ / 2mM EGTA overnight at 4ºC, and were kept in the fixative for up to one week. Fixed embryos were washed twice with PBS and then blocked for 1h with PBST / 5% BSA at room temperature with slow agitation. Embryos were incubated overnight at 4ºC with anti-Isl1 antibody, diluted to 1:10 ratio in blocking solution.

Next day, the samples were washed three times for 1h at 4ºC with PBST. Finally, the samples were incubated overnight at 4ºC with the secondary antibody (Alexa Fluor 568), diluted to 1:500 ratio in PBST. And then, washed with PBST, three times for 1h.

4.16. Whole-mount antibody staining on zebrafish embryos after ISH

The same protocol for whole-mount antibody staining on adult zebrafish hearts was followed, with some exceptions: the samples did not undergo dehydration and were not permeabilized because they had been already permeabilized when performing the ISH. The samples were blocked with the previously described blocking buffer. The primary antibody (chicken anti-GFP) was incubated overnight at 4ºC, followed by 30-minute washes for five times with the blocking buffer. The secondary antibody (goat-anti-chicken Alexa Fluor 488) was incubated following the same procedure as with the primary antibody.

4.17. Hyaluronic acid staining on paraffin sections

4.17.1. Tissue preparation

The hearts were fixed overnight at 4ºC with acid-formalin-ethanol fixative, since it best preserves the hyaluronic acid (HA) structure in the tissue (de la Motte and Drazba 2011). Next day, the hearts were gradually dehydrated with series of ten-minute washes with 80% ethanol / H_2O, 90% ethanol / H_2O, 95% ethanol / H_2O, twice with 100% ethanol for ten minutes and then once for 30 minutes. Afterwards, the hearts were placed in a plastic cassette, and then immersed twice in xylene for 20 minutes at room temperature, then in 50% xylene/50% paraffin at 65ºC for 1h. Next, the samples were incubated twice with 100% paraffin for 2-3h at 65ºC. Finally, the samples were mounted in paraffin and were allowed to solidify overnight.

The paraffin blocks were cut to give 8µm thick sections. The slides with the heart sections were put on a hot plate at 40ºC overnight to evaporate all the water. Afterwards, the samples were kept at room temperature until used.

4.17.2. Staining

Before staining, the slides were washed twice in xylene for five minutes to remove all the paraffin. Afterwards, the tissue sections were gradually rehydrated with a series of three-minute washes with ethanol: 100% ethanol, 95% ethanol, 80% ethanol, 70% ethanol, 50% ethanol, then rinsed twice in H_2O and then twice in PBS.

The slides were incubated with blocking buffer for HA staining for 1h at room temperature. Afterwards, the ImmEdge hydrophobic pen was used to draw a contour around the sections. Finally, the slides were incubated overnight at 4ºC with the biotinylated HABP (dilution 4µg/mL) in blocking buffer. Next, the slides were washed three times with PBST, to eliminate the excess of HABP. Afterwards, the slides were incubated at room temperature for 1-2h with Streptavidin Alexa Fluor 555 (dilution 1/700) in blocking buffer. After, the slides were rinsed three times in PBST. Finally, the sections were counterstained with DAPI (dilution 1/3000) for twelve minutes in PBST and then rinsed fresh in PBST. To mount the slides, a drop of Mowiol was added on top of the sections, covered with a coverslide and then allowed to dry overnight in darkness. The slides were imaged with a Zeiss LSM780 confocal microscope.

4.18. DEAB and retinoic acid treatments

DEAB and RA were prepared at a stock solution of 10mM in DMSO and diluted to the desired working solutions with egg water.

For DEAB treatment, groups of 40 eggs were dechorionated at 30% epiboly and incubated with 1μM DEAB (Waxman, Keegan et al. 2008) starting at 40% epiboly, 80% epiboly or tailbud, until collection at eight, 17 or 22 somites stages.

For treatment with excess of RA, groups of 40 eggs were dechorionated at 30% epiboly and incubated with 0.1μM RA for one hour. To eliminate the excess of RA, the embryos were washed twice with egg water and collected at eight, 17 or 22 somites stage (Waxman and Yelon 2009).

Embryos that were treated at 40% epiboly and collected at 22 somites, were selected for positively carrying the *Tg(meis2b-reporter);Tg(myl7:mCherry)* background and were fixed overnight with Fish Fix. Finally, fixed embryos were washed with PBT, the yolk was removed, and the embryos were mounted in 1,1% low-melt agarose and imaged ventrally using a Zeiss LSM880 or LSM780 confocal microscopes.

Embryos that were collected at 8 and 17 somites stages, were sorted for positively carrying *Tg(meis2b-reporter)* background and were fixed overnight. Then, ISH for *ntl* + *hand2* (for 8 somites) or *ntl* + *myl7* (for 17 somites) was performed on the embryos, followed by antibody staining against GFP. Afterwards, the yolk was removed and the embryos were mounted in 1% low-melt agarose and imaged ventrally using a Zeiss LSM880 or LSM780 confocal microscopes.

The percentage of the heart field area that expresses *Tg(meis2b-reporter)*, was calculated by measuring the *myl7*-positive area and the myl7;*Tg(meis2b-reporter)*-positive area with ImageJ/Fiji. The statistical significance of the values was calculated using paired student's t-test with one tail distribution, with the Past (PAleontological STatistics) software.

4.19. Morpholino and plasmid injections

5ng of *isl1* ATG morpholino from Gene Tools, LLC (CCCATGTCAAGAAAGTAAGGCGGTG) were injected into one-cell stage embryo carrying the *Tg(meis2b-reporter);Tg(myl7:mCherry*) (Hutchinson and Eisen 2006). After

injection, the embryos were raised until 48 hpf and the expression of *Tg(meis2b-reporter)* was evaluated by imaging the embryos using a Zeiss LSM700 confocal microscope.

For injections of plasmids containing over-expression constructs of *meis2b*, 1nL of the following solution was injected into one-cell stage embryos: 1µL of Tol2 mRNA + 2µL Phenol Red + 1µL of 250ng/µL of the desired construct + 6µL H_2O. The embryos were raised and sorted for mosaic fluorescence at 2-3 dpf.

4.20. Cryosections

The tissue was dissected and fixed in Fish Fix overnight at 4ºC. Next, the samples were washed with PBS and then transferred to 10% sucrose / PBS until the tissue sank at the bottom of the tube. Afterwards, the samples were incubated overnight at 4ºC in 30% sucrose / PBS. Finally, the samples were mounted in OCT and were stored at -80ºC until used. The sections had 10-12µm thickness.

4.21. Genotyping of *meis2b*

meis2b mutant allele (*meis2b*^{s988}) is characterized by a seven bp deletion and a codon substitution, leading to an earlier stop in the amino acid sequence (Fig. 4.1).

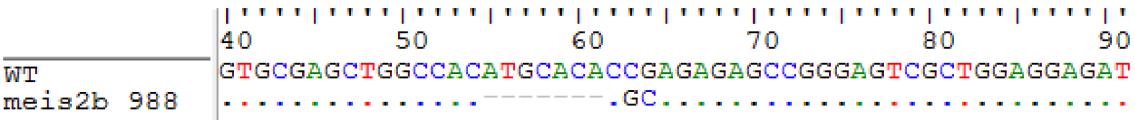

Figure 4.1. *meis2b*^{s988} allele in exon 4. Nucleotide sequences of *meis2b* WT and *meis2b*^{s988} alleles.

To genotype the *meis2b* mutant fish, a PCR was performed, followed by analysis of the PCR product by electrophoresis. The following primers were used:

1. *meis2b* Forward Primer: CCTAACCGCAACAATAAACCA
2. *meis2b* WT Reverse Primer: CCCGGCTCTCTCGGTGTGCAT
3. *meis2b* Mutant Reverse Primer: GACTCCCGGCTCTCTCGC

Two PCR reactions were set for each sample: the first one with *meis2b* Forward Primer, in combination with *meis2b* WT Reverse Primer, giving a product of 210 bp. The second PCR

with *meis2b* Forward Primer, in combination with *meis2b* Mutant Reverse Primer and gives a 207 bp long product. The common *meis2b* Forward Primer binds the end of intron three. The *meis2b* WT Reverse Primer binds exclusively the *meis2b* WT allele. Therefore, the first PCR determines the presence of the WT allele in the DNA sample.

The *meis2b* Mutant Reverse Primer binds exclusively the *meis2b*^{s988} allele. Consequently, the second PCR determines the presence of the mutant allele in the sample (Fig. 4.2).

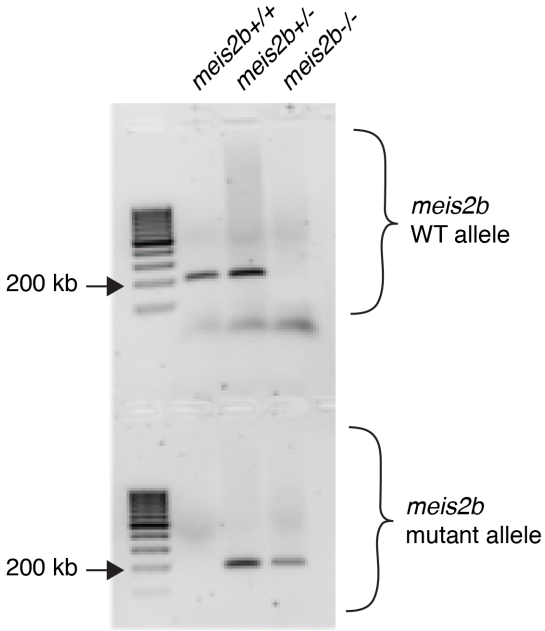

Figure 4.2. Genotyping of *meis2b* alleles by PCR. A PCR made for the *meis2b* WT allele (top panel) and for the *meis2b*^{s988} allele (lower panel). *meis2b*$^{+/+}$ sample shows a band in the PCR for WT allele. *meis2b*$^{+/-}$ sample shows a band in the PCR for WT allele and in the PCR for the mutant allele. *meis2b*$^{-/-}$ sample shows a band only in the PCR for the mutant allele.

4.22. RT-qPCR analysis

All RT-qPCR analyses were done in triplicates using an Illumina Real-Time PCR cycler. Primers were designed using PerlPrimer, and *rpl13* was used for normalization. Primer sequences are listed in Table 4.7; the primer mix was made as follows: 50µL Forward primer + 50µL Reverse primer + 900 µL H_2O. For the RT-qPCR reaction: 5µL Sybr Green 2X Master Mix + 4µL primer mix + 1 µL cDNA, for a total of 10µL.

Table 4.7. List of primers used for RT-qPCR.

Gene	Forward	Reverse
rpl13	TAAGGACGGAGTGAACAACCA	CTTACGTCTGCGGATCTTTCTG
pitx2c	CACACGGTTTCAGACACCTC	CTTGAACCACACTCGGACTC
col18a1	GGTGTGAACGGATATAAAGGAG	CTTCATATCTGCCAAATCTGTCC
stab2	TGAATGTCTGCTGAATCCTCCA	CTCTTGTTCTCCCACTGGCT

4.23. kikGR mRNA injections and photoconversion

4.23.1. *kikGR* mRNA injection

A pCS2+ linearized plasmid containing the kikGR (Kikume Green to Red) sequence was kindly provided by Dr. Michelle Collins. kikGR is a green fluorescence protein (excitation: 488nm) that can be illuminated with UV light at 405nm and be permanently photoconverted to a red fluorescence protein (excitation: 561 nm), this protein is commonly used for lineage tracing experiments (Tsutsui, Karasawa et al. 2005, Nowotschin and Hadjantonakis 2009). The mRNA was synthesized using mMESSAGE mMACHINE SP6 Transcription Kit from Invitrogen, following manufacturer's instructions. 100pg of kikGR were injected into one-cell stage *Tg(myl7:BFP-CAAX)*^{bns193} embryos (this transgenic line allows visualization of the cardiomyocyte membrane with a blue fluorescent protein). The fertilized and successfully injected embryos were raised.

4.23.2. Photoconversion

Dechorionated embryos of 20-23 somites stage were mounted on 0,8% agarose with the dorsal side up, so that the cardiac disc could be easily visualized. The photoconversion was carried as follows: using a Zeiss LSM 880 confocal microscope the "Bleaching" option was selected. Then, the heart disc was visualized, and the anterior or the posterior half of the disc were selected using the option "Regions". Last, the regions of interest were photoconverted using a 405nm wavelength laser, with 15% intensity and seven iterations. After photoconversion, the embryos were transferred to egg water and raised until 48 hpf.

4.23.3. Cell tracking

At 48 hpf, the embryos with photoconverted kikGR were again mounted in 0,8% agarose, and the hearts were visualized with a Zeiss LSM 880 confocal microscope. The hearts were scanned twice: first, the green kikGR together with the photoconverted kikGR were imaged. Then, the hearts the BPF from the cardiomyocyte membrane was visualized, using a 405nm wavelength laser. The channels were later merged using the ImageJ software.

4.24. Microarray

To determine the possible downstream targets of Meis2b, the following expression profiles were compared: 48hpf whole larvae of *meis2b*$^{-/-}$ to *meis2b*$^{+/+}$ siblings, whole heart of three wpf *meis2b*$^{-/-}$ to *meis2b*$^{+/-}$ siblings, atria of three mpf *meis2b*$^{-/-}$ to *meis2b*$^{+/-}$ siblings, and ventricle to atrium of three mpf WT zebrafish (Table 4.8). OakLabs (Hennigsdorf, Germany) performed the microarray using ArrayXS Zebrafish 8x60K.

To determine putative cardiac transcriptional targets of Meis2b, the following selection criteria were used: downregulated or unchanged in 48 hpf *meis2b*$^{-/-}$ larvae, downregulated more than 1.5 fold in three wpf *meis2b*$^{-/-}$ hearts and in three mpf *meis2b*$^{-/-}$ atria, more than fivefold atrial enrichment (Table 4.8).

Table 4.8. Selection criteria for possible Meis2b downstream targets.

genotype	*meis2b* $^{-/-}$	*meis2b* $^{-/-}$	*meis2b* $^{-/-}$	*meis2b* $^{+/+}$
	vs.	vs.	vs.	vs.
genotype	*meis2b* $^{+/+}$	*meis2b* $^{+/-}$	*meis2b* $^{+/-}$	*meis2b* $^{+/+}$
stage	48 hpf	3 wpf	3 mpf	3 mpf
tissue	whole embryo	whole heart	atrium	atrium vs. ventricle
fold change of target genes	unchanged or down	down regulated (>1.5x)	down regulated (>1.5x)	atrial enriched (>5x)

4.25. Image processing

Imaris software was used to count the number of cells in the adult atrium of *meis2b*$^{+/+}$ and *meis2b*$^{+/-}$ after EdU labeling and cardiomyocyte nuclei staining. Imaris was also used to perform 3D rendering of the 48 hpf hearts from *isl1* morphants.

Zen software in Black and Blue editions were used to acquire images from all Zeiss confocal and light sheet microscopes, as well as processing such as: contrast and brightness adjustments, maximum intensity projections and cropping.

Imaging Software NIS-Elements was used to acquire images using the Nikon SMZ25 stereo microscope. The same software was used to adjust the contrast and brightness.

ImageJ was employed to adjust contrast, and brightness and to create maximum intensity projections of confocal images. Additionally, ImageJ was used to merge the red and blue channels from the images obtained with after kikGR photoconversion.

4.26. Generation of *meis2b* overexpression constructs

Three different constructs were made in parallel where *meis2b* was expressed under the control of the atrial specific myosin (*myh6*) promoter. The first construct: *myh6:meis2b*, in which the vector had also integrated *cristallin:GFP*, which allowed to screen for embryos that were carrying the *meis2b* over-expression construct. In the second construct, *myh6:TdTomato-2A-meis2b*, the TdTomato was fused to a 2A self-cleaving peptide, which allows the expression of *TdTomato* in the cells that are overexpressing *meis2b*. And finally, the third construct: *myh6:meis2b-2A-TdTomato*.

Figures 4.3 to 4.5, explain the workflow in which all three constructs were cloned, along with the restriction enzymes used for each construct. *meis2b* CDS was obtained by amplification of cDNA, and the DNA was amplified using primers that added unique restriction sites at the end of the PCR product. The constructs containing the *myh6* promoter, *TdTomato-2A* and *2A-TdTomato* were kindly provided by Dr. Sven Reischauer.

The double digestion reactions with the respective restriction enzymes were as follows:

- 5µg plasmid
- 2µL CutSmart 10X buffer
- 1µL restriction enzyme 1
- 1µL restriction enzyme 2

- H_2O until 20µL
- Overnight incubation at 37ºC

The products were then ligated into the vectors as previously explained.

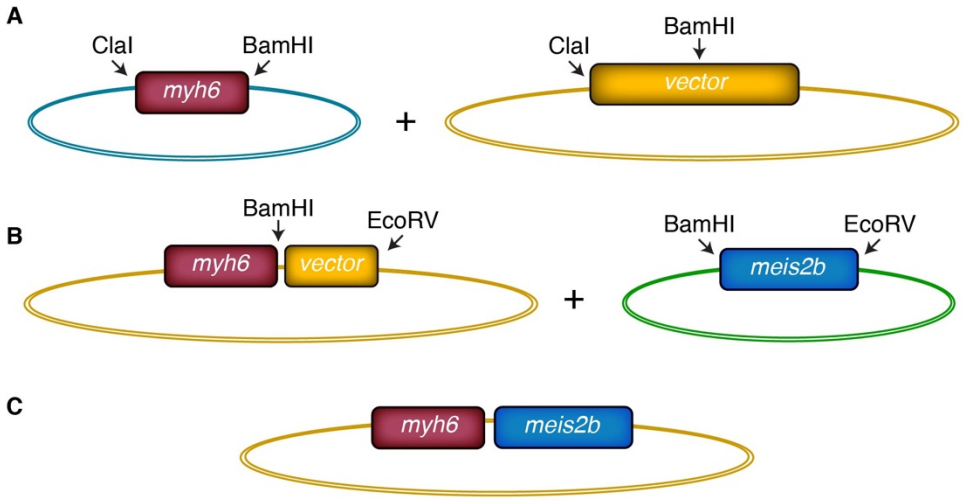

Figure 4.3. Cloning workflow for *myh6:meis2b* construct. **(A)** The plasmid containing the *myh6* promoter and the backbone were digested with ClaI and BamH1 and then ligated together, resulting in the construct shown in **B**. **(B)** The vectors containing *myh6* and *meis2b* were digested with BamH1 and EcoRV. **(C)** After ligation, the final overexpression construct was obtained.

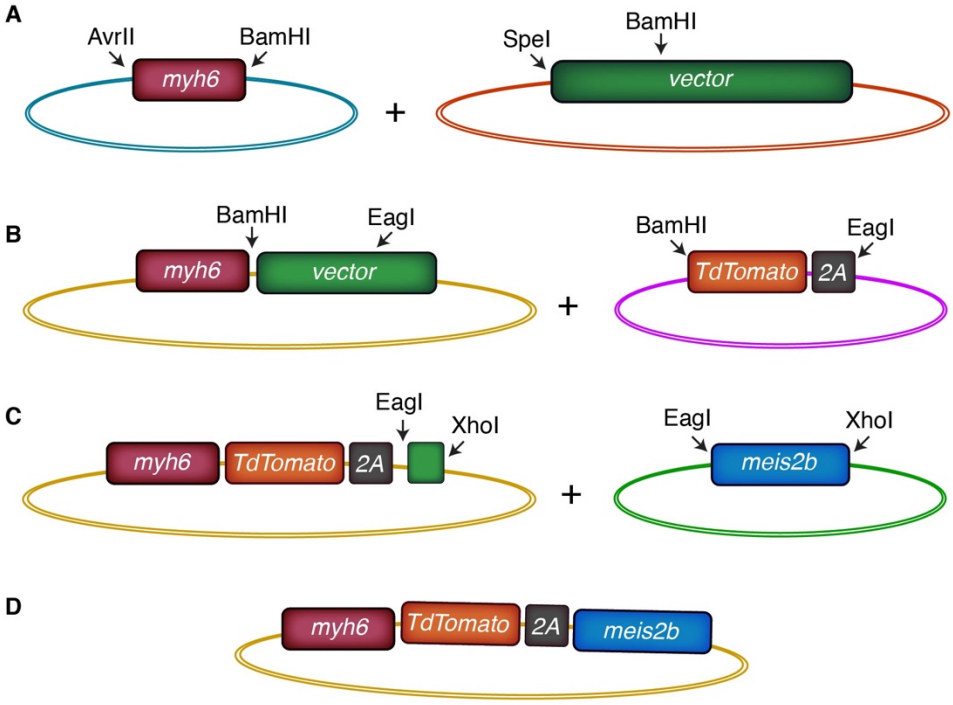

Figure 4.4. Cloning workflow for *myh6:TdTomato-2A-meis2b* construct. **(A)** The plasmid containing *myh6* promoter was digested with AvrII and BamHI, the backbone was

digested with SpeI and BamHI (AvrII and SpeI have compatible ends) and then, the linearized plasmids were ligated together. **(B)** The plasmids containing the *myh6* promoter and *TdTomato-2A* were digested with BamH1 and EagI and then ligated together. **(C)** Plasmids were both digested with EagI and XhoI, and then ligated. **(D)** After a third ligation, the final overexpression construct was obtained.

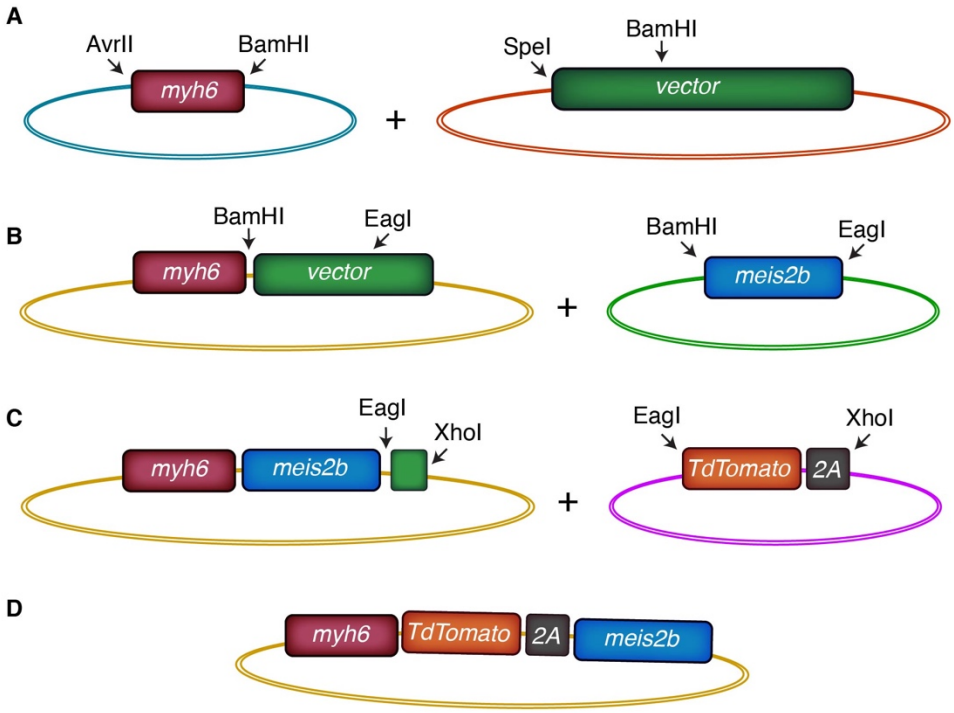

Figure 4.5. Cloning workflow for *myh6:meis2b-2A-TdTomato* construct. **(A)** The plasmid containing *myh6* promoter was digested with AvrII and BamHI, the backbone was digested with SpeI and BamHI (AvrII and SpeI have compatible ends) and then ligated together. **(B)** The plasmids containing *myh6* promoter and *meis2b* CDS were digested with BamH1 and EagI and then ligated together. **(C)** Plasmids were both digested with EagI and XhoI, and the ligated. **(D)** After a third ligation, the final overexpression construct was obtained.

Table 4.9. List of primers used for the creation of the *meis2b* overexpression constructs.

Gene	Forward	Reverse
ClaI-*amhc*-BamHI	ATCGATGCTAAAGTGGCAGTGTGCCG	GGATCCCGTGAATATGGTTTTCAGG
BamHI-*meis2b*-EcoRV	GGATCCATGCTGATGGCTCAACGG	GATATCTTACATGTAGTGCCACTGTCC
AvrII-*amhc*-BamH1	CCTAGGGCTAAAGTGGCAGTGTGCCG	GGATCCCGTGAATATGGTTTTCAGG
BamH1-*TdTomato-2A*-EagI	GGATCCATGGGCTGCATCAAGAGCAAG	CGGCCGTGGGCCAGGATTCTCCTCG
EagI-meis2b-XhoI	CGGCCGATGCTGATGGCTCAACGGTAC	CTCGAGTTACATGTAGTGCCACTGTCC

BamH1-meis2b-EagI	GAAAACCATATTCACGGGATCCATGCTGATGGCTCAACGGTA	AGTAGCTCCGCTTCCCGGCCGTTACATGTAGTGCCACTGTC
EagI-2A-TdTomato-Xho1	TGGCACTACATGTAACGGCCGGGAAGCGGAGCTACTAACTT	CTATAGTTCTAGAGGCTCGAGTTACTTGTACAGCTCGTCCA

V. Results

Note: Parts of this chapter will be included in the article "Distinct myocardial lineages break atrial symmetry during cardiogenesis in zebrafish" from Guerra, A. et al. (manuscript in preparation). All experiments and results shown in this thesis were performed by Almary Guerra. Dr. Sven Reischauer and Prof. Dr. Didier Stainier supervised this project and helped with experimental design. Raoul Freitas and Dr. Sven Reischauer created the *meis2b* mutant line (*meis2b*^{s988}) and the respective genotyping method. The *Tg(myl7:BFP-CAAX)*^{bns193} line used in this study was established by Dr. Suchit Ahuja. Dr. Oliver Stone provided the modified BAC (CH211-128L12), used in creating the *TgBAC(meis2b:GAL4FF)*^{bns15} line.

In humans, mutations in *MEIS2* lead to a great number of congenital malformations, such as cleft palate, facial dysmorphism, epilepsy, mental retardation, delayed motor development, and atrial and ventricular septal defects (Erdogan, Ullmann et al. 2007, Chen, Lin et al. 2008, Crowley, Conlin et al. 2010, Louw, Corveleyn et al. 2015). In mouse, it has been reported that MEIS2 is important in the development of tissues derived from neural crest. *Meis2* deficient mice display defects in facial nerves, in head bones and cartilages, delayed ocular development, small body and liver size compared to WT siblings, and die between E13.5 and E14.5 due to severe hemorrhaging (Machon, Masek et al. 2015). Furthermore, *Meis2* mutant mice also show congenital heart defects, characterized by persistent truncus arteriosus and absence of the aortic and pulmonary valves (Machon, Masek et al. 2015). From studies performed in mammals, it becomes clear that MEIS2 is an important regulator of various processes during embryonic development.

In zebrafish, *Meis2* has two orthologues, *meis2a* and *meis2b*. It has been reported that *meis2b* morphants show delayed cardiac looping and slower heart rate (Paige, Thomas et al. 2012), whereas *meis2a* morphants display defects in craniofacial development (Melvin, Feng et al. 2013). Therefore, this chapter will be dedicated to understanding the effect of the loss-of-function of *meis2b* in the zebrafish heart development and morphogenesis.

Role of Meis2b in zebrafish heart development and asymmetry

Systemic and pulmonary vascular circuits require dedicated left and right cardiac chambers, which are present in terrestrial vertebrates but not in teleost fish. Whether left-right (L-R) chamber specification arose *de novo* in higher vertebrates, or whether it evolved from preexisting molecular patterns, remains to be elucidated. Consequently, mutations interfering with cardiac L-R asymmetry are associated with patterning and septation defects in humans and constitute the leading cause of congenital disorders (Hoffman 1995, Mammi, De Giorgio et al. 1998, Gudbjartsson, Arnar et al. 2007).

In the search for chamber-specific candidate genes that could be linked to atrial and ventricular septation defects, the expression profiles of atria and ventricles of adult zebrafish hearts were compared (Fig. 5.1).

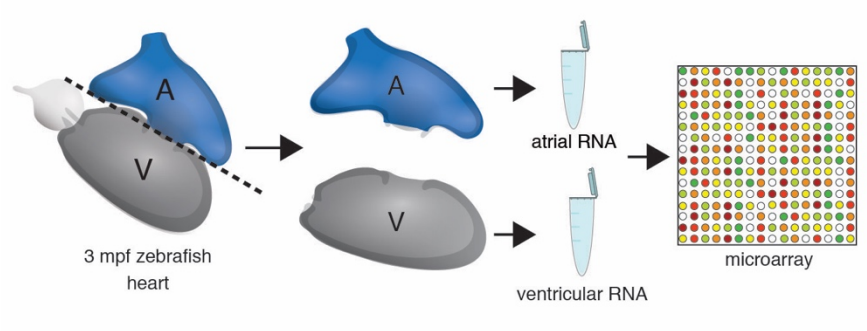

Figure 5.1. Schematic representation of the workflow to determine chamber-specific expression profiles. The hearts of three mpf zebrafish were extracted and the atria dissected from the ventricles. Total RNA of atria and ventricles was isolated and then compared using a microarray.

The expression of atrial enriched transcription factor genes was analyzed and, interestingly, expression of *meis2b* was found to be highly enriched in the atria of three mpf zebrafish (Table 5.1). This result made *meis2b* a very interesting candidate to study its role in heart development, since mutations in *MEIS2* have been associated with atrial and ventricular septal defects in humans (Louw, Corveleyn et al. 2015). Additionally, the expression of *pitx2*, a key regulator of asymmetric cardiac development, was also found to be highly enriched in the atrium, resembling its atrial-specific expression pattern found in the mammalian heart (Franco, Christoffels et al. 2014). *pitx2* and its relationship with *meis2b* will be discussed later in this chapter.

Table 5.1. Expression of chamber-specific transcription factor genes and myosin genes in the zebrafish adult heart. The expression profiles of atria and ventricles were obtained using a microarray. $-\log_2$(fold change Atria vs Ventricles) is shown. Negative values represent atrial-enriched genes and positive values represent ventricular-enriched genes.

Gene	$-\log_2$(Fold Change)
myh6	-5,803683649
meis2b	-5,811560939
pitx2	-4,443606651
id4	-3,700560925
shox2	-3,554771323
vmhcl	5,883161005

5.1. *meis2b* mutants do not show cardiac looping defects

Since *MEIS2* is important in cardiac development in humans, and given its restricted expression pattern in the zebrafish, we decided to study the effect of the loss-of-function of *meis2b* in the zebrafish heart development. For this purpose, a *meis2b* mutant allele was used, which is characterized by a seven bp deletion, followed by a codon substitution (*meis2b*^{s988}).

Earlier published work has shown that knockdown of *meis2b* results in delayed cardiac development and cardiac looping defects (Paige, Thomas et al. 2012). To test whether the *meis2b* mutants recapitulate the phenotype observed in the *meis2b* morphants, a blind experiment was performed, where the overall morphology and looping of the hearts from a *meis2b*$^{+/-}$ incross were evaluated before knowing the genotype of the fish.

The hearts of 32 fish at 48 hpf were observed; to visualize the heart shape and the cardiomyocytes, the *Tg(myl7:LA-GFP)* together with *Tg(-5.1myl7:nDsRed2)* were employed. Interestingly, 28 of 32 hearts were correctly looped at 48 hpf; while only four of 32 were not looped (Fig. 5.2). 17 fish with looped hearts were randomly selected and genotyped, a mendelian ratio was observed, with 50% of the fish *meis2b*$^{+/-}$, 25% for *meis2b*$^{+/+}$, and 25% for *meis2b*$^{-/-}$. The same trend was observed after genotyping the four fish with unlooped hearts (Table 5.2).

Furthermore, no additional cardiac defects were observed during embryonic cardiac development of the *meis2b* mutants. These results indicate that mutations in *meis2b* do not affect embryonic heart development, in contrast to the knockdown experiments that have been previously published (Paige, Thomas et al. 2012).

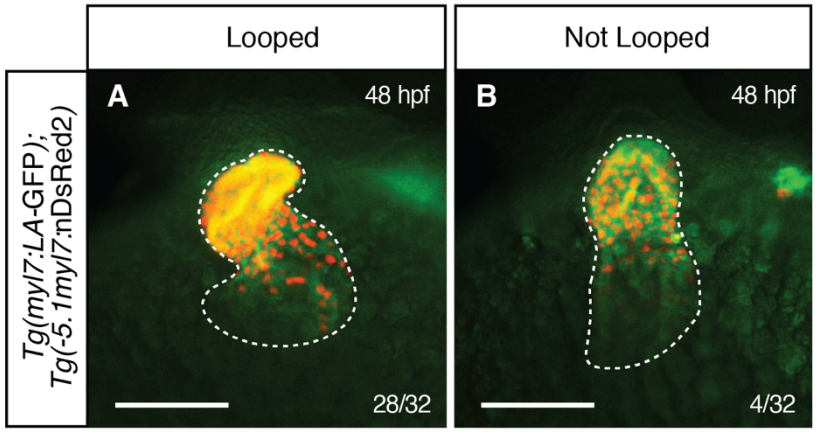

Figure 5.2. *meis2b* mutants do not display early cardiac developmental defects. Brightfield picture of 48 hpf *Tg(myl7:LA*-GFP*)* together with *Tg(-5.1myl7:*nDsRed2*)* embryos from a *meis2b*$^{+/-}$ incross. **(A)** 28 out of 32 hearts were looped. **(B)** four out of 32 hearts failed to loop. Scale bars: 100 μm.

Table 5.2. Genotyping of 48 hpf embryos from a *meis2b*$^{+/-}$ incross, with looped and unlooped hearts.

	***meis2b*$^{+/+}$**	***meis2b*$^{+/-}$**	***meis2b*$^{-/-}$**	**Total**
Looped	4	9	4	17
Not looped	1	2	1	4

5.2. Loss of *meis2b* causes abnormal atrial growth

In contrast to previously published knockdown experiments (Paige, Thomas et al. 2012), no early cardiac morphogenetic defect was observed in *meis2b*$^{-/-}$ at early stages of development. However, starting from three wpf, the atria of the *meis2b*$^{-/-}$ fish were significantly enlarged when compared to WT siblings (data obtained provided by Raoul Freitas. This result has not been published, but is included in Guerra et al., manuscript in preparation). At three mpf, the abnormal atrial growth persisted, causing a pericardial bulge in the adult *meis2b*$^{-/-}$ fish (Fig. 5.3). Interestingly, two different levels of atrial growth were observed in the *meis2b* mutants: less than 5% of the adult *meis2b*$^{-/-}$ developed an extreme atrial growth, which caused a highly prominent pericardial area (Fig. 5.3 C, F, F'), while the majority of the adult *meis2b* mutants exhibited a milder atrial growth and a smaller pericardial bulge. However, trichrome staining and analysis of confocal projections of the adult *meis2b*$^{-/-}$ hearts

revealed that the overall myofibrillar architecture and the formation of the atrioventricular valves in the *meis2b*$^{-/-}$ are normal.

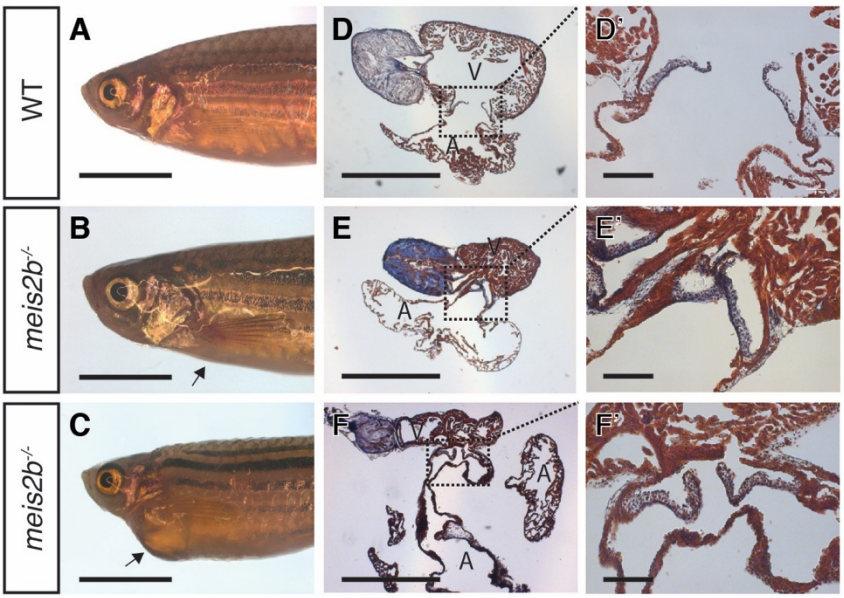

Figure 5.3. *meis2b*$^{-/-}$ display abnormal atrial growth. **(A-C)** 4mpf *meis2b*$^{-/-}$ and WT siblings are shown. Adult *meis2b*$^{-/-}$ display pericardial bulging (arrows). **(D-E)** Trichrome staining on paraffin section of the hearts from the fish in A-C reveals the mild (E) and extreme (F) abnormal atrial growth in *meis2b* mutants. (D'-F') zoom of the atrioventricular canal area of the hearts in D-F shows normal valve formation. A, atrium; V, ventricle. Scale bars: (A-C) 1mm, (D-E) 500µm, (D'-E') 50µm.

5.3. Loss of *meis2b* increases atrial cardiomyocyte proliferation

To elucidate whether the *meis2b* mutants exhibit enlarged atria due to excessive cell proliferation, the atrial proliferation ratio was determined with the help of EdU detection. EdU is a Thymidine analog which is incorporated in proliferating cells and later can be easily detected using a Click reaction (Salic and Mitchison 2008). For this purpose, EdU was injected in three mpf *meis2b* mutants and WT siblings carrying *Tg(-5.1myl7:nDsRed2)*^{f2}. Afterwards, the fish were incubated for four days in the system and later, the hearts were extracted and stained with anti-DsRed, followed by detection of EdU. Finally, the hearts were cleared using iDisco and imaged using a confocal microscope. All proliferating atrial cardiomyocytes were counted with the help of Imaris software.

Adult *meis2b*$^{-/-}$, showed 10,02% (±1.12) of proliferating atrial cardiomyocytes, in contrast to the 2.78% (±0.49) in WT siblings (Fig. 5.4). These results suggest that excessive atrial

cardiomyocyte proliferation greatly contributes to the abnormal atrial growth observed in the *meis2b* mutants.

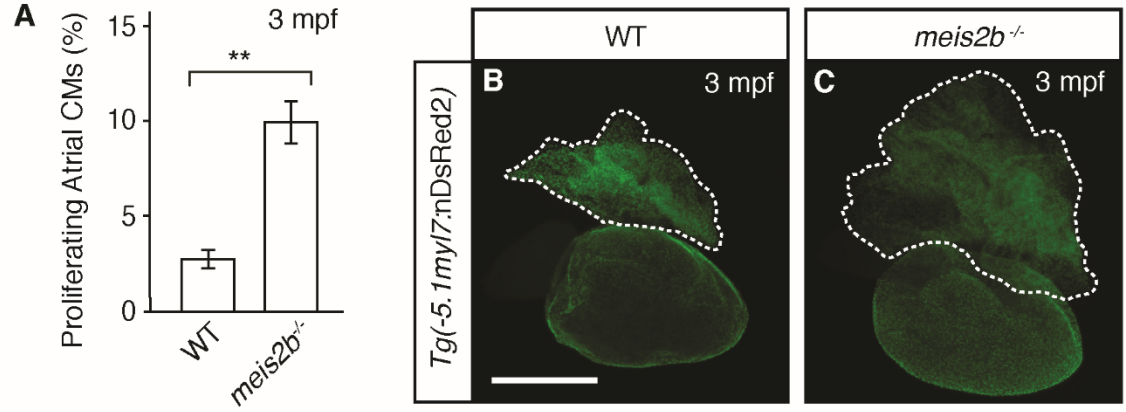

Figure 5.4. Increased atrial cardiomyocyte proliferation in *meis2b*$^{-/-}$. **(A)** Atrial cardiomyocytes from three mpf *meis2b*$^{-/-}$ show significantly increased proliferation in comparison to WT siblings. **(B-C)** Cleared hearts from three mpf fish show the abnormally enlarged atrium in the *meis2b* mutants. Significant differences compared with control are indicated (**p<0,005); error bars indicate ±SD. Scale bar: 1mm.

5.4. *meis2b* expression in the adult heart

To better understand how Meis2b works in the heart, it is important to understand the cardiac expression pattern of *meis2b*. Therefore, an ISH for *meis2b* was performed on paraffin sections of zebrafish adult hearts. Interestingly, ISH experiments revealed that *meis2b* is expressed only on the left side of the atrial myocardium, near the OFT. These results indicate that *meis2b* has an asymmetric expression pattern in the adult zebrafish heart (Fig. 5.5), a characteristic that had not yet been described for any of the *meis* genes in zebrafish or in other species. These results constitute the first evidence of asymmetry in the zebrafish atrium.

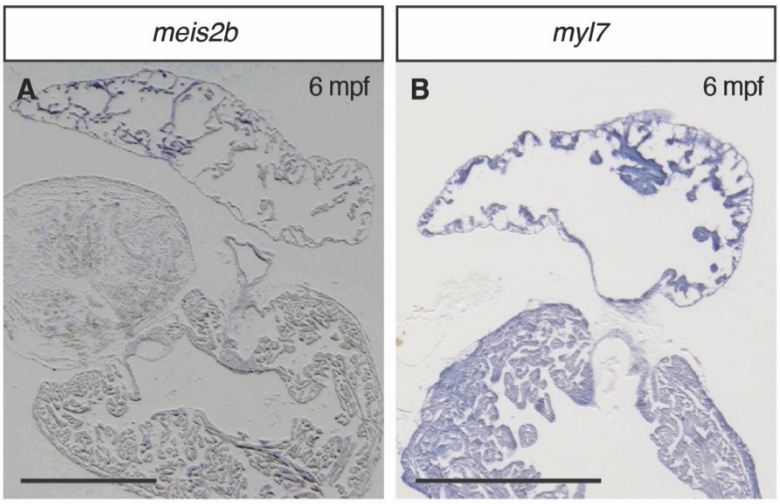

Figure 5.5. *meis2b* is asymmetrically expressed in the atrium. **(A-B)** *In situ* hybridization on paraffin sections of 6 mpf zebrafish hearts for *meis2b* (A) and the cardiomyocyte marker *myl7* (B). The restricted expression of *meis2b* can be observed in (A). Scale bars: 1mm.

5.5 Establishment of the *meis2b* reporter line

A modified BAC (CH211-128L12), containing the *GAL4FF* sequence after the start codon of *meis2b* was kindly provided by Dr. Oliver Stone. 25pg of the modified construct (*meis2b:GAL4FF*) were injected into one-cell stage embryos carrying the *Tg(5xUAS:EGFP)*^{nkuasgfp1a} transgene (Asakawa, Suster et al. 2008). Embryos that were successfully injected and that showed EGFP expression were raised. After three mpf, the adult F0 fish were outcrossed to WT fish, and the F1 progenies were evaluated to determine if the F0 parents carried the *meis2b:GAL4FF* transgene in their germ line (founder fish). Two founders were recovered and the progeny was raised, therefore establishing the *TgBAC(meis2b:GAL4FF)*^{bns15} (Guerra et al., manuscript in preparation).

In order to validate this newly established transgenic line, the expression pattern of the *TgBAC(meis2b:GAL4FF)*^{bns15}*; Tg(5xUAS:EGFP)*^{nkuasgfp1a} (hereon referred to as *Tg(meis2b-reporter)*) was compared to the endogenous expression of *meis2b* observed with ISH, at 24 and 48 hpf. The *Tg(meis2b-reporter)* line was found to recapitulate the expression pattern of the endogenous *meis2b* expression. At 24 hpf, the expression *Tg(meis2b-reporter)* can be observed in the olfactory bulb, brain and neural tube and heart tube. At 48 hpf, the expression of *meis2b* detected with ISH and the expression *Tg(meis2b-reporter)* can be observed in the retinal cells in the eyes, fin buds, brain and neural tube (Fig. 5.6). Interestingly, at 24 and 48 hpf, the *Tg(meis2b-reporter)* is expressed in the cardiac tissue, in contrast to what can be seen in with the ISH, where the expression levels of *meis2b* are too low and cannot be appreciated with conventional ISH.

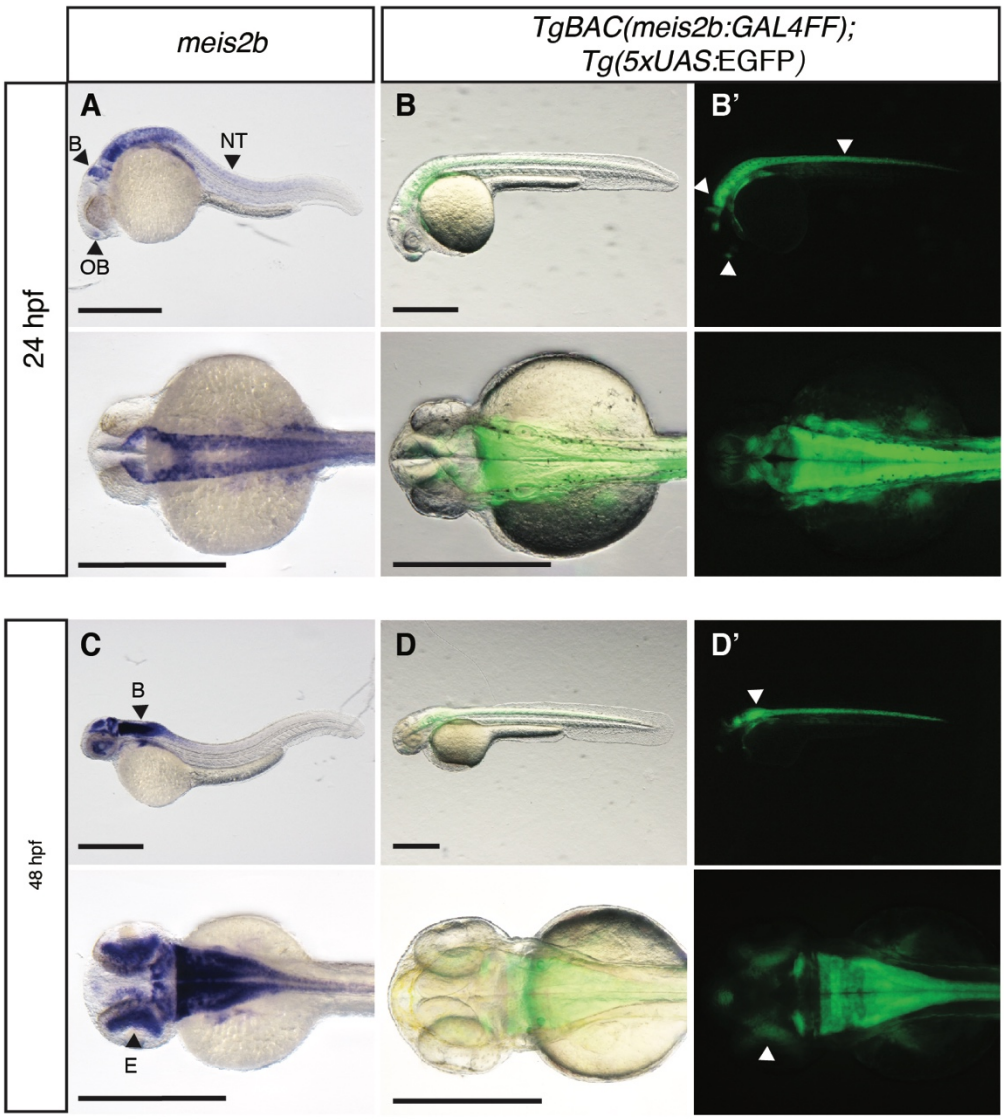

Figure 5.6. Validation of the *Tg(meis2b-reporter)* line. Left column: ISH for *meis2b* at 24 and 48 hpf. Central and right columns: expression of *Tg(meis2b-reporter)* at 24 and 48 hpf. *Tg(meis2b-reporter)* and endogenous *meis2b* are expressed in the same areas of the embryos (arrow heads). B, brain; E, eye; NT, neural tube; OB, olfactory bulb. Scale bars: 100μm.

5.6. Asymmetric expression of *Tg(meis2b-reporter)* in the embryonic heart

To closely follow the expression pattern and dynamics of the *Tg(meis2b-reporter)* throughout heart development, *Tg(meis2b-reporter)* fish were crossed to different transgenic lines that allow the visualization of the distinctive cell types that compose the developing heart.

myosin light chain 7 (*myl7*) is exclusively and highly expressed in the cardiomyocytes; the transgenic line *Tg(myl7:mCherry)* expresses cytosolic mCherry under the control of *myl7*

promoter, which makes this line an excellent tool for visualization of the cardiomyocytes since early stages of development (Langenbacher, Huang et al. 2012).

Tg(meis2b-reporter);Tg(myl7:mCherry) embryos at different developmental stages were fixed, flat-mounted and imaged ventrally using a confocal microscope. Interestingly, at 23 somites stage, after the heart disc has been formed, the *Tg(meis2b-reporter)* is expressed in the cardiomyocytes located in the posterior half of the heart disc (Fig. 5.7 A). This restricted expression pattern is consistent with what has been observed at earlier stages, where *meis2b* is expressed in a more posterior subset of the *gata4*+ cardiomyocyte progenitors in the heart field in the ALMP (Paige, Thomas et al. 2012). Later, due to the migration and rotation of the cardiomyocytes in the heart disc (Rohr, Otten et al. 2008, Smith, Chocron et al. 2008), the *Tg(meis2b-reporter)*-positive cells are found in the ventral region of the heart tube, adopting a dorso-ventral configuration (Fig. 5.7 B).

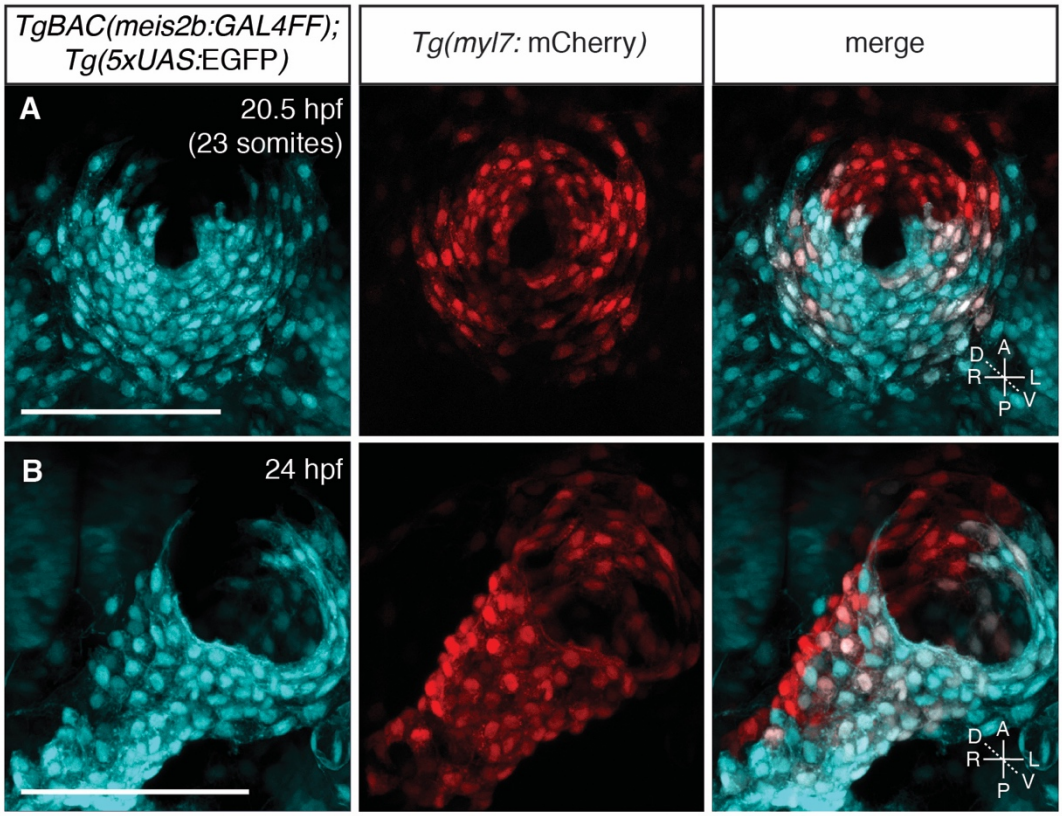

Figure 5.7. *Tg(meis2b-reporter)* is asymmetrically expressed in the embryonic heart. Confocal projections of *Tg(meis2b-reporter);Tg(myl7:*mCherry*)* at 20,5 hpf **(A)** and 24 hpf **(B)**. (A) *Tg(meis2b-reporter)* is expressed in the posterior compartment of the heart disc (n=16). (B) *Tg(meis2b-reporter)* is exclusively expressed in the ventral side of the heart tube (n=14). Ventral views, anterior up. Scale bars: 100µm.

5.7. *Tg(meis2b-reporter)* expression in the larval and mature heart

At three dpf, once the heart tube has looped and the atrium and ventricle are formed, *Tg(meis2b-reporter)* expression can be observed in the dorsal and left side of the atrium, in the inflow tract and in a small portion of the ventricle near the atrioventricular canal (Fig. 5.8A). After six dpf, the expression of *Tg(meis2b-reporter)* is completely restricted to the left side of the atrium, near the outflow tract and no expression in the ventricle can be detected (Fig. 5.8B). In the mature heart, the expression of the *Tg(meis2b-reporter)* resembles the endogenous expression observed with ISH on sections, as shown in Fig. 5.5. At three mpf, the *meis2b* reporter maintains its asymmetric expression in the atrium, being only observed on the left side of the atrium (Fig. 5.8C).

Altogether, these data imply that there is an anterior-posterior asymmetry in the heart disc, which can be evidenced by the restricted expression of the *Tg(meis2b-reporter)*. Later, due to the migration and rotation of the cardiomyocytes, this anterior-posterior asymmetry is translated to a dorso-ventral asymmetry and, after the heart is formed, the dorso-ventral pattern changes to a L-R asymmetry which remains from larval stages until adulthood (Bakkers, Verhoeven et al. 2009, Bakkers 2011).

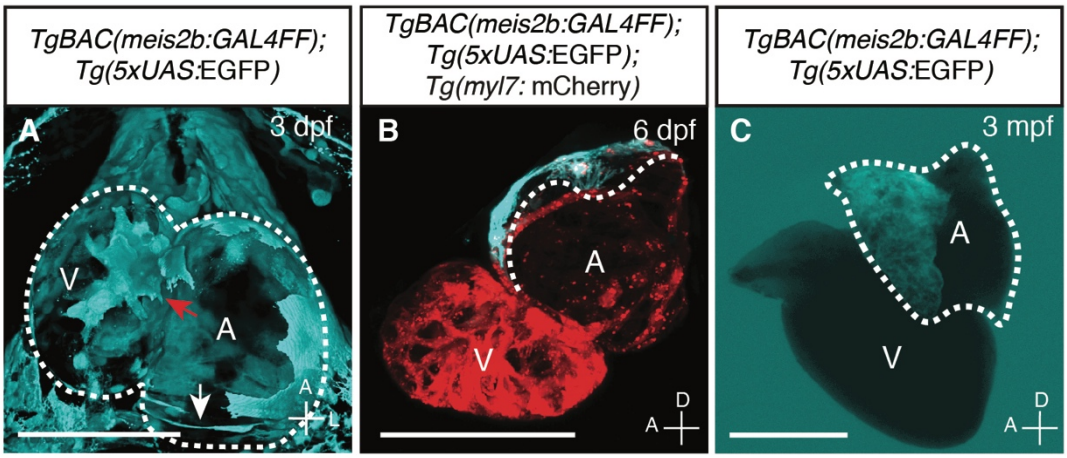

Figure 5.8. *Tg(meis2b-reporter)* is expressed in the left side of the mature atrium. **(A)** At three dpf *Tg(meis2b-reporter)* expression can be observed in the dorsal and distal side of the atrium, in the inflow track (white arrow) and in the ventricle, next to the atrioventricular canal (red arrow) (n=8). **(B)** At six dpf, *meis2b* reporter is exclusively expressed in one side of the atrial myocardium (dotted line) (n=5). **(C)** Expression of *meis2b* reporter is restricted to the left side of the atrium in the adult heart (dotted line) (n=15). (A) ventral view, anterior up; dotted line delimits the heart; (B-C) lateral views, anterior left; A, atrium; V, ventricle. Scale bars: (A-B) 100 µm, (C) 500 µm.

5.8. Expression of *Tg(meis2b-reporter)* in the ventricular progenitors

In the mature heart, *meis2b* is expressed in the atrium. However, during heart development, *Tg(meis2b-reporter)* seems to be expressed in both atrial and ventricular precursors; to determine the extent to which *meis2b* is expressed in the atrial or ventricular progenitors, the *Tg(meis2b-reporter)* was crossed to a *Tg(vmhc:mCherry-NTR)*, which expressed mCherry under the control of the *ventricular myosin heavy chain* (*vmhc*) promoter (Zhang, Han et al. 2013). At 20,5 hpf, *Tg(meis2b-reporter)* can be observed in the ventricular cardiomyocyte precursors in the heart disc, as well as in the atrial cardiomyocyte precursors located in the posterior half of the heart disc (Fig. 5.9 A). At 24 and 30 hpf, the *Tg(meis2b-reporter)* can be observed in the ventricular cardiomyocytes in the ventral side of the heart tube, as well as in the atrial progenitors, which are rostral to the ventricular progenitors (Fig. 5.9 B-C).

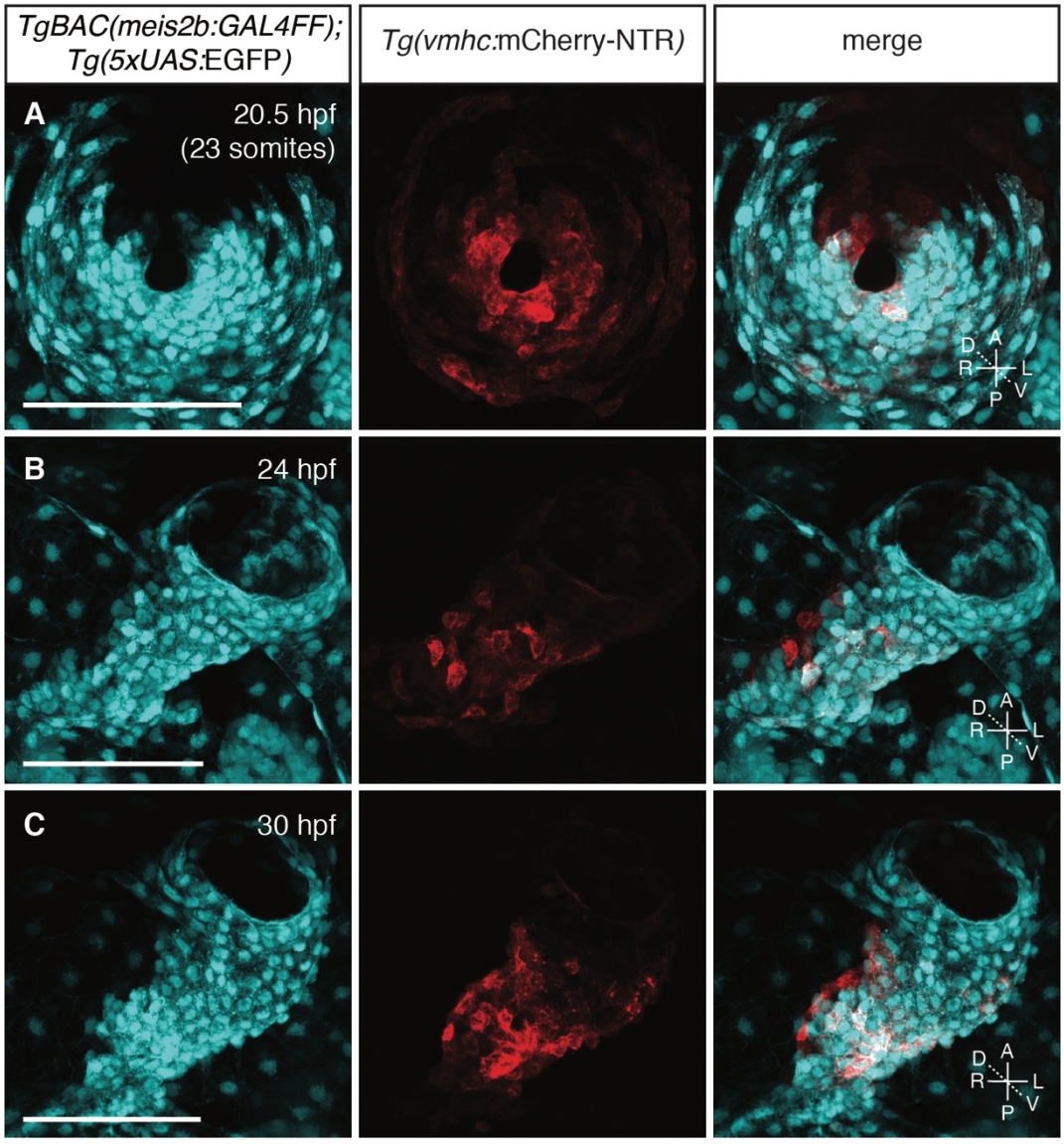

Figure 5.9. *Tg(meis2b-reporter)* is expressed in the ventricular and atrial progenitors. Confocal projections of *Tg(meis2b-reporter);Tg(vmhc:*mCherry-NTR*)* at 20,5 hpf **(A)**, 24 hpf **(B)** and 30 hpf **(C)**. (A) In the heart disc, the *Tg(meis2b-reporter)* colocalizes with *Tg(vmhc:*mCherry-NTR*)* in the ventricular progenitors located in the posterior half of the heart disc (n=5). (B-C) At 24 and 30 hpf, *Tg(meis2b-reporter)* is expressed in the ventricular cardiomyocytes located on the ventral side of the heart tube (n=5). Ventral views, anterior up. Scale bars: 100 μm.

5.9. *Tg(meis2b-reporter)* is not expressed in the endothelial tissue during heart development

During embryonic development, the endocardium and the myocardium are essential for cardiac formation (Staudt and Stainier 2012). To determine if the *Tg(meis2b-reporter)* is expressed exclusively in the cardiomyocytes or if it is also expressed in the endothelial progenitors, the *Tg(meis2b-reporter)* was crossed to the endothelial marker *Tg(kdrl:HRAS-mCherry)* (Chi, Shaw et al. 2008). Neither in the heart disc nor in the forming heart tube, the *Tg(meis2b-reporter)* was found to colocalize with endothelial cells (Fig. 5.10). Instead, at 19 hpf, the *krdl*-positive cells were located ventral and dorsal to the *meis2b*-positive cells. Two streams of *kdrl*-positive cells extended anteriorly to the heart disc were observed, but no coexpression with *Tg(meis2b-reporter)* was detected. Altogether, these data indicate that *Tg(meis2b-reporter)* is expressed exclusively in the myocardium during cardiac development.

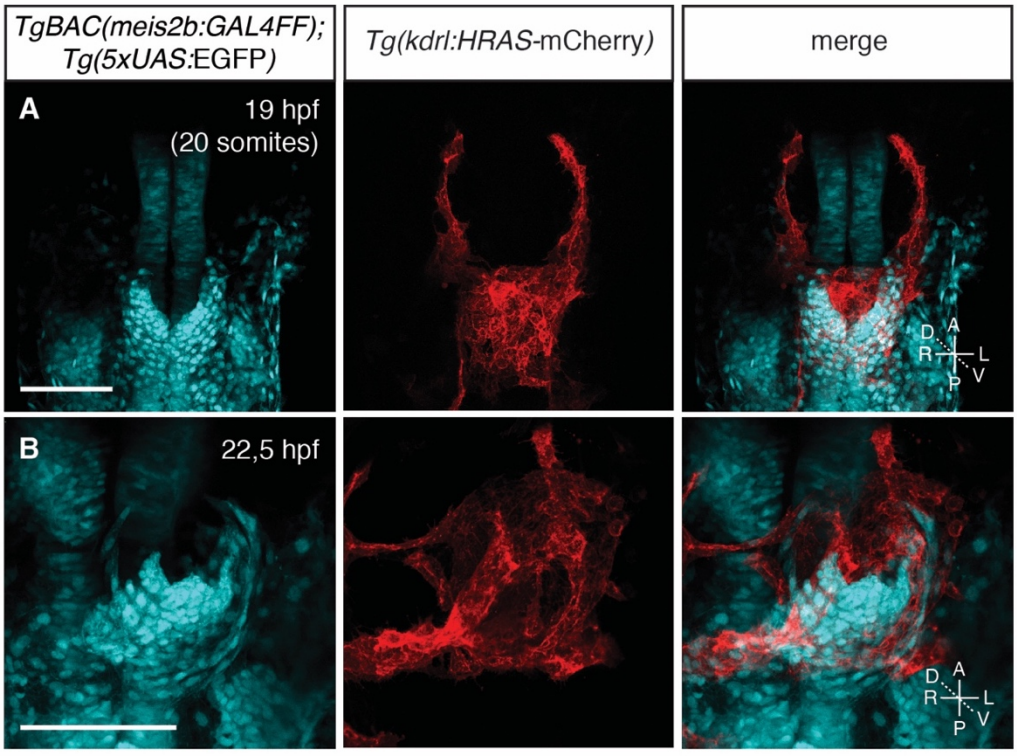

Figure 5.10. *Tg(meis2b-reporter)* is not expressed in endothelial cells. Confocal projections of *Tg(meis2b-reporter);Tg(kdrl:HRAS-mCherry)* embryos at 19 hpf (n=5) **(A)** and 22,5 hpf (n=4) **(B)** indicate that the *Tg(meis2b-reporter)* does not colocalize with the endothelial marker. Ventral views, anterior up. Scale bars: 100µm.

5.10. Anterior-posterior asymmetry in the heart disc is translated to left-right asymmetry in the heart at 48 hpf

A lineage tracing experiment was designed to determine if the *Tg(meis2b-reporter)*-positive cells from the left side of the 48 hpf heart are the same *Tg(meis2b-reporter)*-positive cells from the posterior half of the cardiac disc. 100pg of mRNA of the photoconvertible protein kikGR (Tsutsui, Karasawa et al. 2005, Nowotschin and Hadjantonakis 2009) were injected into *Tg(myl7:BFP-CAAX)*^{bns193} one-cell stage embryos. At 20-23 somites stage, the posterior or the anterior halves of the cardiac disc were photoconverted using an LSM880 confocal microscope (Fig. 5.11). Since kikGR was expressed in all tissues of the embryos, all the tissues that are dorsal or under the posterior half of the heart disc were photoconverted (eg., endocardium, notochord, etc.).

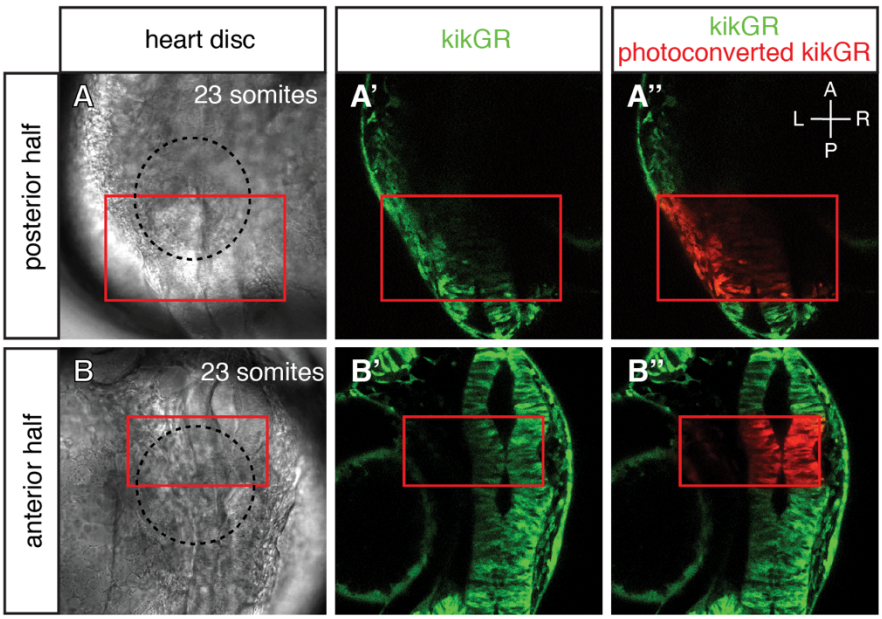

Figure 5.11. Photoconversion of kikGR in the posterior or anterior halves of the heart disc. Top panel: kikGR photoconversion in the posterior half of the heart disc. Lower panel: kikGR photoconversion in the anterior half of the heart disc. **(A, B)** Dorsal view of the heart disc (black, dotted circle) and the region selected for photoconversion (red square). **(A', B')** kikGR expression before photoconversion. **(A'', B'')** kikGR expression after photoconversion.

At 48 hpf, once the cardiac chambers were formed, the hearts were imaged to determine where the cells with photoconverted kikGR are located. In 12 out of 17 samples, the cells from the posterior half of the cardiac disc were located on the left side of the heart at 48 hpf (3.11 A-B). Specifically, the cardiomyocytes with photoconverted kikGR were located around the inflow tract, the left and dorsal side of the atrium and in the AV canal, resembling the *Tg(meis2b-reporter)* expression pattern observed at two and three dpf (Fig. 5.8A and 5.15A).

The endocardial cells that were located in the posterior half of the cardiac disc and were photoconverted were also observed in the heart at 48 hpf. Interestingly, most of the photoconverted endothelial cells were located on the same side of the photoconverted myocardium (Fig. 5.12 B). These results suggest that the endocardium migrates together with the myocardium and form the same side of the heart.

In contrast, in 9 out of 12 embryos, the cardiomyocytes from the anterior half of the heart disc were located on the right side of the heart at 48 hpf (Fig 5.12 C-D), displaying the opposite pattern observed in the cardiomyocytes from the posterior half of the disc. Specifically, the cardiomyocytes from the anterior half of the disc were located in the outer ventricular curvature and in the inner atrial curvature, together with the endocardial cells that were also located in the photoconverted area.

Altogether, these data indicate that the anterior-posterior asymmetry in the cardiac disc is translated to a L-R asymmetry in the heart at 48 hpf.

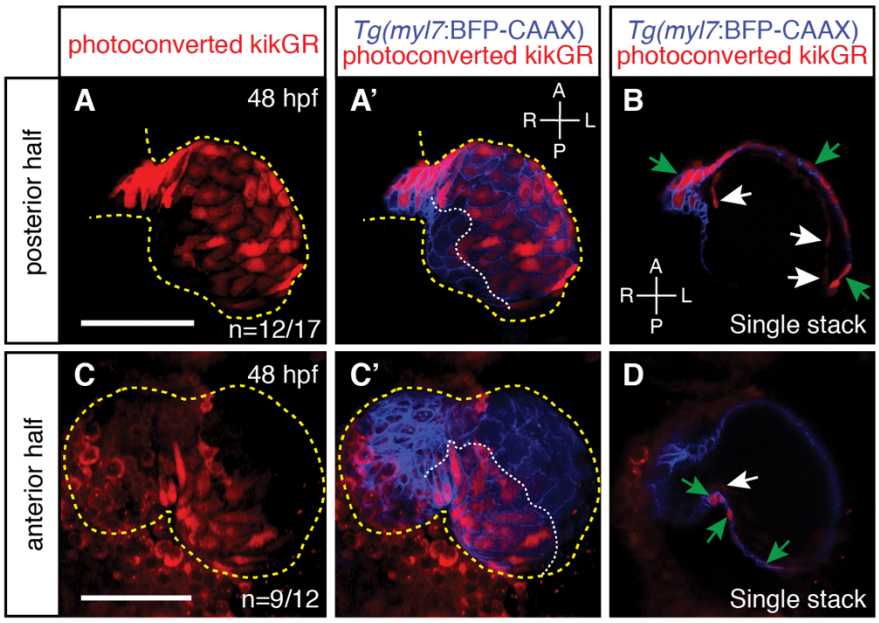

Figure 5.12. Cells from the posterior half of the cardiac disc form the left side of the heart at 48 hpf. Top panel: confocal projections of *Tg(myl7:BFP-CAAX)* and photoconverted

kikGR from the posterior half of the heart disc. Lower panel: confocal projections of photoconverted kikGR from the anterior half of the heart disc. **(A-A')** Confocal projections show that cells from the posterior half of the heart disc are located on the left side of the heart at 48 hpf (n=12/17). **(B, D)** Single stack of the hearts in A and C show the myocardial cells (green arrows) and endocardial cells (white arrows) expressing photoconverted kikGR. **(C)** Confocal projections show that cells from the anterior half of the heart disc are located on the right side of the heart at 48 hpf (n=9/12).

5.11. *Tg(meis2b-reporter)* expression in the adult heart

As previously described in this chapter, the *Tg(meis2b-reporter)* is asymmetrically expressed in the adult atrium; its expression is limited to the left half of the atrium, revealing an inherent L-R atrial asymmetry (Fig 5.13 A). To further characterize the expression pattern of the *Tg(meis2b-reporter)* in the adult heart, the *meis2b* reporter line was crossed to the *Tg(-5.1myl7:nDsRed2)*, which expresses DsRed2 in the nuclei of all cardiomyocytes (Mably, Burns et al. 2003). As expected, the *Tg(meis2b-reporter)* colocalized with *Tg(-5.1myl7:nDsRed2)* in the cardiomyocytes of the atrial trabeculae and the atrial wall (Fig 5.13 B). Furthermore the *meis2b* reporter line was crossed to *Tg(kdrl:NLS-mCherry)*, which allows visualization of the endocardial cells by expressing mCherry under the control of the endothelial specific marker promoter *kdrl* (Wang, Kaiser et al. 2010). The *Tg(meis2b-reporter)* was not found to be expressed in the endocardial cells of the atrium in the adult heart (Fig 5.13 C).

Taken together, these results indicated that *meis2b* is exclusively expressed in the myocardial cells throughout cardiac development and it reveals an inherent L-R asymmetry in the single atrium of the zebrafish.

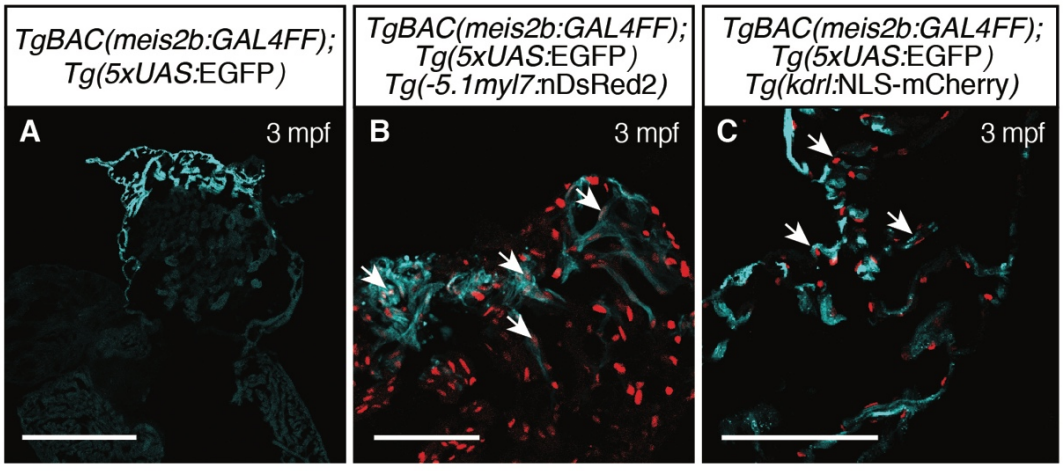

Figure 5.13. *Tg(meis2b-reporter)* is exclusively expressed in myocardial cells. Confocal projections of heart cryosections of *Tg(meis2b-reporter)* **(A)**, *Tg(meis2b-reporter);Tg(-*

5.1myl7:nDsRed2) **(B)**, *Tg(meis2b-reporter);Tg(kdrl:NLS-mCherry)* **(C)**. (B) *Tg(meis2b-reporter)* is expressed in the atrial myocardium (arrows) (n=4). (C) *Tg(meis2b-reporter)* expression cannot be detected in endocardial cells in the atrium (arrows) (n=5). Scale bars: (A) 500µm, (B-C) 100µm.

5.12. Embryonic cardiac expression of *Tg(meis2b-reporter)* and the second heart field

At three dpf, the *Tg(meis2b-reporter)* is expressed in a small portion of the ventricle, near the AVC, in the distal part of the atrium and in the inflow tract. This asymmetric expression of *Tg(meis2b-reporter)* resembles the areas of the heart that are derived from the first heart field (Witzel, Jungblut et al. 2012, Guner-Ataman, Paffett-Lugassy et al. 2013, Mosimann, Panakova et al. 2015). It was hypothesized that if the cardiac *meis2b*-positive cells are derived from the FHF, then they should have a mutually exclusive expression pattern with respect to the cells derived from SHF. Therefore, the expression *Tg(meis2b-reporter)* at 48 hpf was compared to the expression pattern of Islet1 (Isl1), a SHF marker (Hami, Grimes et al. 2011, Witzel, Jungblut et al. 2012).

An antibody staining was performed against Isl1 on *Tg(meis2b-reporter)* hearts at 48 hpf. Around the inflow tract, where most of the Isl1-positive SHF derived cells are present, no correlation between the expression of Isl and *Tg(meis2b-reporter)* was observed (Fig. 5.14).

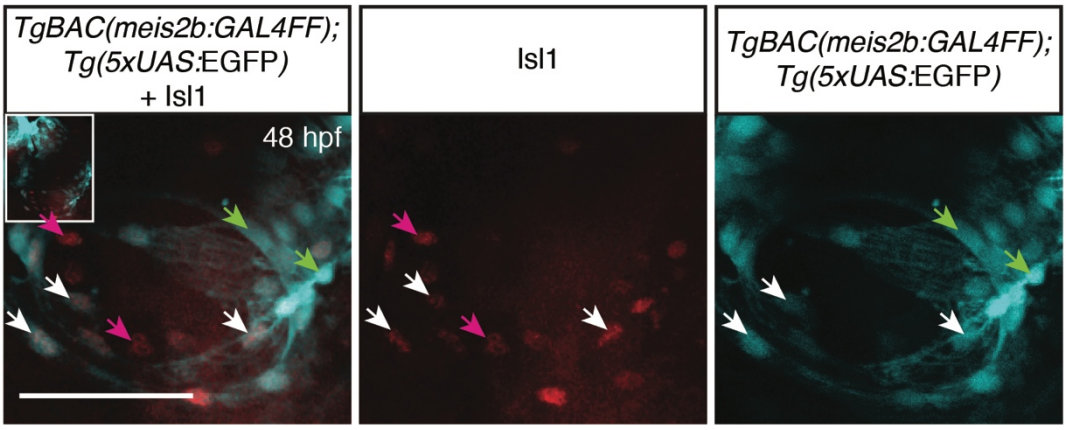

Figure 5.14. Expression of Isl1 and *Tg(meis2b-reporter)* do not correlate. Confocal projections of *Tg(meis2b-reporter)*;Isl1 hearts at 48 hpf in the inflow tract (n=7/7). *meis2b*+/Isl1+ (white arrows), *meis2b*+/Isl1- (green arrows) and *meis2b*-/Isl1+ (pink arrows) cardiomyocytes. Scale bar: 100µm.

5.13. Asymmetric expression of *Tg(meis2b-reporter)* is independent of second heart field contribution

To determine if the absence of SHF derived cells affect the expression of *Tg(meis2b-reporter)*, a morpholino against *isl1* was injected in *Tg(meis2b-reporter)*;*Tg(myl7:mCherry)* one-cell-stage embryos. At 48 hpf, the expression of *Tg(meis2b-reporter)* was not affected by the absence of SHF derived cardiomyocytes (Fig. 5.15 A-B).

isl1 is expressed in a variety of tissues in the zebrafish embryos and, like *meis2b*, it is also expressed in retinal cells in the eye (Nakayama, Miyake et al. 2008, Seth, Machingo et al. 2010). Interestingly, knockdown of *isl1* abolishes the expression of *Tg(meis2b-reporter)* in the retina at 48 hpf (Fig. 5.15 C-D), thus serving as an internal control of the function of the *isl1* morpholino. Altogether, these results indicate that asymmetric expression of *meis2b* is independent of SHF contribution.

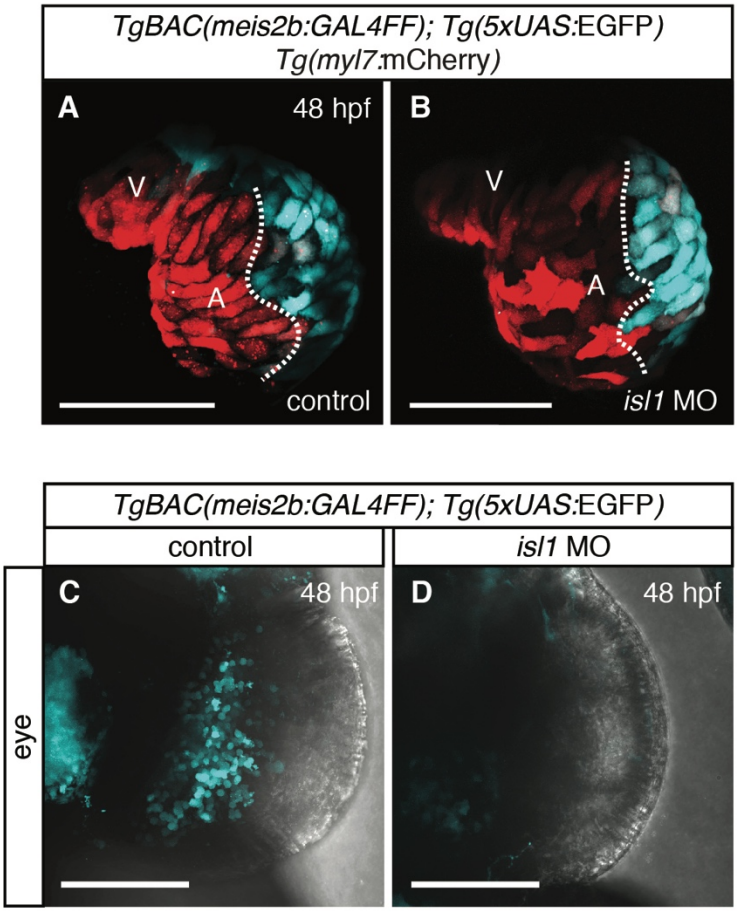

Figure 5.15. Cardiac expression of *Tg(meis2b-reporter)* is independent of SHF contribution. **(A-B)** Confocal projections of control and *isl1* MO injected 48 hpf *Tg(meis2b-reporter);Tg(myl7:mCherry)* hearts [white lines delineate *Tg(meis2b-reporter)* expression]. **(C-D)** Expression of *Tg(meis2b-reporter)* in retinal cells is lost in *isl1*

morphants, serving as an internal control of knockdown efficiency. A, Atrium; V, Ventricle. Scale bars: 100 μm.

5.14. Asymmetric expression of *Tg(meis2b-reporter)* is regulated by retinoic acid signaling

RA signaling plays a key role in anterior-posterior development in vertebrates. Previous works have reported that during gastrulation stages, RA signaling restricts the number of cardiomyocyte progenitors (Keegan, Feldman et al. 2005). Furthermore, in the ALPM, RA signaling regulates the anterior-posterior boundaries between the vascular, cardiomyocyte and forelimb progenitors. Whereby changes in the levels of retinoic acid lead to anterior or posterior shifts in the position of the cardiomyocyte progenitors at the expense of vascular and forelimb progenitors (Waxman, Keegan et al. 2008, Waxman and Yelon 2009, Rydeen and Waxman 2014). As *meis2b* expression shows an anterior-posterior asymmetry in the embryonic heart, the possibility of RA signaling affecting the expression pattern of *meis2b* was tested.

Tg(meis2b-reporter) embryos were dechorionated and treated before gastrulation at 40% epiboly with either 1μM DEAB (a known inhibitor of Aldh, the enzyme that produces RA) or with 0.1μM RA for 1 hour (Waxman, Keegan et al. 2008, Waxman and Yelon 2009).

Under control conditions, the *Tg(meis2b-reporter)*-positive is expressed in 55.1% (±7.6) of cardiomyocytes in the heart disc (Fig. 5.16). In contrast, RA signaling inhibition caused a significant reduction of myocardial progenitors expressing the *Tg(meis2b-reporter)*, where only 7.7% (±2.3) of the cardiomyocytes expressed the *Tg(meis2b-reporter)* and these *meis2b*-positive cells were limited to the posterior end of the heart disc. Embryos exposed to excess RA showed a significant expansion of the *Tg(meis2b-reporter)* expression throughout the cardiac disc, with 92.6% (±6.9) of the cardiomyocytes expressing the *Tg(meis2b-reporter)*, causing the loss of the anterior-posterior asymmetry that is defined by the expression of *Tg(meis2b-reporter)* in the heart disc.

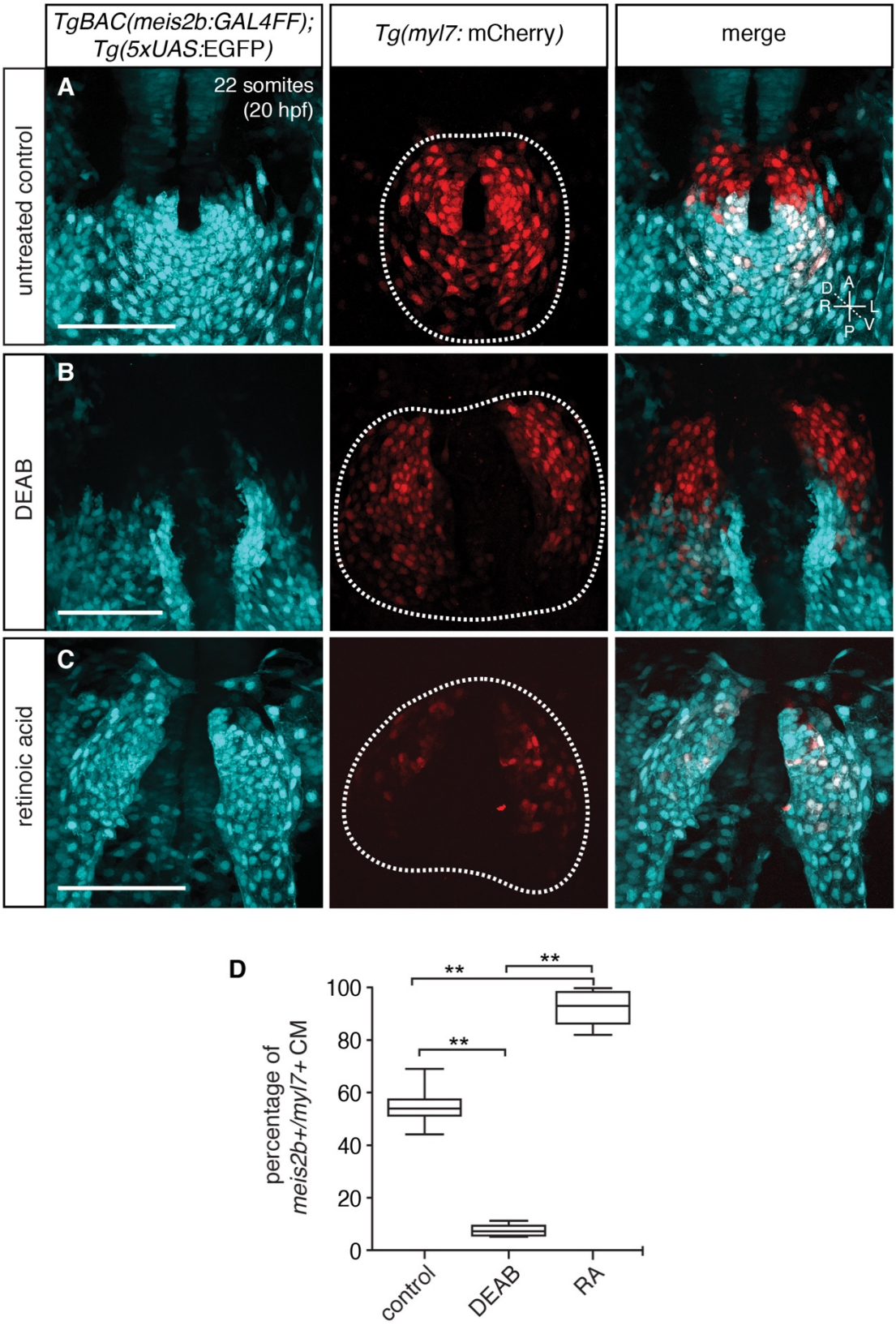

Figure 5.16. Early *Tg(meis2b-reporter)* cardiac expression is regulated by retinoic acid signaling. **(A)** *Tg(meis2b-reporter)* expression in control embryos at 22 somites stage (n=7/7). **(B)** *Tg(meis2b-reporter)* expression decreases and is confined to the most posterior part of the cardiac disc in DEAB treated embryos (n=5/5). **(C)** In embryos

treated with excess of RA, expression of *Tg(meis2b-reporter)* is expanded throughout the cardiac disc (n=5/5). **(D)** Percentage of cardiomyocytes expressing the *Tg(meis2b-reporter)* in the heart disc in control, DEAB and RA treated embryos. (A-C) White dotted lines delineate the cardiac disc. Scale bars: 100 μm. Significant differences compared to controls are indicated (t-test, **p<0.005); error bars indicate ±SD.

5.15. Retinoic acid signaling affects *Tg(meis2b-reporter)* expression during gastrulation

To determine the time window in which RA signaling affects the expression of the *Tg(meis2b-reporter)*, the embryos were exposed either to DEAB or to RA at 40% epiboly, 80% epiboly or at tailbud, and then collected at 17 somites stage, where the expression of *Tg(meis2b-reporter)* in bilateral heart fields starts to be noticeable.

In all cases, embryos treated with excess of RA showed increased expression of *Tg(meis2b-reporter)* throughout the body (Fig. 5.17). This effect was time-dependent, since the embryos that were incubated with exogenous RA at tailbud stage showed a minor increase in the expression of the *Tg(meis2b-reporter)* in comparison to the embryos treated at 40% epiboly. Consistent with previous reports (Stainier and Fishman 1992, Waxman and Yelon 2009), the embryos with increased RA displayed a mild posteriorization of the body, as well as small head and eyes.

Embryos treated with DEAB showed a reduced expression of *Tg(meis2b-reporter)* in the body compared to control. Similar to RA, the effects of DEAB were time-dependent as the embryos treated at tailbud showed a more expanded expression of *Tg(meis2b-reporter)* compared to those treated at 40% epiboly.

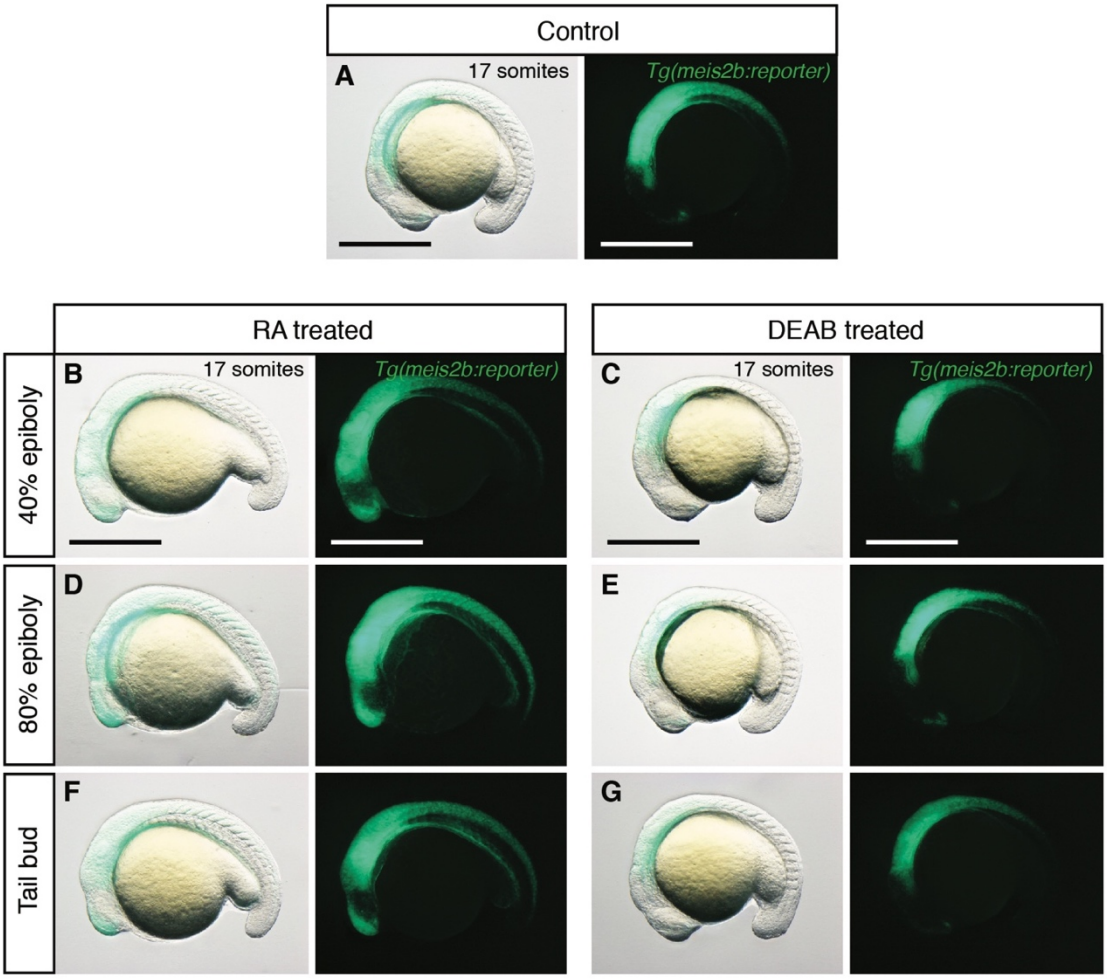

Figure 5.17. Retinoic acid signaling induces *Tg(meis2b-reporter)* expression in a time-dependent manner. Control embryos **(A)**. Embryos treated with exogenous RA (left panel) and embryos treated with DEAB (right panel) at 40% epiboly **(B-C)**, 80% epiboly **(D-E)** and tailbud stage **(F-G)**. Embryos treated with exogenous RA at tailbud stage showed expanded expression of the *Tg(meis2b-reporter)* in the body. Embryos treated with DEAB showed decreased expression of *Tg(meis2b-reporter)*. Scale bars: 100 μm.

5.16. Retinoic acid signaling regulates expression of *Tg(meis2b-reporter)* in the LPM

As previously mentioned, RA signaling is important in the maintenance of boundaries between the forelimb, myocardial and vascular progenitors in the LMP. Furthermore, an excess of RA signaling causes anterior shifts in the heart field, while reduction of RA signaling causes a posterior shift in the region occupied by the bilateral heart field in the LPM (Waxman, Keegan et al. 2008).

To determine how RA signaling affects the expression of *Tg(meis2b-reporter)* in the heart field in the LPM, *in situ* hybridization combined with antibody staining were performed on *Tg(meis2b-reporter)* embryos treated with either excess of RA or DEAB.

The whole-mount *in situ* hybridization was performed for two genes *myl7* and *ntl*. *myl7* marks the cardiomyocyte progenitors in the ALMP (Yelon, Horne et al. 1999), while *ntl* labels the notochord, therefore providing a point of reference for the anterior or posterior shifts of the heart field in the embryos treated with DEAB or RA (Waxman, Keegan et al. 2008). After the *in situ* hybridization, an antibody staining against GFP was performed, to recover the expression of *Tg(meis2b-reporter)*.

Consistent with previously published data, embryos that were treated with excess of RA showed an anterior shift of the heart field with respect to the notochord. In contrast, embryos with decreased RA signaling showed a posterior shift of the heart field in the ALMP (Fig. 5.18).

Using ImageJ, the percentage of the area of cardiomyocyte progenitors that express the *Tg(meis2b-reporter)* with respect to the entire heart field area was measured (% *meis2b*/*myl7* area). In control conditions, *Tg(meis2b-reporter)* is expressed in 64,17% (±4,87) of the entire heart field (Fig. 5.18A, H). In concordance with the previously shown data in this chapter, embryos exposed to excess of RA showed an increase in the percentage of *Tg(meis2b-reporter)*-positive cells in the heart field with respect to control embryos. This effect had a mild variation depending on the time of the start of the RA treatment: *Tg(meis2b-reporter)*-positive cells occupied 79,91% (±6,91), 75,17% (±2,33) or 61,12% (±3,53) of the heart disc upon RA treatment at 40% epiboly, 80% epiboly or tailbud stage, respectively (Fig. 5.18 B, D, F, H).

In embryos exposed to DEAB at 40% epiboly, 45,12% (±5,00) of the heart field expressed *Tg(meis2b-reporter)*; while those treated at 80% epiboly showed 56,26% (±10,07), and those treated at tailbud stage showed 68,44% (±8,86) of the heart field expressing the *Tg(meis2b-reporter)* (Fig. 5.18 C, E, G, H).

Altogether, these data confirm our previous results (Fig. 5.16): RA signaling affects the expression of *Tg(meis2b-reporter)* in the ALPM by regulating the anterior-posterior expression pattern of *meis2b*.

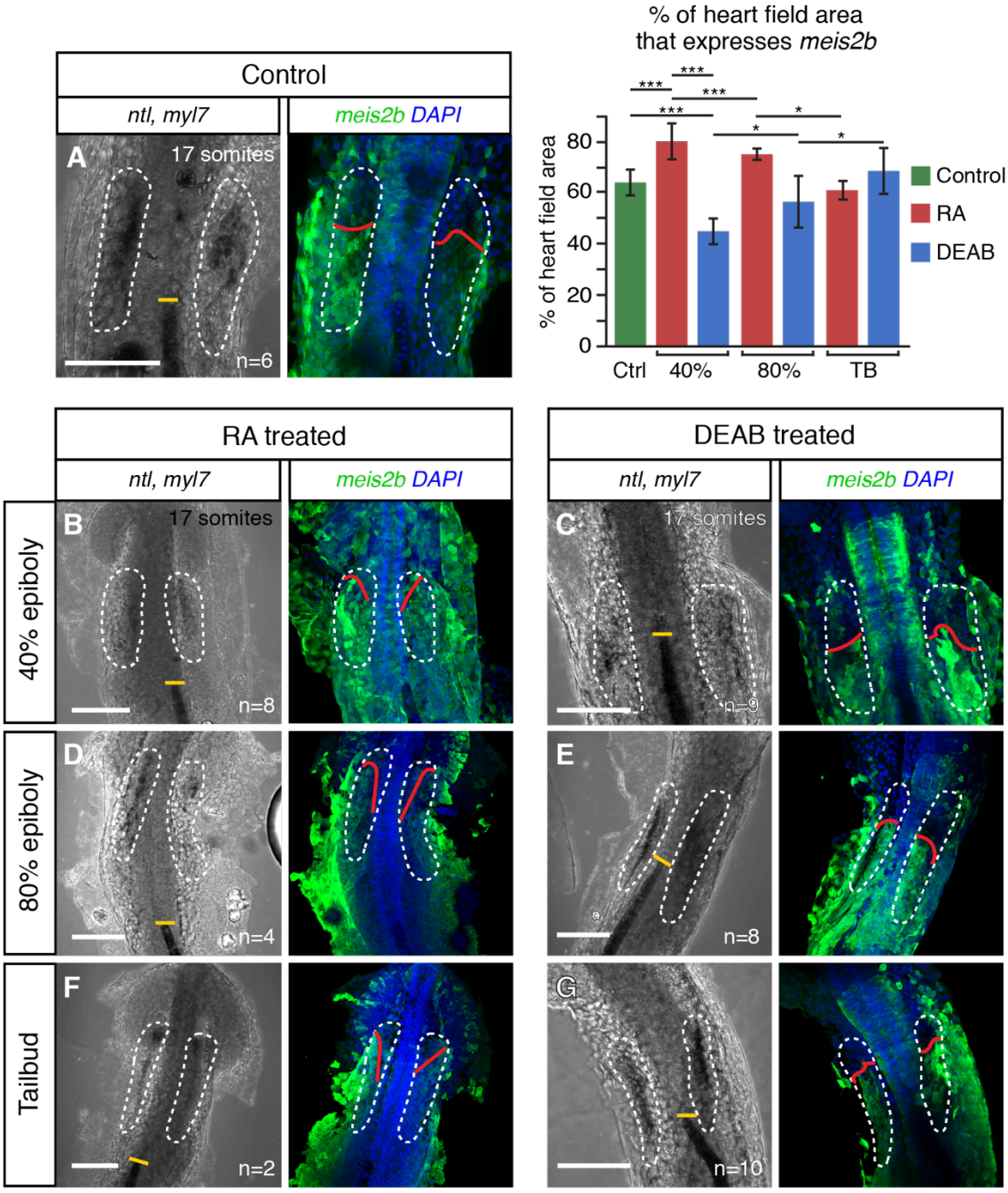

Figure 5.18. Retinoic acid signaling affects expression of *Tg(meis2b-reporter)* in the heart field. *In situ* hybridization and antibody staining on *Tg(meis2b-reporter)* embryos incubated with exogenous RA (left panel) and embryos incubated with DEAB (right panel) at 40% epiboly **(B-C)**, 80% epiboly **(D-E)** and tailbud stage **(F-G)**. **(H)** Quantification of the heart field area that expresses *Tg(meis2b-reporter)* in control conditions, in DEAB and RA treated embryos. Embryos incubated with excess of RA present anteriorly-expanded expression of *Tg(meis2b-reporter)* in the heart field, while those incubated with DEAB show a decreased expression of *Tg(meis2b-reporter)*. RA signaling significantly affects expression of *Tg(meis2b-reporter)* in the heart field before tailbud stage. White dotted lines delineate the heart field. Yellow lines indicate the end of the notochord. Scale bars: 100 μm. Significant differences are indicated (t-test, **p<0.005, *p<0.05); error bars indicate ±SD.

5.17. Meis2b downstream targets

Thus far, I have described the expression pattern of *meis2b* throughout development and the cardiac phenotype of the *meis2b* mutants. However, to further understand the role of Meis2b in the adult heart, it is necessary to study the possible downstream targets of Meis2b, which can help in determining the molecular mechanism through which Meis2b works.

In order to identify the possible downstream targets of Meis2b, expression profiles at different developmental stages were determined and compared: 48 hpf whole embryos of *meis2b*$^{-/-}$ to *meis2b*$^{+/+}$ siblings, whole hearts of three wpf *meis2b*$^{-/-}$ to *meis2b*$^{+/-}$ siblings, atria of three mpf *meis2b*$^{-/-}$ to *meis2b*$^{+/-}$ siblings, and ventricle to atrium of three mpf WT zebrafish (Table 5.3).

Depending on the stage, several subsequent criteria were established for the selection of the different genes. As there is no obvious phenotype that can be appreciated in the *meis2b*$^{-/-}$ at embryonic stages, only genes that were unchanged were further analyzed, with the sole exception of *meis2b*, which (as expected) is downregulated in the *meis2b*$^{-/-}$. As the atrial myocardial enlargement can be observed starting at three wpf until adulthood, only genes that were downregulated in the *meis2b*$^{-/-}$ were taken into account. Finally, as *meis2b* is exclusively expressed in the atrium of the adult heart, only atrial enriched genes were considered in the list of possible downstream targets of Meis2b.

Table 5.3. Comparison of expression profiles of *meis2b* mutants at different developmental stages.

genotype	*meis2b*$^{-/-}$	*meis2b*$^{-/-}$	*meis2b*$^{-/-}$	*meis2b*$^{+/+}$
	vs.	*vs.*	*vs.*	*vs.*
genotype	*meis2b*$^{+/+}$	*meis2b*$^{+/-}$	*meis2b*$^{+/-}$	*meis2b*$^{+/+}$
stage	48 hpf	3 wpf	3 mpf	3 mpf
tissue	whole embryo	whole heart	atrium	atrium vs. ventricle
fold change of target genes	unchanged or down	down regulated	down regulated	atrial enriched

The ten most significantly downregulated genes in the *meis2b* mutant atria are shown in Figure 5.19B. Interestingly, *pitx2*, a transcription factor important for asymmetric organ development, is significantly downregulated in the atria of *meis2b* mutant (Tessari, Pietrobon et al. 2008, Franco, Christoffels et al. 2014). Other candidates of interest are *col18a1*, which encodes a type of collagen, important in normal heart valve development in

mammals (Utriainen, Sormunen et al. 2004). *stab2*, which is a receptor that helps to degrade hyaluronic acid (HA) from the cardiac jelly; HA is especially important in trabeculation and in valve formation in the zebrafish and mouse (Camenisch, Spicer et al. 2000, Walsh and Stainier 2001, Falkowski, Schledzewski et al. 2003).

Comparing this data set to previously published data, the list of the top 10 downregulated genes in the *meis2b* mutant heart was further narrowed down to 3 genes (*meis2b*, *pitx2* and *stab2*). According to ChIPseq data from E11.5 mouse embryos, these genes three are probably directly regulated by Meis2b, as they contain a MEIS1/2 binding site near their enhancer regions (Penkov, Mateos San Martin et al. 2013).

The results obtained by the microarray were further confirmed by RT-qPCR. The $\log_2$ of the fold change for *pitx2c* in 3 mpf atria of *meis2b*$^{-/-}$ to *meis2b*$^{+/-}$ siblings was -4,73 (±0,37). For *col18a1* was -1,36 (±1,08) and for *stab2* was -1,33 (±0,79) (Fig. 5.19C).

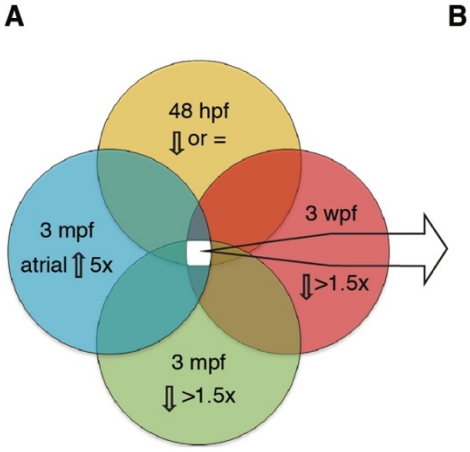

B

gene	FC in *meis2b*$^{-/-}$ vs *meis2b*$^{+/-}$ atria	MEIS1/2 cis reg. binding site
si:dkey76i15.1	-4.55	-
meis2b	-3.34	+
pitx2	-2.77	+
star	-2.28	-
plekhs1	-2.03	-
mia	-1.97	-
dact2	-1.75	-
cthrc1a	-1.62	-
stab2	-1.58	+
col18a1	-1.57	-

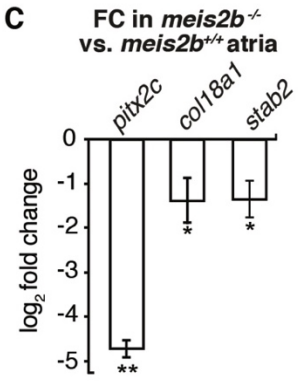

Figure 5.19. Possible downstream targets of Meis2b. **(A)** selection criteria of the candidate genes indicating the fold change for each condition. **(B)** Top ten most downregulated genes in the atria of adult *meis2b* mutant hearts. **(C)** Validation by RT-qPCR of the fold change values obtained by the microarray for *pitx2c*, *col18a1* and *stab2*. Significant differences compared to *meis2b*$^{+/+}$ are indicated (t-test, **p<0.005, *p<0.05); error bars indicate ±SD.

5.17.1 Absence of *meis2b* does not affect cardiac hyaluronic acid distribution

Stabilin 2 (Stab2) is a transmembrane glycoprotein that clears molecules such as hyaluronic acid (Zhou, McGary et al. 2003). HA is a very important component of the cardiac jelly, which is fundamental in heart development since it allows signaling between the endocardium and myocardium, as reviewed by (Peal, Lynch et al. 2011). Furthermore, HA is also required for endothelial to mesenchymal transition (EMT) and heart valve formation in zebrafish and mouse (Stainier, Fouquet et al. 1996, Camenisch, Spicer et al. 2000, Walsh and Stainier 2001). However, besides previous reports showing the importance of HA in EMT during zebrafish heart regeneration (Lagendijk, Szabo et al. 2013, Missinato, Tobita et al. 2015), little is known about the function of HA in the adult heart.

It was hypothesized that reduction of *stab2* in the atrium of *meis2b* mutants would lead to a decrease in HA clearance, which would translate into an accumulation of HA or a change in the distribution of HA in the heart. Therefore, five hearts of adult *meis2b* mutants and WT siblings were extracted and HA was detected through staining of a Hyaluronic Acid Binding Protein (HABP) (Fig. 5.20). No difference in the distribution of atrial HA was observed between the *meis2b* mutant and WT siblings. Additionally, the HABP staining in the atrioventricular valve was not significantly affected, indicating that HA levels and distribution are not affected in the absence of *meis2b*. Thus, the study of *stab2* as a possible target of Meis2b was not pursued.

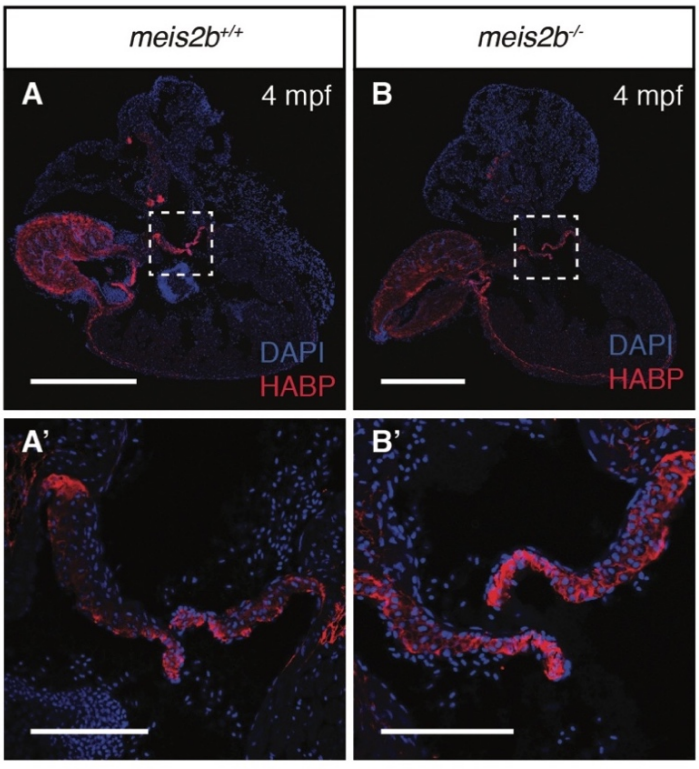

Figure 5.20. Hyaluronic acid is not affected in the heart of adult *meis2b* mutant. Confocal projections of 4 mpf *meis2b*$^{-/-}$ **(A-A')** and WT sibling **(B-B')** with Hyaluronic acid and DAPI staining show no difference in the distribution of HA in the heart or in the valves. White dotted squares indicate the atrioventricular valves. Scale bars: (A-B) 500μm, (A'-B') 100μm.

5.17.2. *pitx2* and *meis2b* colocalize in the left side of the mature atrium

As mentioned in the previous chapter, Pitx2 is a transcription factor which is important in the asymmetric development of the heart and guts in mammals and in zebrafish (Ryan, Blumberg et al. 1998). In the mammalian heart, *Pitx2* is exclusively expressed in the left atrium and has been extensively associated with cardiac septal defects, sinoatrial node formation and maintenance of L-R atrial identity (Tessari, Pietrobon et al. 2008, Wang, Klysik et al. 2010, Franco, Christoffels et al. 2014).

Since *pitx2* is a master regulator of L-R asymmetry that is expressed in the left atrium in higher vertebrates and is significantly downregulated in the hearts of adult *meis2b*$^{-/-}$, the next step was to determine the expression pattern of *pitx2* in the heart in relation to *meis2b*. Since *pitx2* expression levels are low in the adult atrium and conventional *in situ* hybridization could not accurately detect *pitx2* expression pattern, a highly sensitive ISH technology called RNAScope was employed.

Interestingly, *pitx2* transcripts were found to largely colocalize with *Tg(meis2b-reporter)* in five wpf hearts. These results reveal an asymmetrical expression of *pitx2* and for *meis2b* in the zebrafish heart, which are restricted to the left myocardial compartment of the zebrafish atrium (Fig. 5.21).

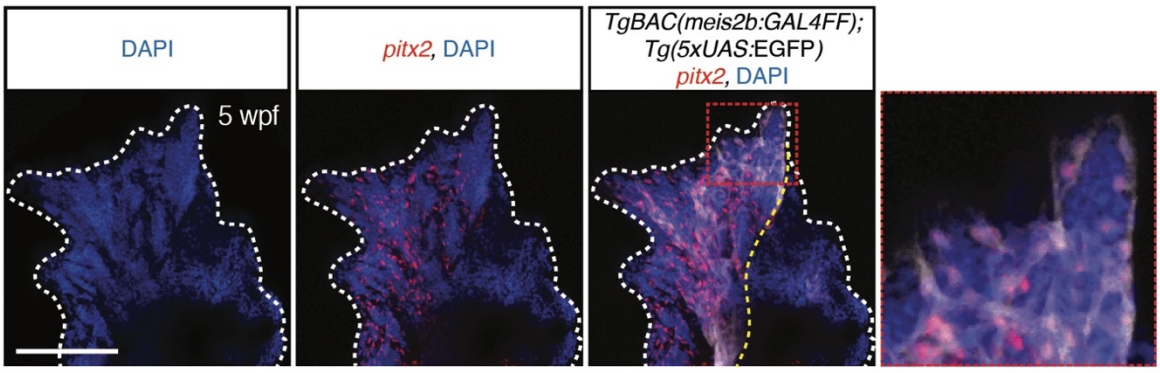

Figure 5.21. *pitx2* and *Tg(meis2b-reporter)* are co-expressed in the left half of the mature atrium. Fluorescent *in situ* hybridization (RNAscope) for *pitx2* expression on a 5 wpf

Tg(meis2b-reporter) zebrafish atrium. White dotted lines delineate the atrium; yellow lines delineate *Tg(meis2b-reporter)* expression. Scale bar: 100 µm.

To further prove that *meis2b* and *pitx2* are significantly enriched in the left side of the atrium, the hearts of adult *Tg(meis2b-reporter)* were dissected and divided into the *Tg(meis2b-reporter)*-positive and the *Tg(meis2b-reporter)*- compartments. cDNA was synthesized from the total RNA from both compartments, and the expression levels of *pitx2* and *meis2b* were determined by RT-qPCR. The results show that in the *Tg(meis2b-reporter)*-positive atrial compartment, the $\log_2$ of the fold change for *meis2b* is 2,56 and 1,37 for *pitx2* (Figure 5.22). Indicating that *pitx2* and *meis2b* are higher expressed in the *Tg(meis2b-reporter)*-positive compartment compared to the *Tg(meis2b-reporter)*-negative compartment.

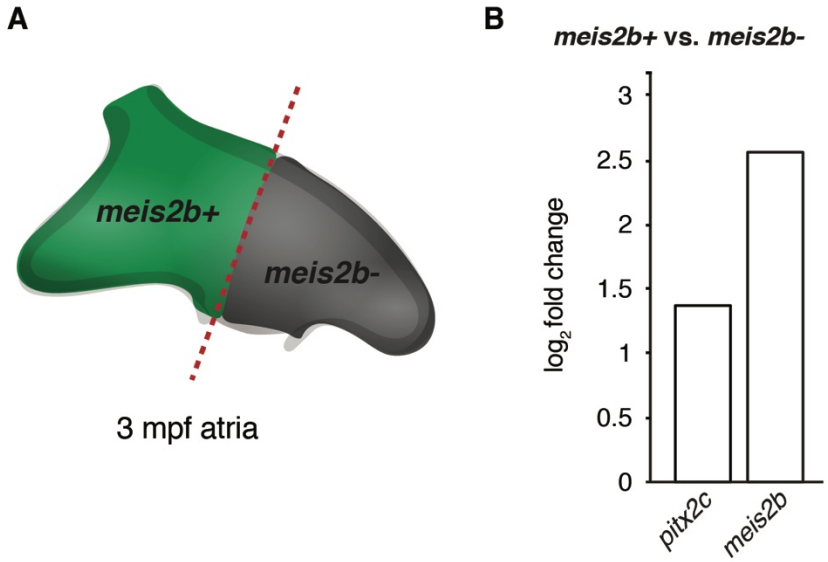

Figure 5.22. *pitx2* and *meis2b* transcripts are enriched in the *Tg(meis2b-reporter)*-positive compartment. **(A)** Schematic representation of *Tg(meis2b-reporter)* adult heart and the *Tg(meis2b-reporter) positive* and *negative* compartments. Red dotted line shows the point of the dissection of the atria, in the boundary between *Tg(meis2b-reporter)*-positive and negative halves. **(B)** $\log_2$ of the fold change of *meis2b* and *pitx2* expressions, obtained by RT-qPCR.

To summarize, this study reveals that both *meis2b* and *pitx2* show asymmetric expression patterns and are both expressed on the left side of the atrium, dividing the single zebrafish atrium into two distinct transcriptional compartments. Furthermore, the cardiac *pitx2* expression is significantly downregulated in *meis2b* mutants. Additionally, published CHIP-seq data show that *Pitx2* contains a MEIS1/2 binding site (Penkov, Mateos San Martin

et al. 2013). Altogether these results suggest that *Meis2b* can directly regulate cardiac expression of *pitx2*, a key regulator in asymmetric heart development.

VI. Discussion

6.1. The relationship between atrial left-right asymmetry in the zebrafish and in the mammalian heart

The cardiovascular systems of mammals and teleost are very different. The mammalian heart is composed of four chambers, with two atria and two ventricles. Due to the function of each cardiac chamber, the mammalian heart can be divided into a left and a right heart: the right half (right atrium and ventricle) receives the deoxygenated blood from the body and pushes it into the pulmonary circuit. After the blood is oxygenated, it enters the left heart (left atrium and ventricle) and then is pumped into the systemic circuit for the transport of oxygen to the body tissues (Vander, Sherman et al. 2001). Furthermore, the ventricular morphology is also very different from the atrial morphology, which allows each chamber to perform a particular function.

There are also morphological and functional differences between the atria, for example: the right atria (but not the left) has the sinoatrial node, which originates the heartbeat. Additionally, these differences can also be observed at the level of gene expression; for example, the left atrium expresses *Pitx2*, a known regulator of cardiac L-R development and of left atrial identity (Franco and Campione 2003, Tessari, Pietrobon et al. 2008, Franco, Chinchilla et al. 2012). Therefore, we can say that, in the mammalian heart, the two atria exhibit different morphology and functions, and asymmetric gene expression profiles.

In contrast, zebrafish possess two-chambered hearts, with only one ventricle and one atrium. Until now, no L-R asymmetry had been described for each cardiac chamber. Instead, it has been reported that L-R asymmetric signals control cardiac jogging and looping (de Campos-Baptista, Holtzman et al. 2008, Smith, Chocron et al. 2008, Bakkers, Verhoeven et al. 2009), and that the FHF and SHF would contribute to cell heterogeneity within each chamber (de Pater, Clijsters et al. 2009, Zhou, Cashman et al. 2011, Liu and Stainier 2012, Witzel, Jungblut et al. 2012, Guner-Ataman, Paffett-Lugassy et al. 2013).

This work presents evidence of an asymmetric gene expression pattern in the single atrium of the teleost heart. This asymmetry is characterized by the differential expression of *meis2b* and *pitx2* in the atrial myocardium. In the mature heart, *pitx2* expression greatly overlaps with *meis2b* expression, which indicates the existence of two different transcriptional compartments in the atrium, a *meis2b*-positive and a *meis2b*-negative compartment. The

meis2b+/*pitx2*+ atrial compartment in the zebrafish can be associated to the left atrium in higher vertebrates, since they both show an enrichment in the expression of *pitx2* (Franco and Campione 2003), which confers a "left atrial identity" to the *meis2b*+/*pitx2*+ atrial compartment.

Furthermore, during evolution, in the transition from aquatic to terrestrial life, one of the most significant and evolutionary advantageous adaptations was the separation of the pulmonary and systemic circulation (Liu and Stainier 2012), and this change involved the septation of the cardiac chambers. However, how atrial septation arose, and how the two-chambered heart of teleost transitioned to the three-chambered heart of amphibians, and finally to the four-chambered hearts of mammalians are still unknown. Nevertheless, this study presents evidence that before the physical separation of the atria, a L-R asymmetry was already present. In addition, these results suggest that atrial septation did not happen *de novo*, but instead, a pre-existing asymmetric pattern can be found in teleost hearts.

6.2. Meis2b could mediate left-right atrial identity through Pitx2

Previous work in mouse has shown that MEIS1/2 can bind near the *Pitx2* enhancer region (Penkov, Mateos San Martin et al. 2013), indicating that *Pitx2* could be a direct downstream target of MEIS1/2. Interestingly, *pitx2* and *meis2b* expression patterns overlap in the left side of the mature zebrafish atrium, and *pitx2* is downregulated in the atria of adult *meis2b*$^{-/-}$ zebrafish. Altogether, these results indicate that *pitx2* could be a direct downstream target of Meis2b in the zebrafish.

Mutations in *Pitx2* in humans and mouse lead to atrial fibrillation due to the misregulation of PITX2 downstream target genes such as *Shox2*, which is involved in the formation of the sinoatrial node (Mommersteeg, Hoogaars et al. 2007, Espinoza-Lewis, Yu et al. 2009). Interestingly, *meis2b* mutant fish also show defects in cardiac conduction (data obtained in collaboration with Prof. Dr. Rima Arnaout. This result has not been published, but is included in Guerra et al., manuscript in preparation), which suggests that Meis2b can act through Pitx2 to properly pattern the cardiac conduction system, possibly involving the Pitx2 downstream target *shox2*. Notably, in humans, the cardiac malformations that result from mutations in *MEIS2* and *PITX2* are similar (Franco, Christoffels et al. 2014, Louw, Corveleyn et al. 2015), which suggest that MEIS2 and PITX2 work together in the same

genetic pathway in mammals. These results would suggest that the genetic pathways of *Meis2* and *Pitx2* are conserved across species.

Furthermore, the progressive atrial chamber enlargement observed in the *meis2b* mutants, has also been observed in *Pitx2* mutant mice, where atrial myocardial proliferation is significantly increased (Chinchilla, Daimi et al. 2011, Lozano-Velasco, Chinchilla et al. 2011). It should be noted that although it is possible that other pathways may be stimulating atrial proliferation or hypertrophy in the *meis2b* mutant hearts, it is likely that the downregulation of *pitx2* is influencing the abnormal atrial growth observed as a mechanism of maintenance of the arrhythmogenic process (Chinchilla, Daimi et al. 2011).

Taken together, the lack of *meis2b*, in the *meis2b* mutants, could be interpreted as the loss of asymmetry between the two atrial compartments of the zebrafish heart. It is possible that, in the zebrafish heart, the role of Meis2b is to mediate the identity of the left atrial compartment through regulating the cardiac expression of *pitx2*.

Additionally, one of the genes that was most downregulated in the hearts of *meis2b*$^{-/-}$ and that may be a potential direct target of Meis2b is *stab2*, a transmembrane glycoprotein that clears hyaluronic acid (Zhou, McGary et al. 2003). However, no changes in HA distribution in the hearts of *meis2b*$^{-/-}$ were observed (Fig. 5.20); which suggests that the reduction in the atrial expression of *stab2* is not significant enough to induce an obvious change in the distribution and levels of HA, and that Meis2b is not the only factor that regulates cardiac *stab2* expression.

6.3. Retinoic acid signaling regulates early compartmentalization of the cardiac disc

In the ALMP, RA signaling is important in maintaining the boundaries between the vascular, cardiomyocyte and forelimb progenitors (Waxman, Keegan et al. 2008, Rydeen and Waxman 2014). Imbalance in the levels of RA during gastrulation can alter the number of cardiomyocyte progenitors. More specifically, the level of RA is inversely proportional to the number of cardiomyocytes (Keegan, Feldman et al. 2005), which is evident even before the fusion of the bilateral heart fields.

A decrease in RA creates a surplus of cardiomyocytes, but a significant decrease in the number of *Tg(meis2b-reporter)*-expressing cells. In contrast, an excess of RA results in a decrease in the number of cardiomyocytes, but a significant increase in the number of *Tg(meis2b-reporter)*-expressing cardiomyocytes (Fig. 5.15-18). Therefore, a loss of A-P

asymmetric pattern is lost when RA levels are misregulated, which indicates that RA signaling regulates early compartmentalization of the cardiac disc by inducing the expression of *meis2b* in the cardiomyocytes.

Several publications have reported that *Meis1* and *Meis2* are RA signaling targets (Oulad-Abdelghani, Chazaud et al. 1997, Savory, Edey et al. 2014) in mouse and chick (Mercader, Leonardo et al. 1999, Mercader, Leonardo et al. 2000, Fernandes-Silva, Vaz-Cunha et al. 2017). These data support the observation that *meis2b* expression can be regulated by RA signaling in zebrafish, although further investigation is needed to determine if *meis2b* is directly controlled by RA signaling.

During the experiments, it became evident that the effect of excess RA seems stronger than the effect of adding DEAB (inhibiting Aldh enzymes). It is possible that adding exogenous RA has a stronger effect because RA is directly integrated in the pathway; hence, a faster and more dramatic effect can be achieved. Additionally, it is likely that inhibition of Aldh enzymes with DEAB may not be as efficient as other RA signaling inhibitors such as BMS, which antagonizes RA by binding the RA receptors without activating them (Schulze, Clay et al. 2001, Waxman, Keegan et al. 2008).

6.4. The role of Meis2b during embryonic cardiac patterning and in the maintenance of left-right atrial asymmetry in adult zebrafish heart

Paige et al. reported that knockdown of *meis2b* leads to delayed cardiac development, failure of the heart to loop and slower heart rate (Paige, Thomas et al. 2012). However, these results significantly differ from the observations in this study; *meis2b* mutants do not show evident cardiac formation delay or cardiac looping defects (Fig. 5.2). Although Paige et al. showed that the morpholino effectively blocks *meis2b* pre-mRNA splicing, the possibility that the *meis2b* morphant phenotype is due to an off-target effect cannot be excluded (Bedell, Westcot et al. 2011, Blum, De Robertis et al. 2015).

The levels of *meis2b* transcripts are very low in *meis2b* mutants (Fig. 5.19), suggesting a significant loss-of-function of *meis2b* in the zebrafish. However, even though *meis2b* expression pattern during heart formation reveals an unknown previously-uncharacterized anterior-posterior asymmetry, no evident defect is observed during embryonic heart formation. This observation suggests that Meis2b function during heart development is not essential, and other factors may be needed in the A-P patterning of the heart. It is possible

that Meis2a and Meis2b could have redundant functions during heart development, as the DNA sequence of both paralogues are highly conserved (Force, Lynch et al. 1999, Longobardi, Penkov et al. 2014); and that *meis2a* expression can also be regulated by RA signaling.

In contrast to what is observed in the embryo, adult *meis2b*$^{-/-}$ zebrafish exhibit a cardiac phenotype, characterized by a progressive atrial enlargement (which produces pericardial bulging in the fish) and cardiac conduction defects. Furthermore, it is clear that the *Tg(meis2b-reporter)* reveals a previously unknown L-R asymmetry in the atrium, which, as discussed above, could be regulated together with Pitx2.

As previously mentioned in the Introduction section, the Meis proteins are important interaction partners of Pbx and Hox transcription factors (Longobardi, Penkov et al. 2014, Merabet and Mann 2016). It has been suggested that, during heart development in mouse, MEIS1 and PBX1 work together, and the absence of one of them causes VSD and overriding aorta (Stankunas, Shang et al. 2008). Therefore, it would be interesting to determine which Meis2b interaction partners are important for the role of Meis2b in the establishment of the atrial L-R asymmetry and patterning of the cardiac conduction system.

Furthermore, published data revealed that in mouse, MEIS1/2 could bind near its own enhancer region (Fig. 5.19) (Penkov, Mateos San Martin et al. 2013), suggesting that MEIS1/2 may regulate its expression via a feedback loop.

In summary, the current research focuses on the cardiac function of the transcription factor Meis2b, and reveals an unexpected L-R asymmetry in the single atrium of the zebrafish heart. The evolution of the cardiac compartments from the simple two-chambered heart of the teleost to the four-chambered heart of mammals, remains a puzzling problem, whose evolutionary, developmental and genetic bases still have to be discovered. However, the results obtained in this study suggest that before atrial septation and the emergence of the two physically separated left and right atria, there was a pre-existing transcriptional pattern present in the heart of the teleost fish, which confers an individual identity to the two transcriptional compartments, and includes the participation of genes involved in the establishment of cardiac L-R asymmetry.

Furthermore, this study also reinforces the idea that proper heart formation requires the orchestration of different mechanisms and cell lineages, which include the first and

secondary heart fields, L-R signaling pathways and, importantly anterior-posterior patterning. The latter is mainly controlled by RA signaling, and can also be evidenced by the expression of *meis2b* during heart development.

VII. Conclusion

- The present study shows the first evidence of the existence of a L-R atrial asymmetric pattern in the zebrafish heart, which preceded the evolutionary emergence of the atrial septum in higher vertebrates. This L-R asymmetry can be evidenced by the expression pattern of *meis2b* and divides the atrium into two distinct transcriptional compartments.
- Initial anterior-posterior patterning of the cardiac disc in the zebrafish is regulated by RA signaling.
- Loss of *meis2b* function leads to progressive chamber enlargement and cardiac conduction defects.
- *pitx2* and *meis2b* expression patterns overlap in the left atrial compartment. Furthermore, Meis2b could directly regulate the expression *pitx2* in the heart.

7.1. Future Directions

A research project never ends, as soon as a question is answered many more questions and experiments come to mind. Scientific research requires dedication, discipline, curiosity and vocation. Therefore, this section is dedicated to summarizing some ideas of experiments that can be done to answer some questions derived from the results presented in this dissertation:

- *meis2b* overexpression: This project has revealed the cardiac defects originated from a mutation in *meis2b*. However, it will be interesting to investigate what happens in the opposite case, regarding atrial cardiomyocyte proliferation, expression of Meis2b downstream targets (*pitx2*), cardiac embryonic phenotype and cardiac conduction. This is an ongoing investigation, and several *meis2b* overexpression constructs were synthesized; at the time of submission of this Thesis dissertation to the Johann Wolfgang Goethe University, the injected fish are being screened for founders.
- MEIS2 in heart development and asymmetry in mammals: Mammals only have one *MEIS2* orthologue; however, several splice isoforms are derived from *MEIS2* (Dunwoodie, Rodriguez et al. 1998, Longobardi, Penkov et al. 2014). It would be useful to determine which isoforms are expressed in the mouse heart, if they are asymmetrically expressed, and if they can also regulate cardiac *Pitx2* expression.

- Meis2b interaction partners during heart development: As previously mentioned, Meis1 and 2 are important interaction partners of Pbx and Hox transcription factors. It would be interesting to dissect how these interactions contribute to the cardiac phenotype observed in the *meis2b* mutants in this study.
- Meis2a in heart development: In contrast to *meis2b*, *meis2a* is expressed in both atrium and ventricle (with a slight ventricular enrichment). Due to the interesting anterior-posterior expression pattern of *meis2b* in the early stages of cardiac development, but an absence of phenotype in the embryonic heart, it is possible that Meis2a, at least in part, compensate for the loss of Meis2b. Therefore, close evaluation of heart development in *meis2a* and *meis2b* mutants could provide some answers in this matter.

VIII. References

Amin, S., I. J. Donaldson, D. A. Zannino, J. Hensman, M. Rattray, M. Losa, F. Spitz, F. Ladam, C. Sagerstrom and N. Bobola (2015). "Hoxa2 selectively enhances Meis binding to change a branchial arch ground state." Dev Cell **32**(3): 265-277.

Anderson, R. H., S. Webb, N. A. Brown, W. Lamers and A. Moorman (2003). "Development of the heart: (2) Septation of the atriums and ventricles." Heart **89**(8): 949-958.

Ang, Y. S., R. N. Rivas, A. J. Ribeiro, R. Srivas, J. Rivera, N. R. Stone, K. Pratt, T. M. Mohamed, J. D. Fu, C. I. Spencer, N. D. Tippens, M. Li, A. Narasimha, E. Radzinsky, A. J. Moon-Grady, H. Yu, B. L. Pruitt, M. P. Snyder and D. Srivastava (2016). "Disease Model of GATA4 Mutation Reveals Transcription Factor Cooperativity in Human Cardiogenesis." Cell **167**(7): 1734-1749 e1722.

Asakawa, K., M. L. Suster, K. Mizusawa, S. Nagayoshi, T. Kotani, A. Urasaki, Y. Kishimoto, M. Hibi and K. Kawakami (2008). "Genetic dissection of neural circuits by Tol2 transposon-mediated Gal4 gene and enhancer trapping in zebrafish." Proc Natl Acad Sci U S A **105**(4): 1255-1260.

Baker, K., N. G. Holtzman and R. D. Burdine (2008). "Direct and indirect roles for Nodal signaling in two axis conversions during asymmetric morphogenesis of the zebrafish heart." Proc Natl Acad Sci U S A **105**(37): 13924-13929.

Bakkers, J. (2011). "Zebrafish as a model to study cardiac development and human cardiac disease." Cardiovasc Res **91**(2): 279-288.

Bakkers, J., M. C. Verhoeven and S. Abdelilah-Seyfried (2009). "Shaping the zebrafish heart: from left-right axis specification to epithelial tissue morphogenesis." Dev Biol **330**(2): 213-220.

Bedell, V. M., S. E. Westcot and S. C. Ekker (2011). "Lessons from morpholino-based screening in zebrafish." Brief Funct Genomics **10**(4): 181-188.

Begemann, G., T. F. Schilling, G. J. Rauch, R. Geisler and P. W. Ingham (2001). "The zebrafish neckless mutation reveals a requirement for raldh2 in mesodermal signals that pattern the hindbrain." Development **128**(16): 3081-3094.

Bisgrove, B. W., J. J. Essner and H. J. Yost (1999). "Regulation of midline development by antagonism of lefty and nodal signaling." Development **126**(14): 3253-3262.

Blum, M., E. M. De Robertis, J. B. Wallingford and C. Niehrs (2015). "Morpholinos: Antisense and Sensibility." Dev Cell **35**(2): 145-149.

Bruneau, B. G. (2008). "The developmental genetics of congenital heart disease." Nature **451**(7181): 943-948.

Bruneau, B. G., G. Nemer, J. P. Schmitt, F. Charron, L. Robitaille, S. Caron, D. A. Conner, M. Gessler, M. Nemer, C. E. Seidman and J. G. Seidman (2001). "A murine model of Holt-Oram syndrome defines roles of the T-box transcription factor Tbx5 in cardiogenesis and disease." Cell **106**(6): 709-721.

Buckingham, M., S. Meilhac and S. Zaffran (2005). "Building the mammalian heart from two sources of myocardial cells." Nat Rev Genet **6**(11): 826-835.

Burglin, T. R. (1997). "Analysis of TALE superclass homeobox genes (MEIS, PBC, KNOX, Iroquois, TGIF) reveals a novel domain conserved between plants and animals." Nucleic Acids Res **25**(21): 4173-4180.

Bussmann, J., J. Bakkers and S. Schulte-Merker (2007). "Early endocardial morphogenesis requires Scl/Tal1." PLoS Genet **3**(8): e140.

Cai, C. L., X. Liang, Y. Shi, P. H. Chu, S. L. Pfaff, J. Chen and S. Evans (2003). "Isl1 identifies a cardiac progenitor population that proliferates prior to differentiation and contributes a majority of cells to the heart." Dev Cell **5**(6): 877-889.

Camenisch, T. D., A. P. Spicer, T. Brehm-Gibson, J. Biesterfeldt, M. L. Augustine, A. Calabro, Jr., S. Kubalak, S. E. Klewer and J. A. McDonald (2000). "Disruption of hyaluronan synthase-2 abrogates normal cardiac morphogenesis and hyaluronan-mediated transformation of epithelium to mesenchyme." J Clin Invest **106**(3): 349-360.

Campione, M., M. A. Ros, J. M. Icardo, E. Piedra, V. M. Christoffels, A. Schweickert, M. Blum, D. Franco and A. F. Moorman (2001). "Pitx2 expression defines a left cardiac lineage of cells: evidence for atrial and ventricular molecular isomerism in the iv/iv mice." Dev Biol **231**(1): 252-264.

Capdevila, J., T. Tsukui, C. Rodriquez Esteban, V. Zappavigna and J. C. Izpisua Belmonte (1999). "Control of vertebrate limb outgrowth by the proximal factor Meis2 and distal antagonism of BMPs by Gremlin." Mol Cell **4**(5): 839-849.

Chang, C. P., Y. Jacobs, T. Nakamura, N. A. Jenkins, N. G. Copeland and M. L. Cleary (1997). "Meis proteins are major in vivo DNA binding partners for wild-type but not chimeric Pbx proteins." Mol Cell Biol **17**(10): 5679-5687.

Chen, C. P., S. P. Lin, F. J. Tsai, S. R. Chern, C. C. Lee and W. Wang (2008). "A 5.6-Mb deletion in 15q14 in a boy with speech and language disorder, cleft palate, epilepsy, a ventricular septal defect, mental retardation and developmental delay." Eur J Med Genet **51**(4): 368-372.

Cheng, S. K., F. Olale, A. H. Brivanlou and A. F. Schier (2004). "Lefty blocks a subset of TGFbeta signals by antagonizing EGF-CFC coreceptors." PLoS Biol **2**(2): E30.

Chi, N. C., R. M. Shaw, S. De Val, G. Kang, L. Y. Jan, B. L. Black and D. Y. Stainier (2008). "Foxn4 directly regulates tbx2b expression and atrioventricular canal formation." Genes Dev **22**(6): 734-739.

Chinchilla, A., H. Daimi, E. Lozano-Velasco, J. N. Dominguez, R. Caballero, E. Delpon, J. Tamargo, J. Cinca, L. Hove-Madsen, A. E. Aranega and D. Franco (2011). "PITX2

insufficiency leads to atrial electrical and structural remodeling linked to arrhythmogenesis." Circ Cardiovasc Genet **4**(3): 269-279.

Chocron, S., M. C. Verhoeven, F. Rentzsch, M. Hammerschmidt and J. Bakkers (2007). "Zebrafish Bmp4 regulates left-right asymmetry at two distinct developmental time points." Dev Biol **305**(2): 577-588.

Crowley, M. A., L. K. Conlin, E. H. Zackai, M. A. Deardorff, B. D. Thiel and N. B. Spinner (2010). "Further evidence for the possible role of MEIS2 in the development of cleft palate and cardiac septum." Am J Med Genet A **152A**(5): 1326-1327.

de Campos-Baptista, M. I., N. G. Holtzman, D. Yelon and A. F. Schier (2008). "Nodal signaling promotes the speed and directional movement of cardiomyocytes in zebrafish." Dev Dyn **237**(12): 3624-3633.

de la Motte, C. A. and J. A. Drazba (2011). "Viewing hyaluronan: imaging contributes to imagining new roles for this amazing matrix polymer." J Histochem Cytochem **59**(3): 252-257.

de Pater, E., L. Clijsters, S. R. Marques, Y. F. Lin, Z. V. Garavito-Aguilar, D. Yelon and J. Bakkers (2009). "Distinct phases of cardiomyocyte differentiation regulate growth of the zebrafish heart." Development **136**(10): 1633-1641.

Dong, P. D., C. A. Munson, W. Norton, C. Crosnier, X. Pan, Z. Gong, C. J. Neumann and D. Y. Stainier (2007). "Fgf10 regulates hepatopancreatic ductal system patterning and differentiation." Nat Genet **39**(3): 397-402.

Dunwoodie, S. L., T. A. Rodriguez and R. S. Beddington (1998). "Msg1 and Mrg1, founding members of a gene family, show distinct patterns of gene expression during mouse embryogenesis." Mech Dev **72**(1-2): 27-40.

Erdogan, F., R. Ullmann, W. Chen, M. Schubert, S. Adolph, C. Hultschig, V. Kalscheuer, H. H. Ropers, C. Spaich and A. Tzschach (2007). "Characterization of a 5.3 Mb deletion in 15q14 by comparative genomic hybridization using a whole genome "tiling path" BAC array in a girl with heart defect, cleft palate, and developmental delay." Am J Med Genet A **143A**(2): 172-178.

Espinoza-Lewis, R. A., L. Yu, F. He, H. Liu, R. Tang, J. Shi, X. Sun, J. F. Martin, D. Wang, J. Yang and Y. Chen (2009). "Shox2 is essential for the differentiation of cardiac pacemaker cells by repressing Nkx2-5." Dev Biol **327**(2): 376-385.

Essner, J. J., J. D. Amack, M. K. Nyholm, E. B. Harris and H. J. Yost (2005). "Kupffer's vesicle is a ciliated organ of asymmetry in the zebrafish embryo that initiates left-right development of the brain, heart and gut." Development **132**(6): 1247-1260.

Falkowski, M., K. Schledzewski, B. Hansen and S. Goerdt (2003). "Expression of stabilin-2, a novel fasciclin-like hyaluronan receptor protein, in murine sinusoidal endothelia, avascular tissues, and at solid/liquid interfaces." Histochem Cell Biol **120**(5): 361-369.

Fernandes-Silva, H., P. Vaz-Cunha, V. B. Barbosa, C. Silva-Goncalves, J. Correia-Pinto and R. S. Moura (2017). "Retinoic acid regulates avian lung branching through a molecular network." Cell Mol Life Sci.

Force, A., M. Lynch, F. B. Pickett, A. Amores, Y. L. Yan and J. Postlethwait (1999). "Preservation of duplicate genes by complementary, degenerative mutations." Genetics **151**(4): 1531-1545.

Franco, D. and M. Campione (2003). "The role of Pitx2 during cardiac development. Linking left-right signaling and congenital heart diseases." Trends Cardiovasc Med **13**(4): 157-163.

Franco, D., A. Chinchilla and A. E. Aranega (2012). "Transgenic insights linking pitx2 and atrial arrhythmias." Front Physiol **3**: 206.

Franco, D., V. M. Christoffels and M. Campione (2014). "Homeobox transcription factor Pitx2: The rise of an asymmetry gene in cardiogenesis and arrhythmogenesis." Trends Cardiovasc Med **24**(1): 23-31.

Garg, V., I. S. Kathiriya, R. Barnes, M. K. Schluterman, I. N. King, C. A. Butler, C. R. Rothrock, R. S. Eapen, K. Hirayama-Yamada, K. Joo, R. Matsuoka, J. C. Cohen and D. Srivastava (2003). "GATA4 mutations cause human congenital heart defects and reveal an interaction with TBX5." Nature **424**(6947): 443-447.

Gross-Thebing, T., A. Paksa and E. Raz (2014). "Simultaneous high-resolution detection of multiple transcripts combined with localization of proteins in whole-mount embryos." BMC Biol **12**: 55.

Gudbjartsson, D. F., D. O. Arnar, A. Helgadottir, S. Gretarsdottir, H. Holm, A. Sigurdsson, A. Jonasdottir, A. Baker, G. Thorleifsson, K. Kristjansson, A. Palsson, T. Blondal, P. Sulem, V. M. Backman, G. A. Hardarson, E. Palsdottir, A. Helgason, R. Sigurjonsdottir, J. T. Sverrisson, K. Kostulas, M. C. Ng, L. Baum, W. Y. So, K. S. Wong, J. C. Chan, K. L. Furie, S. M. Greenberg, M. Sale, P. Kelly, C. A. MacRae, E. E. Smith, J. Rosand, J. Hillert, R. C. Ma, P. T. Ellinor, G. Thorgeirsson, J. R. Gulcher, A. Kong, U. Thorsteinsdottir and K. Stefansson (2007). "Variants conferring risk of atrial fibrillation on chromosome 4q25." Nature **448**(7151): 353-357.

Guner-Ataman, B., N. Paffett-Lugassy, M. S. Adams, K. R. Nevis, L. Jahangiri, P. Obregon, K. Kikuchi, K. D. Poss, C. E. Burns and C. G. Burns (2013). "Zebrafish second heart field development relies on progenitor specification in anterior lateral plate mesoderm and nkx2.5 function." Development **140**(6): 1353-1363.

Hamada, H. (2010). Heart Development and Regeneration. Londond, Academic Press Elsevier.

Hami, D., A. C. Grimes, H. J. Tsai and M. L. Kirby (2011). "Zebrafish cardiac development requires a conserved secondary heart field." Development **138**(11): 2389-2398.

Harvey, R. P. (2002). "Patterning the vertebrate heart." Nat Rev Genet **3**(7): 544-556.

Hillenius, W. J. and J. A. Ruben (2004). "The evolution of endothermy in terrestrial vertebrates: Who? When? Why?" Physiol Biochem Zool **77**(6): 1019-1042.

Hoffman, J. I. (1995). "Incidence of congenital heart disease: I. Postnatal incidence." Pediatr Cardiol **16**(3): 103-113.

Hoffman, J. I. (1995). "Incidence of congenital heart disease: II. Prenatal incidence." Pediatr Cardiol **16**(4): 155-165.

Holtzman, N. G., J. J. Schoenebeck, H. J. Tsai and D. Yelon (2007). "Endocardium is necessary for cardiomyocyte movement during heart tube assembly." Development **134**(12): 2379-2386.

Horne-Badovinac, S., M. Rebagliati and D. Y. Stainier (2003). "A cellular framework for gut-looping morphogenesis in zebrafish." Science **302**(5645): 662-665.

Hutchinson, S. A. and J. S. Eisen (2006). "Islet1 and Islet2 have equivalent abilities to promote motoneuron formation and to specify motoneuron subtype identity." Development **133**(11): 2137-2147.

Ilagan, R., R. Abu-Issa, D. Brown, Y. P. Yang, K. Jiao, R. J. Schwartz, J. Klingensmith and E. N. Meyers (2006). "Fgf8 is required for anterior heart field development." Development **133**(12): 2435-2445.

Keegan, B. R., J. L. Feldman, G. Begemann, P. W. Ingham and D. Yelon (2005). "Retinoic acid signaling restricts the cardiac progenitor pool." Science **307**(5707): 247-249.

Keegan, B. R., D. Meyer and D. Yelon (2004). "Organization of cardiac chamber progenitors in the zebrafish blastula." Development **131**(13): 3081-3091.

Kelly, R. G., N. A. Brown and M. E. Buckingham (2001). "The arterial pole of the mouse heart forms from Fgf10-expressing cells in pharyngeal mesoderm." Dev Cell **1**(3): 435-440.

Kim, J. S., S. Viragh, A. F. Moorman, R. H. Anderson and W. H. Lamers (2001). "Development of the myocardium of the atrioventricular canal and the vestibular spine in the human heart." Circ Res **88**(4): 395-402.

Knoepfler, P. S., K. R. Calvo, H. Chen, S. E. Antonarakis and M. P. Kamps (1997). "Meis1 and pKnox1 bind DNA cooperatively with Pbx1 utilizing an interaction surface disrupted in oncoprotein E2a-Pbx1." Proc Natl Acad Sci U S A **94**(26): 14553-14558.

Koshiba-Takeuchi, K., A. D. Mori, B. L. Kaynak, J. Cebra-Thomas, T. Sukonnik, R. O. Georges, S. Latham, L. Beck, R. M. Henkelman, B. L. Black, E. N. Olson, J. Wade, J. K. Takeuchi, M. Nemer, S. F. Gilbert and B. G. Bruneau (2009). "Reptilian heart development and the molecular basis of cardiac chamber evolution." Nature **461**(7260): 95-98.

Lagendijk, A. K., A. Szabo, R. M. Merks and J. Bakkers (2013). "Hyaluronan: a critical regulator of endothelial-to-mesenchymal transition during cardiac valve formation." Trends Cardiovasc Med **23**(5): 135-142.

Lamers, W. H. and A. F. Moorman (2002). "Cardiac septation: a late contribution of the embryonic primary myocardium to heart morphogenesis." Circ Res **91**(2): 93-103.

Langenbacher, A. D., J. Huang, Y. Chen and J. N. Chen (2012). "Sodium pump activity in the yolk syncytial layer regulates zebrafish heart tube morphogenesis." Dev Biol **362**(2): 263-270.

Li, Y., N. T. Klena, G. C. Gabriel, X. Liu, A. J. Kim, K. Lemke, Y. Chen, B. Chatterjee, W. Devine, R. R. Damerla, C. Chang, H. Yagi, J. T. San Agustin, M. Thahir, S. Anderton, C. Lawhead, A. Vescovi, H. Pratt, J. Morgan, L. Haynes, C. L. Smith, J. T. Eppig, L. Reinholdt, R. Francis, L. Leatherbury, M. K. Ganapathiraju, K. Tobita, G. J. Pazour and C. W. Lo (2015). "Global genetic analysis in mice unveils central role for cilia in congenital heart disease." Nature **521**(7553): 520-524.

Lin, C. R., C. Kioussi, S. O'Connell, P. Briata, D. Szeto, F. Liu, J. C. Izpisua-Belmonte and M. G. Rosenfeld (1999). "Pitx2 regulates lung asymmetry, cardiac positioning and pituitary and tooth morphogenesis." Nature **401**(6750): 279-282.

Liu, C., W. Liu, J. Palie, M. F. Lu, N. A. Brown and J. F. Martin (2002). "Pitx2c patterns anterior myocardium and aortic arch vessels and is required for local cell movement into atrioventricular cushions." Development **129**(21): 5081-5091.

Liu, J. and D. Y. Stainier (2012). "Zebrafish in the study of early cardiac development." Circ Res **110**(6): 870-874.

Lo, C. W., Q. Yu, C. Y. Shen, L. Leatherbury, R. Francis, X. Q. Zhao, Z. Zhang, A. Wessels, G. Y. Huang and B. Chatterjee (2010). Heart Development and Regeneration. Londond, Academic Press Elsevier.

Long, S., N. Ahmad and M. Rebagliati (2003). "The zebrafish nodal-related gene southpaw is required for visceral and diencephalic left-right asymmetry." Development **130**(11): 2303-2316.

Longobardi, E., D. Penkov, D. Mateos, G. De Florian, M. Torres and F. Blasi (2014). "Biochemistry of the tale transcription factors PREP, MEIS, and PBX in vertebrates." Dev Dyn **243**(1): 59-75.

Louw, J. J., A. Corveleyn, Y. Jia, G. Hens, M. Gewillig and K. Devriendt (2015). "MEIS2 involvement in cardiac development, cleft palate, and intellectual disability." Am J Med Genet A **167A**(5): 1142-1146.

Lozano-Velasco, E., A. Chinchilla, S. Martinez-Fernandez, F. Hernandez-Torres, F. Navarro, G. E. Lyons, D. Franco and A. E. Aranega (2011). "Pitx2c modulates cardiac-specific transcription factors networks in differentiating cardiomyocytes from murine embryonic stem cells." Cells Tissues Organs **194**(5): 349-362.

Mably, J. D., C. G. Burns, J.-N. Chen, M. C. Fishman and M.-A. P. K. Mohideen (2003). "heart of glass Regulates the Concentric Growth of the Heart in Zebrafish." Current Biology **13**(24): 2138-2147.

Machon, O., J. Masek, O. Machonova, S. Krauss and Z. Kozmik (2015). "Meis2 is essential for cranial and cardiac neural crest development." BMC Dev Biol **15**: 40.

Mahmoud, A. I., F. Kocabas, S. A. Muralidhar, W. Kimura, A. S. Koura, S. Thet, E. R. Porrello and H. A. Sadek (2013). "Meis1 regulates postnatal cardiomyocyte cell cycle arrest." Nature **497**(7448): 249-253.

Mammi, I., P. De Giorgio, M. Clementi and R. Tenconi (1998). "Cardiovascular anomaly in Rieger Syndrome: heterogeneity or contiguity?" Acta Ophthalmol Scand **76**(4): 509-512.

Marques, S. R., Y. Lee, K. D. Poss and D. Yelon (2008). "Reiterative roles for FGF signaling in the establishment of size and proportion of the zebrafish heart." Dev Biol **321**(2): 397-406.

Martin, J. F., B. A. Amendt and N. A. Brown (2010). Heart Development and Regeneration. Londond, Academic Press Elsevier.

Melvin, V. S., W. Feng, L. Hernandez-Lagunas, K. B. Artinger and T. Williams (2013). "A morpholino-based screen to identify novel genes involved in craniofacial morphogenesis." Dev Dyn **242**(7): 817-831.

Meno, C., K. Gritsman, S. Ohishi, Y. Ohfuji, E. Heckscher, K. Mochida, A. Shimono, H. Kondoh, W. S. Talbot, E. J. Robertson, A. F. Schier and H. Hamada (1999). "Mouse Lefty2 and zebrafish antivin are feedback inhibitors of nodal signaling during vertebrate gastrulation." Mol Cell **4**(3): 287-298.

Meno, C., Y. Ito, Y. Saijoh, Y. Matsuda, K. Tashiro, S. Kuhara and H. Hamada (1997). "Two closely-related left-right asymmetrically expressed genes, lefty-1 and lefty-2: their

distinct expression domains, chromosomal linkage and direct neuralizing activity in Xenopus embryos." Genes Cells **2**(8): 513-524.

Meno, C., A. Shimono, Y. Saijoh, K. Yashiro, K. Mochida, S. Ohishi, S. Noji, H. Kondoh and H. Hamada (1998). "lefty-1 is required for left-right determination as a regulator of lefty-2 and nodal." Cell **94**(3): 287-297.

Merabet, S. and R. S. Mann (2016). "To Be Specific or Not: The Critical Relationship Between Hox And TALE Proteins." Trends Genet **32**(6): 334-347.

Mercader, N., E. Leonardo, N. Azpiazu, A. Serrano, G. Morata, C. Martinez and M. Torres (1999). "Conserved regulation of proximodistal limb axis development by Meis1/Hth." Nature **402**(6760): 425-429.

Mercader, N., E. Leonardo, M. E. Piedra, A. C. Martinez, M. A. Ros and M. Torres (2000). "Opposing RA and FGF signals control proximodistal vertebrate limb development through regulation of Meis genes." Development **127**(18): 3961-3970.

Missinato, M. A., K. Tobita, N. Romano, J. A. Carroll and M. Tsang (2015). "Extracellular component hyaluronic acid and its receptor Hmmr are required for epicardial EMT during heart regeneration." Cardiovasc Res **107**(4): 487-498.

Mommersteeg, M. T., W. M. Hoogaars, O. W. Prall, C. de Gier-de Vries, C. Wiese, D. E. Clout, V. E. Papaioannou, N. A. Brown, R. P. Harvey, A. F. Moorman and V. M. Christoffels (2007). "Molecular pathway for the localized formation of the sinoatrial node." Circ Res **100**(3): 354-362.

Monteiro, R., M. van Dinther, J. Bakkers, R. Wilkinson, R. Patient, P. ten Dijke and C. Mummery (2008). "Two novel type II receptors mediate BMP signalling and are required to establish left-right asymmetry in zebrafish." Dev Biol **315**(1): 55-71.

Moretti, A., L. Caron, A. Nakano, J. T. Lam, A. Bernshausen, Y. Chen, Y. Qyang, L. Bu, M. Sasaki, S. Martin-Puig, Y. Sun, S. M. Evans, K. L. Laugwitz and K. R. Chien (2006). "Multipotent embryonic isl1+ progenitor cells lead to cardiac, smooth muscle, and endothelial cell diversification." Cell **127**(6): 1151-1165.

Mosimann, C., D. Panakova, A. A. Werdich, G. Musso, A. Burger, K. L. Lawson, L. A. Carr, K. R. Nevis, M. K. Sabeh, Y. Zhou, A. J. Davidson, A. DiBiase, C. E. Burns, C. G. Burns, C. A. MacRae and L. I. Zon (2015). "Chamber identity programs drive early functional partitioning of the heart." Nat Commun **6**: 8146.

Moyes, C. D. and P. M. Schulte (2005). Principles of Animal Physiology. San Francisco, Pearson Education Inc., publishing as Benjamin Cummings.

Nakayama, Y., A. Miyake, Y. Nakagawa, T. Mido, M. Yoshikawa, M. Konishi and N. Itoh (2008). "Fgf19 is required for zebrafish lens and retina development." Dev Biol **313**(2): 752-766.

Newbury-Ecob, R. A., R. Leanage, J. A. Raeburn and I. D. Young (1996). "Holt-Oram syndrome: a clinical genetic study." J Med Genet **33**(4): 300-307.

Niederreither, K. and P. Dollé (2010). Heart Development and Regeneration. Londond, Academic Press Elsevier.

Niederreither, K., V. Subbarayan, P. Dolle and P. Chambon (1999). "Embryonic retinoic acid synthesis is essential for early mouse post-implantation development." Nat Genet **21**(4): 444-448.

Niederreither, K., J. Vermot, N. Messaddeq, B. Schuhbaur, P. Chambon and P. Dolle (2001). "Embryonic retinoic acid synthesis is essential for heart morphogenesis in the mouse." Development **128**(7): 1019-1031.

Nowotschin, S. and A. K. Hadjantonakis (2009). "Use of KikGR a photoconvertible green-to-red fluorescent protein for cell labeling and lineage analysis in ES cells and mouse embryos." BMC Dev Biol **9**: 49.

Olson, E. N. (2006). "Gene regulatory networks in the evolution and development of the heart." Science **313**(5795): 1922-1927.

Oulad-Abdelghani, M., C. Chazaud, P. Bouillet, V. Sapin, P. Chambon and P. Dolle (1997). "Meis2, a novel mouse Pbx-related homeobox gene induced by retinoic acid during differentiation of P19 embryonal carcinoma cells." Dev Dyn **210**(2): 173-183.

Paige, S. L., K. Plonowska, A. Xu and S. M. Wu (2015). "Molecular regulation of cardiomyocyte differentiation." Circ Res **116**(2): 341-353.

Paige, S. L., S. Thomas, C. L. Stoick-Cooper, H. Wang, L. Maves, R. Sandstrom, L. Pabon, H. Reinecke, G. Pratt, G. Keller, R. T. Moon, J. Stamatoyannopoulos and C. E. Murry (2012). "A temporal chromatin signature in human embryonic stem cells identifies regulators of cardiac development." Cell **151**(1): 221-232.

Peal, D. S., S. N. Lynch and D. J. Milan (2011). "Patterning and development of the atrioventricular canal in zebrafish." J Cardiovasc Transl Res **4**(6): 720-726.

Penkov, D., D. Mateos San Martin, L. C. Fernandez-Diaz, C. A. Rossello, C. Torroja, F. Sanchez-Cabo, H. J. Warnatz, M. Sultan, M. L. Yaspo, A. Gabrieli, V. Tkachuk, A. Brendolan, F. Blasi and M. Torres (2013). "Analysis of the DNA-binding profile and function of TALE homeoproteins reveals their specialization and specific interactions with Hox genes/proteins." Cell Rep **3**(4): 1321-1333.

Plageman, T. F., Jr. and K. E. Yutzey (2005). "T-box genes and heart development: putting the "T" in heart." Dev Dyn **232**(1): 11-20.

Prendiville, T., P. Y. Jay and W. T. Pu (2014). "Insights into the genetic structure of congenital heart disease from human and murine studies on monogenic disorders." Cold Spring Harb Perspect Med **4**(10).

Reischauer, S., R. Arnaout, R. Ramadass and D. Y. Stainier (2014). "Actin binding GFP allows 4D in vivo imaging of myofilament dynamics in the zebrafish heart and the identification of Erbb2 signaling as a remodeling factor of myofibril architecture." Circ Res **115**(10): 845-856.

Renier, N., Z. Wu, D. J. Simon, J. Yang, P. Ariel and M. Tessier-Lavigne (2014). "iDISCO: a simple, rapid method to immunolabel large tissue samples for volume imaging." Cell **159**(4): 896-910.

Rhinn, M. and P. Dolle (2012). "Retinoic acid signalling during development." Development **139**(5): 843-858.

Rochais, F., K. Mesbah and R. G. Kelly (2009). "Signaling pathways controlling second heart field development." Circ Res **104**(8): 933-942.

Rohr, S., C. Otten and S. Abdelilah-Seyfried (2008). "Asymmetric involution of the myocardial field drives heart tube formation in zebrafish." Circ Res **102**(2): e12-19.

Ryan, A. K., B. Blumberg, C. Rodriguez-Esteban, S. Yonei-Tamura, K. Tamura, T. Tsukui, J. de la Pena, W. Sabbagh, J. Greenwald, S. Choe, D. P. Norris, E. J. Robertson, R. M. Evans, M. G. Rosenfeld and J. C. Izpisua Belmonte (1998). "Pitx2 determines left-right asymmetry of internal organs in vertebrates." Nature **394**(6693): 545-551.

Ryckebusch, L., Z. Wang, N. Bertrand, S. C. Lin, X. Chi, R. Schwartz, S. Zaffran and K. Niederreither (2008). "Retinoic acid deficiency alters second heart field formation." Proc Natl Acad Sci U S A **105**(8): 2913-2918.

Rydeen, A. B. and J. S. Waxman (2014). "Cyp26 enzymes are required to balance the cardiac and vascular lineages within the anterior lateral plate mesoderm." Development **141**(8): 1638-1648.

Rydeen, A. B. and J. S. Waxman (2016). "Cyp26 Enzymes Facilitate Second Heart Field Progenitor Addition and Maintenance of Ventricular Integrity." PLoS Biol **14**(11): e2000504.

Salic, A. and T. J. Mitchison (2008). "A chemical method for fast and sensitive detection of DNA synthesis in vivo." Proc Natl Acad Sci U S A **105**(7): 2415-2420.

Savory, J. G., C. Edey, B. Hess, A. J. Mears and D. Lohnes (2014). "Identification of novel retinoic acid target genes." Dev Biol **395**(2): 199-208.

Schier, A. F. and M. M. Shen (2000). "Nodal signalling in vertebrate development." Nature **403**(6768): 385-389.

Schoenebeck, J. J., B. R. Keegan and D. Yelon (2007). "Vessel and blood specification override cardiac potential in anterior mesoderm." Dev Cell **13**(2): 254-267.

Schott, J. J., D. W. Benson, C. T. Basson, W. Pease, G. M. Silberbach, J. P. Moak, B. J. Maron, C. E. Seidman and J. G. Seidman (1998). "Congenital heart disease caused by mutations in the transcription factor NKX2-5." Science **281**(5373): 108-111.

Schulze, G. E., R. J. Clay, L. E. Mezza, C. L. Bregman, R. A. Buroker and J. D. Frantz (2001). "BMS-189453, a novel retinoid receptor antagonist, is a potent testicular toxin." Toxicol Sci **59**(2): 297-308.

Scott, I. C., B. Masri, L. A. D'Amico, S. W. Jin, B. Jungblut, A. M. Wehman, H. Baier, Y. Audigier and D. Y. Stainier (2007). "The g protein-coupled receptor agtrl1b regulates early development of myocardial progenitors." Dev Cell **12**(3): 403-413.

Semina, E. V., R. Reiter, N. J. Leysens, W. L. Alward, K. W. Small, N. A. Datson, J. Siegel-Bartelt, D. Bierke-Nelson, P. Bitoun, B. U. Zabel, J. C. Carey and J. C. Murray (1996). "Cloning and characterization of a novel bicoid-related homeobox transcription factor gene, RIEG, involved in Rieger syndrome." Nat Genet **14**(4): 392-399.

Seth, A., Q. J. Machingo, A. Fritz and B. D. Shur (2010). "Core fucosylation is required for midline patterning during zebrafish development." Dev Dyn **239**(12): 3380-3390.

Shen, M. M. (2007). "Nodal signaling: developmental roles and regulation." Development **134**(6): 1023-1034.

Shimojima, K., Y. Ondo, N. Okamoto and T. Yamamoto (2017). "A 15q14 microdeletion involving MEIS2 identified in a patient with autism spectrum disorder." Hum Genome Var **4**: 17029.

Shiratori, H., R. Sakuma, M. Watanabe, H. Hashiguchi, K. Mochida, Y. Sakai, J. Nishino, Y. Saijoh, M. Whitman and H. Hamada (2001). "Two-step regulation of left-right asymmetric expression of Pitx2: initiation by nodal signaling and maintenance by Nkx2." Mol Cell **7**(1): 137-149.

Shiratori, H., K. Yashiro, M. M. Shen and H. Hamada (2006). "Conserved regulation and role of Pitx2 in situs-specific morphogenesis of visceral organs." Development **133**(15): 3015-3025.

Sirbu, I. O., X. Zhao and G. Duester (2008). "Retinoic acid controls heart anteroposterior patterning by down-regulating Isl1 through the Fgf8 pathway." Dev Dyn **237**(6): 1627-1635.

Smith, K. A., S. Chocron, S. von der Hardt, E. de Pater, A. Soufan, J. Bussmann, S. Schulte-Merker, M. Hammerschmidt and J. Bakkers (2008). "Rotation and asymmetric development of the zebrafish heart requires directed migration of cardiac progenitor cells." Dev Cell **14**(2): 287-297.

Stainier, D. Y. (2001). "Zebrafish genetics and vertebrate heart formation." Nat Rev Genet **2**(1): 39-48.

Stainier, D. Y. and M. C. Fishman (1992). "Patterning the zebrafish heart tube: acquisition of anteroposterior polarity." Dev Biol **153**(1): 91-101.

Stainier, D. Y., B. Fouquet, J. N. Chen, K. S. Warren, B. M. Weinstein, S. E. Meiler, M. A. Mohideen, S. C. Neuhauss, L. Solnica-Krezel, A. F. Schier, F. Zwartkruis, D. L. Stemple, J. Malicki, W. Driever and M. C. Fishman (1996). "Mutations affecting the formation and function of the cardiovascular system in the zebrafish embryo." Development **123**: 285-292.

Stainier, D. Y., R. K. Lee and M. C. Fishman (1993). "Cardiovascular development in the zebrafish. I. Myocardial fate map and heart tube formation." Development **119**(1): 31-40.

Stankunas, K., C. Shang, K. Y. Twu, S. C. Kao, N. A. Jenkins, N. G. Copeland, M. Sanyal, L. Selleri, M. L. Cleary and C. P. Chang (2008). "Pbx/Meis deficiencies demonstrate multigenetic origins of congenital heart disease." Circ Res **103**(7): 702-709.

Stanley, E. G., C. Biben, A. Elefanty, L. Barnett, F. Koentgen, L. Robb and R. P. Harvey (2002). "Efficient Cre-mediated deletion in cardiac progenitor cells conferred by a 3'UTR-ires-Cre allele of the homeobox gene Nkx2-5." Int J Dev Biol **46**(4): 431-439.

Staudt, D. and D. Stainier (2012). "Uncovering the molecular and cellular mechanisms of heart development using the zebrafish." Annu Rev Genet **46**: 397-418.

Takeuchi, J. K., M. Ohgi, K. Koshiba-Takeuchi, H. Shiratori, I. Sakaki, K. Ogura, Y. Saijoh and T. Ogura (2003). "Tbx5 specifies the left/right ventricles and ventricular septum position during cardiogenesis." Development **130**(24): 5953-5964.

Targoff, K. L., T. Schell and D. Yelon (2008). "Nkx genes regulate heart tube extension and exert differential effects on ventricular and atrial cell number." Dev Biol **322**(2): 314-321.

Tessari, A., M. Pietrobon, A. Notte, G. Cifelli, P. J. Gage, M. D. Schneider, G. Lembo and M. Campione (2008). "Myocardial Pitx2 differentially regulates the left atrial identity and ventricular asymmetric remodeling programs." Circ Res **102**(7): 813-822.

Thisse, C. and B. Thisse (2008). "High-resolution in situ hybridization to whole-mount zebrafish embryos." Nat Protoc **3**(1): 59-69.

Trinh, L. A. and D. Y. Stainier (2004). "Fibronectin regulates epithelial organization during myocardial migration in zebrafish." Dev Cell **6**(3): 371-382.

Tsutsui, H., S. Karasawa, H. Shimizu, N. Nukina and A. Miyawaki (2005). "Semi-rational engineering of a coral fluorescent protein into an efficient highlighter." EMBO Rep **6**(3): 233-238.

Uribe, R. A. and M. E. Bronner (2015). "Meis3 is required for neural crest invasion of the gut during zebrafish enteric nervous system development." Mol Biol Cell **26**(21): 3728-3740.

Utriainen, A., R. Sormunen, M. Kettunen, L. S. Carvalhaes, E. Sajanti, L. Eklund, R. Kauppinen, G. T. Kitten and T. Pihlajaniemi (2004). "Structurally altered basement membranes and hydrocephalus in a type XVIII collagen deficient mouse line." Hum Mol Genet **13**(18): 2089-2099.

Vander, A., J. Sherman and D. Luciano (2001). Human Physiology: The Mechanisms of Body Function. New York, McGraw-Hill Higher Education.

Waldo, K. L., D. H. Kumiski, K. T. Wallis, H. A. Stadt, M. R. Hutson, D. H. Platt and M. L. Kirby (2001). "Conotruncal myocardium arises from a secondary heart field." Development **128**(16): 3179-3188.

Walsh, E. C. and D. Y. Stainier (2001). "UDP-glucose dehydrogenase required for cardiac valve formation in zebrafish." Science **293**(5535): 1670-1673.

Wang, J., E. Klysik, S. Sood, R. L. Johnson, X. H. Wehrens and J. F. Martin (2010). "Pitx2 prevents susceptibility to atrial arrhythmias by inhibiting left-sided pacemaker specification." Proc Natl Acad Sci U S A **107**(21): 9753-9758.

Wang, Y., M. S. Kaiser, J. D. Larson, A. Nasevicius, K. J. Clark, S. A. Wadman, S. E. Roberg-Perez, S. C. Ekker, P. B. Hackett, M. McGrail and J. J. Essner (2010). "Moesin1 and Ve-cadherin are required in endothelial cells during in vivo tubulogenesis." Development **137**(18): 3119-3128.

Waxman, J. S., B. R. Keegan, R. W. Roberts, K. D. Poss and D. Yelon (2008). "Hoxb5b acts downstream of retinoic acid signaling in the forelimb field to restrict heart field potential in zebrafish." Dev Cell **15**(6): 923-934.

Waxman, J. S. and D. Yelon (2009). "Increased Hox activity mimics the teratogenic effects of excess retinoic acid signaling." Dev Dyn **238**(5): 1207-1213.

Webb, S., N. A. Brown, A. Wessels and R. H. Anderson (1998). "Development of the murine pulmonary vein and its relationship to the embryonic venous sinus." Anat Rec **250**(3): 325-334.

Wessels, A., R. H. Anderson, R. R. Markwald, S. Webb, N. A. Brown, S. Viragh, A. F. Moorman and W. H. Lamers (2000). "Atrial development in the human heart: an immunohistochemical study with emphasis on the role of mesenchymal tissues." Anat Rec **259**(3): 288-300.

Westerfield, M. (2000). The zebrafish book. A guide for the laboratory use of zebrafish (Danio rerio).
, Univ. of Oregon Press, Eugene.

Williams, T. M., M. E. Williams and J. W. Innis (2005). "Range of HOX/TALE superclass associations and protein domain requirements for HOXA13:MEIS interaction." Dev Biol **277**(2): 457-471.

Witzel, H. R., B. Jungblut, C. P. Choe, J. G. Crump, T. Braun and G. Dobreva (2012). "The LIM protein Ajuba restricts the second heart field progenitor pool by regulating Isl1 activity." Dev Cell **23**(1): 58-70.

Xavier-Neto, J., B. Davidson, M. S. Simoes-Costa, R. A. Castro, A. Coelho Sampaio and A. P. Azambuja (2010). Heart Development and Regeneration. Londond, Academic Press Elsevier.

Xie, L., A. D. Hoffmann, O. Burnicka-Turek, J. M. Friedland-Little, K. Zhang and I. P. Moskowitz (2012). "Tbx5-hedgehog molecular networks are essential in the second heart field for atrial septation." Dev Cell **23**(2): 280-291.

Yelon, D., S. A. Horne and D. Y. Stainier (1999). "Restricted expression of cardiac myosin genes reveals regulated aspects of heart tube assembly in zebrafish." Dev Biol **214**(1): 23-37.

Yokoyama, T., N. G. Copeland, N. A. Jenkins, C. A. Montgomery, F. F. Elder and P. A. Overbeek (1993). "Reversal of left-right asymmetry: a situs inversus mutation." Science **260**(5108): 679-682.

Zaffran, S., R. G. Kelly, S. M. Meilhac, M. E. Buckingham and N. A. Brown (2004). "Right ventricular myocardium derives from the anterior heart field." Circ Res **95**(3): 261-268.

Zaidi, S. and M. Brueckner (2017). "Genetics and Genomics of Congenital Heart Disease." Circ Res **120**(6): 923-940.

Zeng, X. X., T. P. Wilm, D. S. Sepich and L. Solnica-Krezel (2007). "Apelin and its receptor control heart field formation during zebrafish gastrulation." Dev Cell **12**(3): 391-402.

Zhang, R., P. Han, H. Yang, K. Ouyang, D. Lee, Y. F. Lin, K. Ocorr, G. Kang, J. Chen, D. Y. Stainier, D. Yelon and N. C. Chi (2013). "In vivo cardiac reprogramming contributes to zebrafish heart regeneration." Nature **498**(7455): 497-501.

Zhao, C. M., L. Y. Peng, L. Li, X. Y. Liu, J. Wang, X. L. Zhang, F. Yuan, R. G. Li, X. B. Qiu and Y. Q. Yang (2015). "PITX2 Loss-of-Function Mutation Contributes to Congenital Endocardial Cushion Defect and Axenfeld-Rieger Syndrome." PLoS One **10**(4): e0124409.

Zhou, B., C. T. McGary, J. A. Weigel, A. Saxena and P. H. Weigel (2003). "Purification and molecular identification of the human hyaluronan receptor for endocytosis." Glycobiology **13**(5): 339-349.

Zhou, Y., T. J. Cashman, K. R. Nevis, P. Obregon, S. A. Carney, Y. Liu, A. Gu, C. Mosimann, S. Sondalle, R. E. Peterson, W. Heideman, C. E. Burns and C. G. Burns (2011). "Latent TGF-beta binding protein 3 identifies a second heart field in zebrafish." Nature **474**(7353): 645-648.

Summary

Introduction

Zebrafish heart development: The heart of the zebrafish is the first organ to form and function during embryonic development, and is composed by one atrium and one ventricle. Between 5-17 somites stage, the cardiomyocyte precursors form the bilateral cardiac fields in the anterior lateral plate mesoderm (ALMP); where the endocardial precursors are located anterior to the cardiac fields (Zeng, Wilm et al. 2007). Then, the pools of endocardial and myocardial precursors fuse at the midline and form the heart disc; where atrial cardiomyocytes are located around, the ventricular cardiomyocytes are located in the center of the heart disc, and the future endocardium is located in a ventral position relative to the cardiomyocytes (Bakkers 2011).

After the heart disc is formed, the cardiomyocyte progenitors start to migrate and rotate asymmetrically to form the heart tube (de Campos-Baptista, Holtzman et al. 2008, Rohr, Otten et al. 2008, Smith, Chocron et al. 2008). This process is followed by a rightward bending of the heart tube, and the arterial and venous poles rotate at different speed and directions (a process known as heart looping) (Smith, Chocron et al. 2008). The heart looping process results in a ventricle located on the right side and a more posterior atrium located on the left side with respect to the midline; at this point the atrium and ventricle are separated by a fine segment called the atrioventricular canal, where the valves will be formed (Staudt and Stainier 2012).

The second heart field (SHF) is a pool of cardiac progenitors that are specified later during the formation of the heart disc and until the heart looping stages. The SHF contributes with cells to the distal side of the ventricle, the outflow and inflow tracts, and is important for the specification of the cardiac conduction system (de Pater, Clijsters et al. 2009, Hami, Grimes et al. 2011, Zhou, Cashman et al. 2011, Witzel, Jungblut et al. 2012, Guner-Ataman, Paffett-Lugassy et al. 2013).

Mammalian heart development: Mammals have four-chambered hearts comprised of two atria and two ventricles. Despite anatomical differences, the genetic pathways regulating heart development in mammals are very similar to those in the zebrafish (Staudt and Stainier 2012). In mouse, at E7.5, the cardiac progenitors are located at both sides of the LPM, forming the cardiac crescent that contains the FHF and SHF progenitors. These pool of

progenitors will fuse at the midline and form the linear heart tube (Harvey 2002). Afterwards, the cardiac chambers start to balloon as the atrial and ventricular cells differentiate and proliferate. The interatrial, the interventricular septation processes start at stage E10 and are only completed after birth (Paige, Plonowska et al. 2015). However, correct chamber septation is fundamental for the proper function of the heart, and defects in heart septation lead to mixing of deoxygenated and oxygenated blood, which in severe cases, can lead to lethality. Cardiac septation allows the separation of the systemic and pulmonary circulations, constituting an evolutionary advantage in comparison to the teleost fish, who only have two-chambered hearts; however, the evolutionary transition from two- to four-chambered hearts is a question that remains to be elucidated.

Congenital heart diseases (CHDs) constitute the most common type of birth defects, and arise when the heart is not correctly formed during embryonic development, impeding the proper function of the heart (Hoffman 1995). Some of the most common types of CHDs are atrial and ventricular septal defects (ASD and VSD, respectively) and atrioventricular canal defects (Bruneau 2008).

Mutations in genes involved in the establishment of cardiac left-right (L-R) asymmetry often lead to ASDs and VSDs (Liu, Liu et al. 2002, Plageman and Yutzey 2005, Tessari, Pietrobon et al. 2008). PITX2 is a homeobox transcription factor that is key in L-R patterning of the heart. During cardiac development, *Pitx2* is expressed on the left side of the heart tube, and then its expression becomes restricted to the left atrium (Franco and Campione 2003). In mammals, mutations in *Pitx2* have been linked to ASDs, VSDs, as well as endocardial cushion defects and atrial fibrillation (Mammi, De Giorgio et al. 1998, Gudbjartsson, Arnar et al. 2007, Franco, Chinchilla et al. 2012, Zhao, Peng et al. 2015).

Retinoic Acid Signaling: RA is a signaling molecule important for embryonic anterior-posterior (A-P) patterning, morphogenesis and organogenesis (Niederreither and Dollé 2010). In the zebrafish, RA signaling regulates the boundaries between the pool of cardiac progenitors and the adjacent vascular and forelimb progenitors by restricting the number of cardiomyocytes in the ALMP (Waxman, Keegan et al. 2008, Rydeen and Waxman 2014). Additionally, the levels of RA are inversely proportional to the number of cardiomyocytes. And excess of RA results in hearts with atrial dominance, suggesting that A-P cardiac patterning is influenced by RA signaling (Xavier-Neto, Davidson et al. 2010).

Meis transcription factors: The Meis transcription factors are major interaction partners of Hox and Pbx proteins, and together they are important in A-P axis development and

organogenesis. *Meis2* expression and activity have been shown to be regulated by RA signaling during limb and lung development in chick (Mercader, Leonardo et al. 2000, Fernandes-Silva, Vaz-Cunha et al. 2017). In humans, mutations in *MEIS2* lead to a great number of congenital malformations, including ASDs and VSDs (Erdogan, Ullmann et al. 2007, Chen, Lin et al. 2008, Crowley, Conlin et al. 2010, Louw, Corveleyn et al. 2015). *Meis2* deficient mice die between E13.5 and E14.5 due to severe hemorrhaging and show congenital heart defects, characterized by persistent truncus arteriosus and absence of the aortic and pulmonary valves (Machon, Masek et al. 2015). In zebrafish, *Meis2* has two orthologues, *meis2a* and *meis2b*. It has been reported that *meis2b* morphants showed delayed heart development, cardiac looping defects, and slower heart rate (Paige, Thomas et al. 2012),

However, the exact role of *MEIS2* and its orthologue *meis2b*, during heart formation is not clear. Therefore, the main goal of this project was to determine the function of *meis2b* in cardiac development by: a) determining the expression pattern of *meis2b* throughout heart development; b) studying the effect of *meis2b* loss-of-function in heart development and function; c) determining possible upstream regulators of Meis2b; and d) possible downstream targets of Meis2b in the heart.

Results and Discussion

meis2b mutant: In an unbiased comparison of the transcription profiles of the atrium and ventricle of the adult zebrafish heart, *meis2b* expression was found to be highly enriched in the atrium. Together with *meis2b*, the expressions of *myh6*, *pitx2*, *id4* and *shox2*, are also highly enriched in the atrium and lowly expressed in the ventricle.

Since *MEIS2* is important in cardiac development in humans, and given its restricted expression pattern in the zebrafish heart, *meis2b* became an interesting candidate to study its role in heart development. For this purpose, a *meis2b* mutant allele was used, which is characterized by a frameshift mutation. However, no cardiac defects were observed during embryonic cardiac development of the *meis2b* mutants. In contrast to the knockdown experiments that have been previously published, these results indicate that mutations in *meis2b* do not affect embryonic heart development (Paige, Thomas et al. 2012). Nevertheless, starting from 3 wpf, a progressive atrial enlargement was detected in the *meis2b* mutants, which caused bulging in the pericardial area of the adult fish.

To determine if proliferation is increased in the hearts of *meis2b* mutants, the atrial proliferation ratio was determined in 3 mpf fish. Adult *meis2b*$^{-/-}$, showed 10,02% (±1.12) of proliferating atrial cardiomyocytes, in contrast to the 2.78% (±0.49) in WT siblings. These results suggest that excessive atrial cardiomyocyte proliferation greatly contributes to the abnormal atrial growth observed in the *meis2b* mutants.

Establishment of the *meis2b* reporter line: To closely follow the expression pattern of *meis2b* during heart development, transgenic line was created: *TgBAC(meis2b:GAL4FF); Tg(5xUAS:EGFP)* (hereon referred to as *Tg(meis2b-reporter)*). At 24 and 48 hpf, the expression *Tg(meis2b-reporter)* in the body closely resembles the endogenous expression of *meis2b*, detected by *in situ* hybridization (ISH). Interestingly, at 24 and 48 hpf, the *Tg(meis2b-reporter)* is expressed in the cardiac tissue, in contrast to what can be seen in with ISH, given that the expression levels of *meis2b* are too low and cannot be appreciated with conventional ISH.

Taking advantage of the possibility of visualization of *Tg(meis2b-reporter)* in the heart at embryonic stages, *Tg(meis2b-reporter);Tg(myl7:mCherry)* embryos at different developmental stages were imaged. Interestingly, at 23 somites stage, after the heart disc is formed, the *Tg(meis2b-reporter)* is expressed in the cardiomyocytes located in the posterior half of the heart disc. This restricted expression pattern is consistent with what has been observed at earlier stages, where *meis2b* is expressed in a more posterior subset of the *gata4*-positive cardiomyocyte progenitors in the bilateral heart fields in the ALMP (Paige, Thomas et al. 2012). Later, due to the migration and rotation of the cardiomyocytes in the heart disc, the *Tg(meis2b-reporter)*-positive cells are found in the ventral region of the heart tube, adopting a dorso-ventral configuration.

At three dpf, once the cardiac chambers are formed, *Tg(meis2b-reporter)* is expressed in the dorsal and left side of the atrium, in the inflow tract and in a small portion of the ventricle near the atrioventricular canal. After six dpf, the expression of *Tg(meis2b-reporter)* is completely restricted to the left side of the atrium, near the outflow tract and no expression in the ventricle can be detected. At three mpf, the *Tg(meis2b-reporter)* maintains its asymmetric expression pattern, being only observed on the left side of the atrium, and resembling the endogenous expression observed with ISH on sections. Throughout heart development, the *Tg(meis2b-reporter)* is expressed exclusively in the cardiomyocytes.

Lineage tracing experiments indicated that the cardiomyocytes from the posterior half of the cardiac disc, form the left side of the heart at 48 hpf; while cells from the anterior half of the

disc, are located mainly on the right side of the heart at 48 hpf. These results indicate that the A-P asymmetry in the cardiac disc is translated to a L-R asymmetry in the heart and, and this L-R is maintained until adulthood. Furthermore, these data reveal a L-R asymmetric gene expression pattern in the single atrium of the zebrafish heart, preceding the evolutionary emergence of the interatrial septum of terrestrial vertebrates; and divides the atrium into a *meis2b*-positive and a *meis2b*-negative compartment.

Upstream regulators of *meis2b*: To determine if the asymmetric expression pattern of *meis2b* at 48 hpf depends on the cellular contributions of the FHF and SHF to the heart, a morpholino against *isl1* (a SHF marker) was injected in *Tg(meis2b-reporter)*; *Tg(myl7:mCherry)* embryos. However, at 48 hpf, the expression of *Tg(meis2b-reporter)* was not affected by the absence of SHF derived cardiomyocytes. Suggesting that the asymmetric expression of *Tg(meis2b-reporter)* is independent of SHF contribution.

Since RA signaling is important for A-P axis development during heart formation, and it has been shown that RA restricts the number of cardiomyocyte progenitors (Keegan, Feldman et al. 2005), *Tg(meis2b-reporter)* embryos were treated before gastrulation with either DEAB (a known inhibitor of Aldh, the enzyme that produces RA) or with excess of RA (Waxman, Keegan et al. 2008, Waxman and Yelon 2009).

Under control conditions, the *Tg(meis2b-reporter)* is expressed in 55.1% (±7.6) of cardiomyocytes in the heart disc. In contrast, inhibiting RA signaling caused a significant reduction in the number of *Tg(meis2b-reporter)*-positive cells, where only 7.7% (±2.3) of the cardiomyocytes expressed the *Tg(meis2b-reporter)* and these *meis2b*-positive cells were limited to the posterior end of the heart disc. Embryos exposed to excess of RA showed a significant expansion of the *Tg(meis2b-reporter)* expression throughout the cardiac disc, with 92.6% (±6.9) of the cardiomyocytes expressing the *Tg(meis2b-reporter)*. Therefore, the A-P asymmetric pattern is lost when RA levels are misregulated, which indicates that RA signaling regulates early compartmentalization of the heart disc by inducing the expression of *meis2b* in the cardiomyocytes.

Downstream targets of Meis2b: In order identify the possible downstream targets of Meis2b, expression profiles at different developmental stages were determined and compared using a microarray. Interestingly, within the ten most downregulated genes in the atria of adult *meis2b* mutants are: *meis2b* (as expected) and *pitx2*. Surprisingly, and according to previously published data (Penkov, Mateos San Martin et al. 2013), MEIS1/2 in mouse, can

bind near *Meis2* and *Pitx2* enhancer sites, which suggests that *pitx2* could be a direct downstream target of Meis2b in the zebrafish as well.

Interestingly, *pitx2* transcripts were found to largely colocalize with *Tg(meis2b-reporter)* in five wpf hearts. This result was further confirmed by RT-qPCR, by comparing the transcriptional profiles of *meis2b*-positive and *meis2b*-negative atrial compartments of three mpf zebrafish hearts. These data revealed that *pitx2* and *meis2b* expressions are significantly enriched in the left atrial compartment of the zebrafish atrium, and indicates that cardiac expression of *pitx2* could be regulated by Meis2b. Given that *Pitx2* is a key factor in maintenance of the left atrial identity in mammals (Tessari, Pietrobon et al. 2008, Franco, Christoffels et al. 2014), it is possible that, in the zebrafish heart, the role of Meis2b is to mediate the identity of the left atrial compartment through regulating the cardiac expression of *pitx2*.

In summary, the current research emphasizes on the cardiac function of Meis2b and reveals an unexpected L-R asymmetry in the single atrium of the zebrafish heart. The evolution of the cardiac compartments from the simple two-chambered heart of the teleost, to the four-chambered heart of mammals, remains a puzzling problem whose evolutionary, developmental and genetic bases still have to be discovered. In contrast, the results obtained in this study suggest that before atrial septation, there was a pre-existing transcriptional pattern present in the heart of the teleost fish; which confers an individual identity to the two transcriptional compartments (*meis2b*-positive and *meis2b*-negative compartments), and includes the participation of genes involved in the establishment of cardiac L-R asymmetry.

Zusammenfassung

Einleitung

Herzentwicklung des Zebrafisches: Das Herz des Zebrafisches ist das erste gebildete und funktionsfähige Organ während der Embryonenentwicklung und setzt sich aus einem Herzvorhof und einem Ventrikel zusammen. Zwischen dem 5. und dem 17. Somitenstadium formen die Kardiomyozytenvorläufer die bilateralen Herzfelder im vorderen lateralen Plattenmesoderm (VLPM), wo sich die Endokardiumvorläufer vor den Herzfeldern befinden. Dann verschmelzen die Zellverbände der Endokardium- und der Myokardiumvorläufer auf der Mittellinie und bilden die Herzscheibe, bei welcher die Ventrikelkardiomyozyten im Zentrum lokalisiert sind und von den Herzvorhofkardiomyozyten umgeben sind. In einer ventralen Position relativ zu den Kardiomyozyten befindet sich das zukünftige Endokardium.

Nachdem sich die Herzscheibe gebildet hat, beginnen die Kardiomyozytenvorläufer, asymmetrisch zu migrieren und zu rotieren, um die Herzröhre zu bilden. Anschließend neigt sich die Röhre auf die rechte Seite des Embryos und die Arterien- und Venenpole rotieren in verschiedenen Richtungen und Geschwindigkeiten (ein Prozess, welcher als „heart looping“ bezeichnet wird). Dieser Prozess resultiert in einem Ventrikel, welcher auf der rechten Seite lokalisiert ist und einem Herzvorhof, welcher sich weiter hinten auf der linken Seite gegenüber der Mittellinie befindet. Zu diesem Zeitpunkt sind dann sowohl der Herzvorhof, als auch der Ventrikel durch einen dünnen Abschnitt separiert, dem sogenannten atrioventrikulären Kanal, wo sich die Ventile bilden.

Das sekundäre Herzfeld (SHF) ist ein Verband aus Herzvorläuferzellen, welche sich später während der Formierung der Herzscheibe und bis zu den „heart looping“-Stadien spezifizieren. Das SHF trägt Zellen zu der distalen Seite des Ventrikels, dem Einfluss- und dem Ausflusstrakt bei und ist wichtig für die Spezifizierung des Herzleitungssystems.

Herzentwicklung der Säugetiere: Säugetiere besitzen Vierkammerherzen, welche aus zwei Herzvorhöfen und zwei Ventrikeln bestehen. Abgesehen von den offensichtlichen anatomischen Differenzen sind die zellulären und genetischen Mechanismen, welche die Herzentwicklung in Säugetieren kontrollieren, sehr ähnlich zu denen in Zebrafischen. In der Maus, bei E7.5, sind die Herzvorläuferzellen in der LPM gruppiert und formen damit die Herzsichel, welche die FHF- und die SHF-Vorläufer beinhaltet, die auf der Mittellinie

verschmelzen und die lineare Herzröhre bilden. Danach beginnen die Herzkammern sich aufzublähen, indem die Atrium- und Ventrikelzellen differenzieren und proliferieren. Der Interatrium- und Interventrikelseptationsprozess starten bei Stadium E10 und sind erst nach der Geburt vollendet. Jedoch ist die korrekte Septation der Kammern grundlegend für die einwandfreie Funktionsfähigkeit des Herzens und Defekte in der Herzseptation führen zu der Vermischung von sauerstoffarmen mit sauerstoffreichem Blut, was in schweren Fällen tödlich enden kann. Die Herzseptation erlaubt die Trennung des Körper- und des Lungenkreislaufs, was einen evolutionären Vorteil zu den Teleostfischen darstellt, welche nur Zweikammerherzen besitzen. Jedoch ist der evolutionäre Übergang von Zweikammerherzen zu Vierkammerherzen eine noch ungeklärte Fragestellung.

Erblich bedingte Herzerkrankungen stellen den häufigsten Fall von Geburtdefekten dar und treten auf, wenn das Herz während der Embryonenentwicklung nicht korrekt ausgebildet wurde, was die Funktionsfähigkeit des Herzens einschränkt. Einige der häufigsten Typen von erblich bedingten Herzerkrankungen sind Herzvorhofseptum- und Ventrikelseptumdefekte, sowie atrioventrikuläre Kanaldefekte.

Mutationen von Genen, welche in der Etablierung der Herz-Links-Rechts-Asymmetrie (L-R) involviert sind, führen häufig zu ASDs und VSDs. PITX2 ist ein Homeobox-Transkripitionsfaktor, welcher eine Schlüsselrolle in der Bildung des L-R-Musters des Herzen spielt. Während der Herzentwicklung wird *Pitx2* zunächst in der linken Hälfte der Herzröhre exprimiert, anschließend wird seine Expression auf den linken Herzvorhof beschränkt. In Säugetieren wurden Mutationen von *Pitx2* in Verbindung mit ASDs, VSDs, Defekten des Endokardkissens, sowie Herzvorhofflimmern gebracht.

Der Retinolsäurensignalweg: RA ist ein Signalmolekül, welches während der embryonalen Anterior-Posterior-Musterbildung (A-P), der Morphogenese und der Organogenese wichtig ist. Im Zebrafisch reguliert RA die Grenzen zwischen den Herzvorläuferzellen und den benachbarten Gefäß- und Vordergliedmaßenvorläufern, indem es die Anzahl an Kardiomyozyten im ALMP begrenzt. Zusätzlich ist die Menge an RA umgekehrt proportional zu der Anzahl an Kardiomyozyten. Ein Überschuss an RA resultiert in einem Herzen mit Herzvorhofdominanz, was zu der Vermutung führt, dass die A-P-Herzmusterung durch die Signalwirkung von RA beeinflusst wird.

Meis-Transkriptionsfaktoren: Die Meis-Transkriptionsfaktoren sind Hauptinteraktionspartner der Hox- und Pbx-Proteine und zusammen sind sie wichtig in der A-P-Axen-Entwicklung und der Organogenese. Es wurde beobachtet, dass in Küken

während der Entwicklung der Extremitäten und der Lunge die *Meis2*-Expression und –Aktivität durch RA-Signalwege reguliert wird. Im Menschen führen Mutationen in *MEIS2* zu einer großen Anzahl an angeborenen Missbildungen, beispielsweise ASDs und VSDs. *Meis2*-defiziente Mäuse sterben bedingt durch schwere Blutungen zwischen E13.5 und E14.5 und zeigen angeborene Herzdefekte, charakterisiert durch einen persistenten Truncus arteriosus und dem Fehlen der Aorten- und Lungenventile. Im Zebrafisch hat *Meis2* zwei Orthologe, *meis2a* und *meis2b*. Es wurde berichtet, dass *meis2b*-Morphanten eine verzögerte Herzentwicklung, Herzschlaufendefekte und eine verringerte Herzrate aufweisen.

Allerdings ist die exakte Rolle von *MEIS2* und seinem Ortholog *meis2b* während der Formierung des Herzens nicht klar. Daher ist es das Hauptziel dieses Projektes, die Funktion von *meis2b* in der Herzentwicklung zu untersuchen, a) durch die Untersuchung des Expressionsmusters von *meis2b* während der Herzentwicklung, b) durch das Studieren des Effekts eines *meis2b*-Funktionsverlustes auf die Herzentwicklung und –Funktion, c) durch die Untersuchung der möglichen Regulatoren stromaufwärts und d) stromabwärts von Meis2b im Herzen.

Ergebnisse und Diskussion

meis2b-Mutanten: In einem objektiven Vergleich der Transkriptionsprofile des Herzvorhofs und des Ventrikels des erwachsenen Zebrafischherzens wurde gefunden, dass die *meis2b*-Expression im Atrium stark angereichert ist. Zusammen mit *meis2b* sind die Expressionen von *myh6*, *pitx2*, *id4* und *shox2* ebenso stark im Herzvorhof angereichert und wenig exprimiert im Ventrikel.

Da *MEIS2* wichtig für die Herzentwicklung vom Menschen ist und da es ein beschränktes Expressionsmuster im Zebrafischherzen zeigt, wurde *meis2b* ein interessanter Kandidat, um seine Rolle in der Herzentwicklung zu studieren. Für dieses Ziel wurde ein *meis2b*-Mutantenallel verwendet, welches durch eine Framshiftmutation charakterisiert ist. Allerdings konnten keine Herzdefekte während der embryonalen Herzentwicklung der *meis2b*-Mutanten festgestellt werden. Im Kontrast zu den knockdown-Experimenten, welche kürzlich publiziert wurden, zeigen diese Ergebnisse, dass Mutationen in *meis2b* die embryonale Herzentwicklung nicht beeinflussen. Trotzdem wurde, beginnend bei drei

Wochen nach der Befruchtung, eine beständige Herzvorhofvergrößerung in den *meis2b*-Mutanten festgestellt, was Ausbeulungen im Perikard des erwachsenen Fisches auslöste.

Um herauszufinden, ob die Proliferation in den Herzen der *meis2b*-Mutanten erhöht ist, wurde die Herzvorhofproliferationsrate in drei Monate alten Fischen geprüft. Erwachsene *meis2b*$^{-/-}$ zeigten 10,02% (±1,12) an proliferierenden Herzvorhofkardiomyozyten, im Gegensatz zu den 2,78% (±0,49) in Wildtypgeschwistern. Diese Ergebnisse suggerieren, dass eine exzessive Proliferation in den Herzvorhofkardiomyozyten stark zu dem abnormen Herzvorhofwachstum beiträgt, welches in *meis2b*-Mutanten beobachtet wurde.

Etablierung der *meis2b*-Reporterlinie: Um das Expressionsmuster von *meis2b* während der Herzentwicklung genau verfolgen zu können, wurde eine transgene Linie kreiert: *TgBAC(meis2b:GAL4FF); Tg(5xUAS:EGFP)* (kurz als *Tg(meis2b-reporter)* bezeichnet). 24 und 48 Stunden nach der Befruchtung gleicht die Expression von *Tg(meis2b-reporter)* im Körper stark der endogenen Expression von *meis2b*, wenn sie durch in situ-Hybridisierung (ISH) detektiert wurde. Interessanterweise wird 24 und 48 Stunden nach der Befruchtung der *Tg(meis2b-reporter)* im Herzgewebe exprimiert, im Gegensatz zu dem, was mit ISH gesehen werden kann, da die Expressionslevel von *meis2b* zu gering sind und daher nicht mit konventioneller ISH eingeschätzt werden können.

Dank dieses Vorteils der Visualisierung von *Tg(meis2b-reporter)* im Herzen während embryonalen Stadien, konnten *Tg(meis2b-reporter);Tg(myl7:mCherry)*-Embryos während verschiedenen Entwicklungsstadien abgebildet werden. Interessanterweise wird der *Tg(meis2b-reporter)* während des 23. Somitenstadiums, nachdem sich die Herzscheibe gebildet hat, in den Kardiomyozyten, welche sich in der hinteren Hälfte der Herzscheibe befinden, exprimiert. Dieses beschränkte Expressionsmuster liegt im Einklang mit dem, was in früheren Stadien beobachtet wurde, wobei *meis2b* eher im hinteren Teil der *gata4*+-Kardiomyozytenvorläufer im bilateralen Herzfeld im ALMP exprimiert wird. Später, durch Migration und Rotation der Kardiomyozyten in der Herzscheibe, wurden die *Tg(meis2b-reporter)*-positiv-Zellen in der ventralen Region der Herzröhre gefunden, wo sie eine dorso-ventrale Konfiguration annehmen.

Drei Tage nach der Befruchtung, sobald die Herzkammern geformt wurden, wird der *Tg(meis2b-reporter)* in der dorsalen und linken Seite des Atriums exprimiert, sowohl im Einstromtrakt als auch in einem kleinen Bereich des Ventrikels nahe des Herzvorhof-Ventrikelkanals. Sechs Tage nach der Befruchtung ist die Expression von *Tg(meis2b-reporter)* komplett beschränkt auf die linke Seite des Atriums, nahe des Ausflusstraktes und

es kann keine Expression im Ventrikel detektiert werden. Drei Monate nach der Befruchtung, behält der *Tg(meis2b-reporter)* sein asymmetrisches Expresionsmuster bei, da es nur auf der linken Seite des Herzvorhofes beobachtet werden kann, was der endogenen Expression ähnelt, welche mit ISH in Querschnitten beobachtet werden kann. Während der Herzentwicklung wird der *Tg(meis2b-reporter)* exklusiv nur in den Kardiomyozyten exprimiert.

Linienverfolgungsexperimente ergaben, dass die Kardiomyozyten aus der hinteren Hälfte der Herzscheibe bei 48 Stunden nach der Befruchtung die linke Seite des Herzens bilden, während Zellen von der vorderen Hälfte der Scheibe 48 Stunden nach der Befruchtung hauptsächlich auf der rechten Seite lokalisiert sind. Diese Ergebnisse induzieren, dass sich die A-P-Asymmetrie in der Herzscheibe zu einer L-R-Asymmetrie im Herzen umwandelt und dieses L-R bis zum Erwachsenenalter beibehalten wird. Weiterhin zeigen diese Daten auf, dass ein asymmetrisches L-R-Genexpressionsmuster in dem einzelnen Herzvorhof des Zebrafischherzens existiert, welches dem evolutionären Hervortreten des interatrialen Septums von Landwirbeltieren vorrausgeht und den Herzvorhof in ein *meis2b*+ und ein *meis2b*- Kompartiment unterteilt.

Regulatoren stromaufwärts von *meis2b*: Um herauszufinden, ob das asymmetrische Expressionsmuster von *meis2b* bei 48 Stunden nach der Befruchtung von dem zellulären Beitrag des FHF und des SHF zum Herzen abhängt, wurde ein Morpholino gegen *isl1* (einem SHF-Marker) in *Tg(meis2b-reporter)*; *Tg(myl7:mCherry)*-Embryos injiziert. Allerdings wurde bei 48 Stunden nach der Befruchtung die Expression von *Tg(meis2b-reporter)* nicht durch die Abwesenheit von SHF-abgeleiteten Kardiomyozyten beeinflusst. Dies suggeriert, dass die asymmetrische Expression von *Tg(meis2b-reporter)*unabhängig von dem SHF-Beitrag ist.

Da die RA-Signalwege während der Herzbildung wichtig sind für die A-P-Axenentwicklung und da gezeigt wurde, dass RA die Anzahl an Kardiomyozytenvorläufern beschränkt, wurden *Tg(meis2b-reporter*)-Embryos entweder mit DEAB (einem bekannten Inhibitor von Aldh, dem Enzym welches RA produziert) oder mit einem Überschuss an RA vor der Gastrulation behandelt.

Unter Kontrollbedingungen wird der *Tg(meis2b-reporter)* in 55,1% (±7,6) der Kardiomyozyten in der Herzscheibe exprimiert. Im Gegensatz dazu führte die Inhibierung von RA zu einer signifikanten Reduktion der Anzahl an *Tg(meis2b-reporter)*-positiv-Zellen,

bei welchen nur 7,7% (±2,3) der Kardiomyozyten den *Tg(meis2b-reporter)* exprimierten und diese *meis2b*+-Zellen waren limitiert auf das hintere Ende der Herzscheibe. Embryos, die einem Überschuss an RA ausgesetzt waren zeigten eine signifikante Expansion der *Tg(meis2b-reporter)*-Expression in der gesamten Herzscheibe, wobei 92,6% (±6,9) der Kardiomyozyten den *Tg(meis2b-reporter)* exprimierten. Somit geht das A-P-Asymmetriemuster verloren, wenn die RA-Level dysreguliert sind, was zu der Annahme führt, dass RA die frühe Kompartimentalisierung der Herzscheibe reguliert, indem es die Expression von *meis2b* in den Kardiomyozyten induziert.

Ziele stromabwärts von Meis2b: Um die möglichen Ziele stromabwärts von Meis2b zu identifizieren, wurden die Expressionsprofile bei unterschiedlichen Entwicklungsstadien bestimmt und mithilfe eines Microarrays verglichen. Interessanterweise sind unter den zehn der am meisten herunterregulierten Gene in den Herzvorhöfen von erwachsenen *meis2b*-Mutanten: *meis2b* (wie erwartet) und *pitx2*. Überraschenderweise und entsprechend der zuvor publizierten Daten kann MEIS1/2 in Mäusen nahe *Meis2*- und *Pitx2*-Enhancerstellen binden, was zu der Vermutung führt, dass *pitx2* ebenfalls ein direktes Ziel stromabwärts von Meis2b im Zebrafisch sein könnte.

Interessanterweise wurde beobachtet, dass fünf Wochen nach der Befruchtung *pitx2*-Transkripte stark mit *Tg(meis2b-reporter)* im Herzen kolokalisieren. Dieses Ergebnis wurde weiter bestätigt durch RT-qPCR, indem die Transkriptionsprofile von den *meis2b*+ und den *meis2b*- Herzvorhofkompartimenten in Zebrafischherzen drei Monate nach der Befruchtung verglichen wurden. Diese Daten decken auf, dass die Expressionen von *pitx2* und *meis2b* in dem linken Herzvorhofkompartiment des Zebrafischherzvorhofes signifikant erhöht sind und sie indizieren, dass die Herzexpression von *pitx2* durch Meis2b reguliert werden könnte. Da *Pitx2* ein Schlüsselfaktor für die Aufrechterhaltung der linken Herzvorhofidentität in Säugetieren ist, ist es möglich, dass die Aufgabe von Meis2b im Zebrafischherzen die Vermittlung der Identität des linken Herzvorhofkompartiments ist, indem es die Herzexpression von *pitx2* reguliert.

Alles in allem betont die aktuelle Forschung die Funktion von Meis2b im Herzen und sie deckt eine unerwartete L-R-Asymmetrie im einzelnen Herzvorhof des Zebrafischherzens auf. Die Evolution der Herzkompartimente von einem einfachen Zweikammerherzen der Teleostfische zu einem Vierkammerherzen von Säugetieren bleibt ein rätselhaftes Problem, dessen evolutionäre, genetische und Entwicklungsgrundlagen noch immer erforscht werden müssen. Trotzdem weisen die Ergebnisse aus dieser Studie darauf hin, dass vor der

Herzvorhofseptation ein bereits existierendes Transkriptionsmuster im Herzen der Teleostfische präsent war, welches den beiden Transktiptionskompartimenten (*meis2b*+ und *meis2b*- Kompartimente) eine individuelle Identität gewährt und die Beteiligung von Genen einschließt, welche in der Etablierung der Herz-L-R-Asymmetrie involviert sind.